

Journal of Electrochemical Science and Engineering

J. Electrochem. Sci. Eng. 9(1) 2019, 1-73





Open Access: ISSN 1847-9286

www.jESE-online.org

Original scientific paper

Electroorganic synthesis of disulfonamide substituted *p*-benzoquinone by hydroquinone electrochemical oxidation

Seba Nassif^{1,⊠}, Deeb Bakeer¹, Rushdi Madwar¹, Waleed Khadam², Abeer Nakhla²

¹Department of Chemistry, Faculty of Science, Al-Baath University, Homs, Syria

Received: June 4, 2018; Revised: July 30, 2018; Accepted: August 1, 2018

Abstract

This study illustrates electrochemical behavior of hydroquinone and 4-amino-6-chlorobenzene-1,3-disulfonamide in the phosphate buffer solution evaluated by cyclic voltammetry. It was found that the peak of the hydroquinone oxidation potential in the presence of 4-amino-6-chlorobenzene-1,3-disulfonamide is shifted to more positive values compared to hydroquinone alone. Based on these results, the electrochemical synthesis of new disulfonamide substituted p-benzoquinone is proposed and carried out via electrochemical oxidation of hydroquinone in the presence of 4-amino-6-chlorobenzene-1,3-disulfonamide in the electrolytic cell. It has been concluded that hydroquinone is converted into disulfonamide substituted p-benzoquinone via an ECE mechanism. The successful electrochemical synthesis was conducted in the water/ethanol mixture under green conditions without any toxic reagents or solvents and with high atom economy.

Keywords

Cyclic voltammetry; electrochemical synthesis; hydroquinone; disulfonamide

Introduction

Electrochemistry provides a versatile way for electrosynthesis of biologically active intermediates and kinetic studies of different reagents that are of pharmaceutical importance [1]. Since electrochemical methods are simple and rapid, they are normally used to study electroactive compounds in pharmaceutical forms and physiological fluids. Quinones are classified in a large group of natural pigments that show excellent photochemical properties [2] and act as intermediates in a biosynthesis of important antibiotics [3]. Quinones exhibit biological activities such as antidiabetic [4] and are frequently used as charge transfer complexes [5]. Also, the change from hydroquinone to quinine plays an important role in redox processes occurring in living organisms. Quinones also act as electron—proton carriers for carrying oxygen in biochemical

²Faculty of Pharmacy, Al-Baath University, Homs, Syria.

[™]Corresponding author E-mail: s nassif81@hotmail.com

reactions [6]. There are many works addressed to electro-oxidation of hydroquinone and its derivatives followed by the addition reaction with different nucleophiles such as 1-methylindole—triphenylphosphine-1,3-dimethylbarbituric acid [7-9]. Contrary to conventional organic synthetic methods that take place in organic solvents such as benzene, only few papers on the electrolytic synthesis of the sulfonamide derivatives have already been published. This is somewhat strange because conventional organic synthetic reactions suffer from the necessity of heating, long reaction time and low atom economy [10,11].

Sulfonamides are synthetic drugs that have various therapeutic potential uses such as antimetalloprotease [12], antibacterial, anti-diabetic [13], anti-carbonic anhydrase, diuretic [14], antithyroid, and antiviral activities [15].

Based on all these information, we believed that the synthesis of an organic compound with a structure of both sulfonamide and quinone groups would be useful from the perspective of pharmaceutical properties. This idea encouraged us to investigate the electrochemical oxidation of hydroquinone in the presence of disulfonamide as a nucleophile. The reaction is carried out in a single step with high atom economy under ambient conditions using a carbon anode.

Experimental

Apparatus and reagents

Cyclic voltammetry experiments were performed using an ampere-metric station model (Amel-433Analyser, Milano, Italy). The electrolytic cell with the glassy carbon working electrode was used. Ag/AgCl electrode as the reference, and a platinum wire as an auxiliary electrode were used. NMR ¹H and ¹³C spectra were taken at 400 MHz Bruker. Infrared spectrum was taken on FT-IR-4100 from Jasco. All chemicals including 4-amino-6-chlorobenzene-1,3-disulfonamide and hydroquinone were purchased from Merck Laboratories and were analytical grade materials. Phosphate salt and solvents were all of pro-analysis quality and used without further purification. The water utilized in all studies was double-distilled and deionized.

Procedure

All voltammetric experiments were performed in water (phosphate buffer, c = 0.2 M)/ethanol (50/50 v/v) solution. Electroorganic synthesis of new substituted disulfonamide-para-benzoquinone was carried out in a single step, by using the electrolytic cell.

In a typical procedure, 70 ml of phosphate buffer solution (0.2 M, pH 8.0) was added to the water/ethanol mixture (35/65 v/v). This mixture contains 0.05 M of hydroquinone and 0.05 M of 4-amino-6-chlorobenzene-1,3-disulfonamide. The total solution was electrolyzed in a divided cell equipped with a zinc cathode, two carbon rods-anode and DC power supply set at 0.08 A. Current density was 6.413×10^{-3} A/cm².

The reaction was electrolyzed with constant stirring using a magnetic stirrer for two hours. The progress of the reaction was monitored by TLC plate. Then, evaporation of the solution was conducted and a brown colored product was obtained. This product was washed with ethanol and isolated at yield of 98 %. The product was characterized by spectroscopy (IR, ¹H NMR).

Results and discussion

Electrochemical behavior of hydroquinone

The cyclic voltammogram of glassy carbon electrode in a solution of hydroquinone (0.005 M) in a water (phosphate buffer, c = 0.2 M, pH 8.0)/ethanol mixture is shown in Figure 1. Anodic peak (A)

at 95 mV and a corresponding cathodic peak (B) at -57 mV can be clearly observed. These peaks correspond to the conversion of hydroquinone to *p*-benzoquinone and vice versa, proceeding by a quasi-reversible two electrons process.

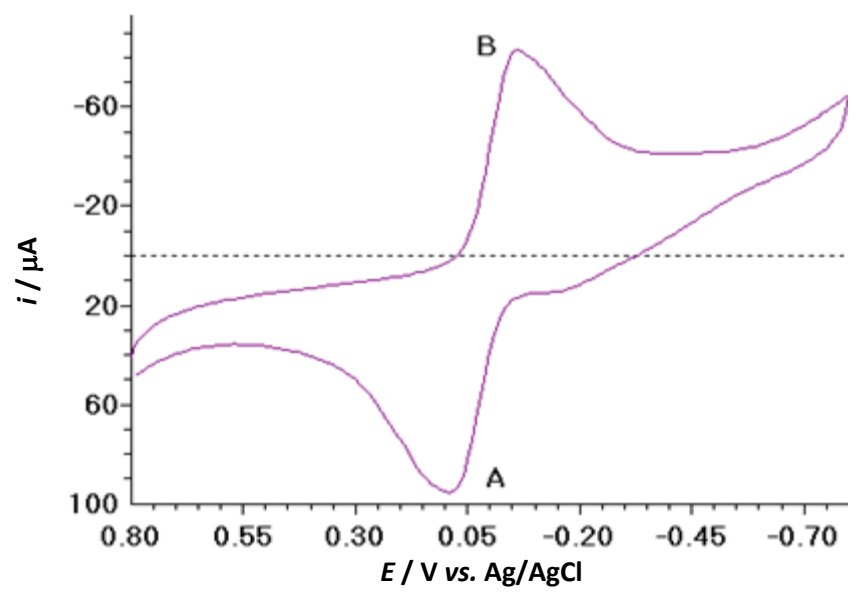


Figure 1. Cyclic voltammogram hydroquinone (0.005M) on glassy carbon electrode. Scan rate: 100 mv s^{-1} Solvent water (phosphate buffer, c = 0.2M, pH 8.0)/ethanol.

If, however, 1.0 mM solution of disulfonamide was put in the solution instead hydroquinone, not any peak was observed in the cyclic voltammogram recorded under same applied conditions.

The effect of pH on the voltammetric behavior of hydroquinone was monitored and it was seen that the peak (A) shifts to the negative potential by increasing pH value. Figure 2 represents the potential-pH diagram.

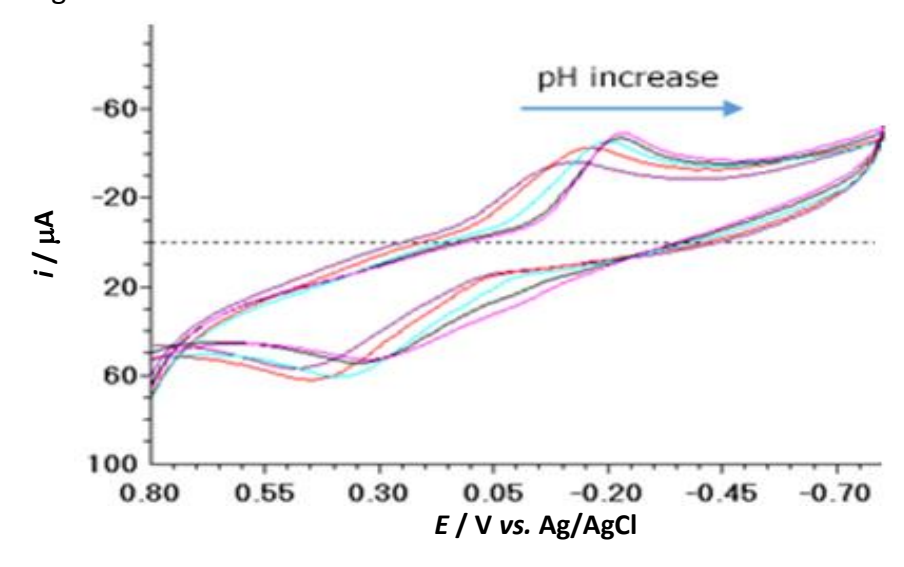


Figure 2. Cyclic voltammogram of hydroquinone in phosphate buffer solution with various pH values on glassy carbon electrode. pH are 4.0, 5.0, 6.0, 7.0 and 8.0, scan rate 100 mv s^{-1} .

The anodic peak potential (E_{pA}) is given by [16]:

$$E_{pA} = E_{pA(pH0)} - 2.303 \frac{mRT}{2F} pH$$

where m is the number of protons involved in the reaction, $E_{pA(pH\ 0)}$ is the anodic peak potential at (pH 0.0), while R, T, and F have their usual meanings. It is seen in Figure 3 that E_{pA} is shifted to less positive potentials with the slope of 62.2 mV/pH. This slope is in agreement with the theoretical slope (2.303 mRT/2F) of 59 mV/pH for m=2. Based on this slope, it can be concluded that the electrode reaction is a two electron—two proton process. The ratio of the number of protons to electrons (m/n) indicates the slope of the potential-pH diagram. Upon increasing pH, the hydroxyl group dissociates to its anionic form. In other words, the proton of hydroxyl group does not participate in the electrochemical oxidation process. Hence, the potential-pH diagram is independent of the hydroxyl proton.

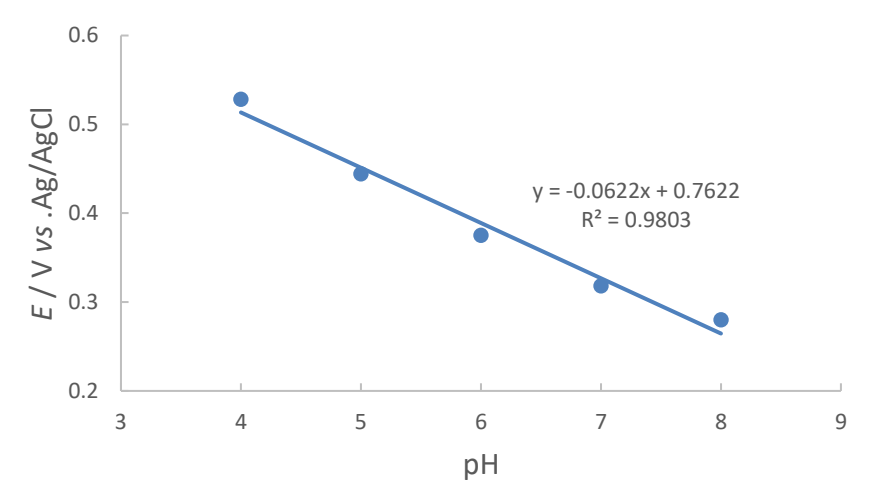


Figure 3. Potential – pH diagram of hydroquinone

Figure 4 shows cyclic voltammograms of hydroquinone with and without the presence of 4-amino-6-chlorobenzene-1,3-disulfonamide.

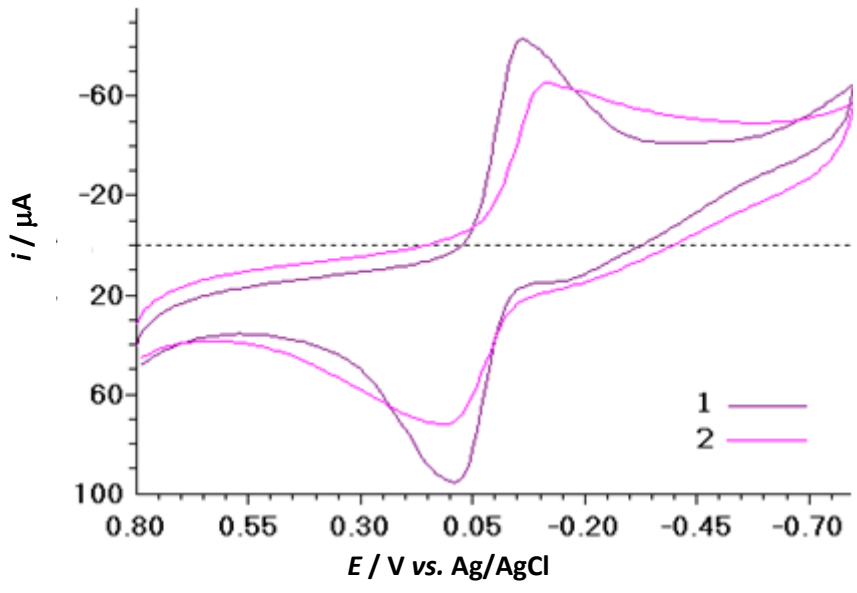


Figure 4. Cyclic voltammograms of: (1) hydroquinone, (2) hydroquinone in the presence of 4-amino-6-chlorobenzene-1,3-disulfonamide on glassy carbon electrode, scan rate: 100 mv s⁻¹ Solvent: water (phosphate buffer,c=0.2M,pH=8.0)/ethanol

In the presence of sulfonamide, the current peak heights of hydroquinone are decreased and peak potentials are slightly shifted toward higher potentials, *i.e.* cathodic peak toward more

negative values while anodic peak shifted toward more positive values. Obviously, the presence of sulfonamide affects the reaction of hydroquinone at GC electrode, probably due to their chemical or physical association in the solution decreasing diffusion coefficient.

Electroorganic synthesis

In order to investigate the possibility of synthetic utilization of the reaction, a preparative electrochemical oxidation of hydroquinone in the presence of 4-amino-6-chlorobenzen-1,3-disulfonamide was carried out in a divided cell containing 0.025 M of hydroquinone, 0.05 M of 4-amino-6-chlorobenzen-1,3-disulfonamide, and phosphate buffer solution (0.2 M, pH 8.0). The cell was equipped with a zinc cathode and two carbon rods anodes.

After 576 C (As) of electricity passed, the reaction was stopped and the resulting product isolated as described in Experimental section. The spectroscopic data of final product (IR, ¹H NMR, ¹³C NMR) allowed us to propose the following pathway of the electrochemical oxidation of hydroquinone in the presence of 4-amino-6-chlorobenzen-1,3-disulfonamide:

1. Firstly, hydroquinone oxidizes at the carbon anode by an electrochemical reaction into *p*-benzoquinone. Then, this product reacts with disulfonamide to produce a substituted hydroquinone. The reaction follows the Michael's addition mechanism.

2. Secondly, the substituted hydroquinone oxidizes into substituted *p*-benzoquinone in an electrooxidation reaction. This oxidation takes place at lower potentials than hydroquinone oxidation, what is due to the presence of the electron-donating amine functional group.

Hence, the overall reaction mechanism of the electrochemical synthesis followed the ECE mechanism and can be described as follows:

Spectral data:

 1 H NMR (400 MHz, DMSO-d6) δ ppm: 8.11(s,H, NH)- 7.3 (d, J=66Hz, 2H, quinone)- 6.9 (s, H, aromatic) - 6.6 (s, H, aromatic)- 3.3(s,2H, NH₂)- 3.7(s,2H, NH₂).

¹³C NMR(DMSO-d6) δppm: 55.9, 104.3, 120.2, 129.6, 133.6,147.87, 158.13, 180.75,182 (C=O). IR (KBr) v/cm^{-1} : 3407-3361 (NH₂), 3279 (NH), 1630 - 1552 (C=O), 1170 (S=O).

The atom economy was calculated for the synthesis substituted disulfonamide p-benzoquinone according to Eissen and coworkers (Eq. 1) [17]:

Atom economy,
$$\% = \frac{\text{Atom mass (in desired product)}}{\text{Atom mass (in reactant)}} \times 100$$
 (1)

The calculated atom economy for the synthesis of substituted disulfonamide p-benzoquinone is 99.09 %. The high atom economy indicates that all atoms, except four hydrogen atoms from the starting materials are incorporated into the product.

The substituted disulfonamide p-benzoquinone compound was tested to evaluate its antibacterial activity by Agar-well diffusion method [18]. *Escherichia coli* (*E. coli* Gram-negative) was the bacteria used in this experiment. The created well was filled with 3 mg of substituted disulfonamide *p*-benzoquinone. The inhibition zone surrounding the wells (in millimeters) was measured to evaluate antibacterial activity. The results showed that *E. coli* has a little sensitivity to substituted disulfonamide *p*-benzoquinone. An outer membrane might be established and a set of multidrug resistance pumps in Gram-negative bacteria, such as *E.coli*, are quite effective barriers for antimicrobial compounds [19].

Conclusions

In summary, the pharmacological properties of disulfonamide and quinone encouraged us to synthesize a new compound containing disulfonamide and *p*-benzoquinone by electrochemical method. The results of cyclic voltammetric studies illustrated the ECE reaction mechanism. This mechanism started in electrooxidation reaction through hydroquinone oxidation to generate *p*-benzoquinone. Then this middle product was attacked by disulfonamide to produce the final product.

The synthesis of substituted disulfonamide *p*-benzoquinone was conducted in high atom economy and in accordance with the principles of green chemistry. These principles were the reaction in water/ethanol mixture instead of toxic solvents, running the reaction under room temperature, and the utilization of electrode as an electron source instead of the usage of any toxic reagents.

(cc) BY

References

- [1] H. Lund and O. Hammerich, Organic Electrochemistry 4th, CRC Press, New York, (2001), p.1-95.
- [2] S. Patai, Z. Rappoport, The Chemistry of the Quinonoid Compounds. John Wiley and Sons, London, (1974) 737-791.
- [3] S. Patai, Z. Rappoport, The Chemistry of the Quinonoid Compounds Volume 2, John Wiley and Sons., London, (1988), p.1293-1349.
- [4] B. Zhang, G. Salituro, D. Li. Z. Szalkowski, Y. Zhang, I. Royo, D. Vilella, M. T. Diez, F.Pelaez, C. Ruby, R.L. Kendall, X. Mao, P. Griffin, J. Calaycay, J. R. Zierath, J. V. Heck, R. G. Smith, D. E. Moller, *Science Journals* **284** (1999) 974–977.
- [5] T. Murata, Y. Morita, K. Fukui, K. Sato, D. Shiomi, T. Takui, M. Maesato, H. Yamochi, G. Saito, K. A. Nakasuji, *Chemie International Edition* **43** (2004) 6343–6346.
- [6] F. A. Khan, S. Choudhury, *Tetrahedron Letters* **51** (2010) 2541–2544.
- [7] D. Nematollahi, V. Hedayatfar, Journal of Chemical Sciences 123 (2011) 709–717.
- [8] D. Nematollahi, R. Esmaili, Journal of the Iranian Chemical Society 7 (2010) 260-268.
- [9] D. Nematollahi, H. Goodarzi, *Journal of Organic Chemistry* **67** (2002) 5036-5039.
- [10] F. Ramirez, S. Dershowitz, Journal of the American Chemical Society 78 (1956) 5614.
- [11] A. Solhy, W. Amer, M. Karkouri, R. Tahir, A. E. Bouari, A. Fihri, M. Bousmina, M. Zahouily, *Journal of Molecular Catalysis* **336** (2011) 8–15.
- [12] C. T. Supuran, A. Casini, A. Scozzafava, Medicinal Research Reviews 23 (2003) 535-558.
- [13] M. Loubatieres-Mariani, *Journal of Social and Biological Structures* **201** (2007) 121-125.
- [14] T. H. Maren, Annual Review of Pharmacology and Toxicology 16 (1976) 309-327.
- [15] F. Comby, J. F. Lagorce, T. Moulard, J. Buxeraud, C. Raby, Veterinary Research 24 (1993) 316-326.
- [16] D. Nematollahi, R. Esmaili, Electrochimica Acta 56 (2011),3899
- [17] M. Eissen, R. Mazur, H. G. Quebbemann, K. H. Pennemann, *Helvetica Chimica Acta* **87** (2004) 524–535
- [18] B. Bonev, J. Hooper, J. Parisot, J. Antimicrob. Chemotherapy **61** (2008) 1295-1301.
- [19] M. M. Cowan, *Clinical Microbiology Reviews* **12** (1999) 564-582.

©2019 by the authors; licensee IAPC, Zagreb, Croatia. This article is an open-access article distributed under the terms and conditions of the Creative Commons Attribution license (http://creativecommons.org/licenses/by/4.0/)



Open Access: ISSN 1847-9286

www.jESE-online.org

Original scientific paper

Studies on electrodeposited Zn-Fe alloy coating on mild steel and its characterization

Ramesh Bhat[⊠], Ampar Chitharanjan Hegde¹

Department of Chemistry, NMAM Institute of Technology, Nitte-574110, India

¹Electrochemistry Research Laboratory, Department of Chemistry, NITK, Surathkal, Srinivasnagar - 575 025, India

[™]Corresponding author: E-mail: <u>rameshbhat@nitte.edu.in</u>; Tel.: +91-8861037310; Fax: 08254-281265

Received: June 27, 2018; Revised: July 19, 2018; Accepted: August 19, 2018

Abstract

Chloride bath containing $ZnCl_2 \cdot 7H_2O$, $FeCl_2 \cdot H_2O$ and a combination of sulphamic acid and citric acid (SA+CA) were optimized for electrodeposition of bright Zn-Fe alloy coating on the mild steel. Bath constituents and operating parameters were optimized by the Hull cell method for highest performance of the coating against corrosion. The effect of current density and temperature on deposit characteristics such as corrosion resistance, hardness, thickness, cathode current efficiency and glossiness, were studied. Potentiodynamic polarization and electrochemical impedance spectroscopic (EIS) methods were used to assess corrosion behaviour. Surface morphology of coatings was examined using scanning electron microscopy (SEM). The Zn-Fe alloy with intense peaks corresponding to Zn (100) and Zn (101) phases, evidenced by X-ray diffraction (XRD) study, showed the highest corrosion resistance. A new and economical chloride bath for electrodeposition of bright Zn-Fe alloy coating on mild steel was proposed and discussed.

Keywords

Zn-Fe alloy; chloride bath; sulphamic/citric acid; corrosion; XRD study

Introduction

Electrodeposition of metals and alloys has become extensively used in many industries, showing distinctive advantages compared to most of other finishing technologies [1]. Implementation of Zn and Zn alloy coatings appears to be one of most original and simplest methods for attainment of high protection against corrosion [2]. The most commonly used metals for Zn alloying are of the Fe group [3-5]. Zn-Fe alloy coatings are characterized by excellent corrosion resistance and good weldability, formability and paint ability. They have numerous important applications such as in chemical and galvanic processes within automobile and aerospace industries [6]. Behaviour of Zn, Fe

and Zn-Fe alloy deposited onto copper from acid chloride solutions containing EDTA and boric acid was investigated by cyclic voltammetry and steady state polarization techniques [7]. Electrodeposition of Zn-Fe alloys from a chloride-based electrolyte has already been studied using electrochemical polarization techniques and other instrumental methods [8]. It was found that the coating of Zn-Fe alloy is formed following the mechanism of nucleation and subsequent growth. The Zn²⁺ ions in the electrolyte were found to inhibit deposition of Fe, while Fe²⁺ ions promote deposition of Zn. It was also found that co-deposition of Zn and Fe behaves anomalously [9]. Sulphate containing bath was developed for the preparation of Zn-Fe alloy coatings by Yang *et al.* [10]. The effects of citric acid and sodium citrate used respectively as a buffer and complexing agent were studied by Diaz *et al.* [11]. It was found that the kinetics of deposition is governed by the interfacial pH. Hegde *et al.* [12] showed that transition of metal alloys shows anomalous co-deposition, occurring as a result of changes in the applied current density during electrodeposition of zinc–nickel, zinc-iron and zinc-nickel alloys in the acidic medium. Eliaz *et al.* [13] concluded that deposition of iron group metals shows good corrosion resistance compared to the single metal deposition.

Electrodeposition of Zn-Fe alloys is generally classified as anomalous co-deposition process due to the preferential deposition of Zn as less noble metal [2]. Several hypotheses have been proposed to explain this anomalous co-deposition [2,14]. Many extensive research works have been reported on deposition mechanism of Zn-Fe group metal alloys, concentrating on anomalous co-deposition and dependency of deposit characteristics on the bath constitution and operating parameters. Not any work, however, has been reported on optimization of Zn-Fe alloy bath containing sulphamic acid (SA) in conjunction with citric acid (CA) for obtaining bright Zn-Fe alloy coatings. In the present study, the role of SA and CA used in a combination, on electrodeposition of Zn-Fe alloy and its corrosion protection performance are investigated. The main focus of this work is related to optimization of the bath composition, operating parameters and characterization of the coatings. Techniques such as scanning electron microscopy (SEM) and X-ray diffraction (XRD) were used to characterize the coatings.

Experimental

Plating solutions were prepared from laboratory grade chemicals and distilled water. Standard Hull cell of 267 ml capacity was used to optimize bath constituents. All depositions were carried out at 303 K and pH 3.0 (except during its deviation). Polished mild steel plates were used as cathode (surface area 7.5 cm²) and a pure zinc plate with the same exposed surface area was used as anode. A PVC cell of 250 cm³ in capacity was used with the cathode-anode space of about 5 cm. All depositions were carried out galvanostatically under constant temperature and pH for duration of 10 minutes using power source (N6705C, Keysight Technologies). A combination of sulphamic acid and citric acid, (SA+CA), was used as an additive for improving the brightness and homogeneity of the coating. The constituents and deposition parameters were optimized on the basis of coating appearance and corrosion resistance.

In order to study the electrochemical properties of coatings, potentiodynamic polarization and electrochemical impedance spectroscopy (EIS) measurements were performed. All electrochemical tests were carried out using a potentiostat/galvanostat (CH instruments) and a three-electrode cell. The working electrode was the coated metal specimen. The counter electrode was a platinum electrode with the same surface area as the working electrode. All electrochemical potentials in this work are referred to the Ag/AgCl electrode. The 5 % NaCl solution was used as a corrosion medium throughout the study. Potentiodynamic polarization study was carried out in a potential ramp of -

0.250 V to +0.250 V around the open circuit potential (OCP), at the scan rate of 1 mV s⁻¹. Corrosion rates were determined by the Tafel's extrapolation method. Impedance measurements were carried out over the frequency range of 100 kHz to 20 mHz, using sine waves of 10 mV amplitude. The microstructure of deposits was examined using SEM (JSM-6380 LA from JEOL, Japan). X-ray diffraction (XRD) patterns were collected by JDX-8P JEOL, Japan, with CuK α radiation (k = 1.5418 Å) as the X-ray source. While the thickness of the coatings was calculated from Faradays law, it was verified using digital thickness tester (Coat measure M&C, ISO-17025). The Fe content in the coating was estimated by spectrophotometer method [14]. The hardness of the deposits (~19 μ m thickness) was measured by Vickers method, using micro hardness tester (CLEMEX). The cathode current efficiency (CCE) of the deposition was determined by knowing the mass and composition of the deposit [2]. The brightness of deposit was measured using Gloss Meter (Nova-Elite, 600).

Results and discussion

Hull cell study

The bath composition and operating parameters of Zn-Fe bath have been optimized by usual Hull cell method [2] at 1.0 A cell current and temperature 30 °C. Varieties of deposits having greyish white/bright/porous bright appearance were obtained over the wide range of current density of 1.0-5.0 A dm⁻². Effect of each bath constituent on Hull cell panels were examined in terms of their appearance and surface morphology. The composition and operating parameters of the optimal bath are collected in Table 1.

Table 1. Composition and operating parameters of optimized bath for electroplating Zn-Fe alloy on mild steel

Bath composition	Amount, g L ⁻¹	Operating parameters
Zinc chloride Ferric chloride Sodium acetate Sulphamic acid Citric acid	70 20 60 1.0 4.0	pH 3.0 Temperature: 303 K Anode: Pure zinc Current density: 3.0 A dm ⁻²

Effect of current density

The current density over wide range (1.0-5.0 A dm⁻²) was found to have a predominant influence on many characteristics of plated deposits. Appearance and corrosion performance of deposit formed at each current density are described with data listed in Table 2. At low current density, the bath produced greyish white coating with ~2.64 wt.% Fe and a porous bright deposit with ~9.81 wt.% Fe at high current density. A sound bright deposit with ~5.87 wt.% Fe was found at 3.0 A dm⁻². Increase in Fe content with current density is attributed to the rapid depletion of more readily depositable Zn²⁺ ions at the cathode coating [2]. As shown in Table 2, the hardness of Zn-Fe alloy deposit increased together with Fe content in the deposit, hardness may ascribed to higher current density of iron compared to zinc (d_{Fe} = 7.90 g cm⁻³ and d_{Zn} = 7.14 g cm⁻³). At high current density, the coating was very thick with increased hardness. Thick and porous bright deposit formed at very high current density is due to the metal hydroxide formation caused by rapid evolution of hydrogen during plating. The reflectance of Zn-Fe alloy coatings at different current densities were also tested and it was found that the deposit formed at very low current density showed lower glossiness, whereas at the optimal current density the glossiness was found to be maximum. At higher current density, glossiness decreased due to increased porosity and thickness. The thickness of deposits was found to increase

substantially with current density, thickness may be due to the adsorbed metal hydroxide at the cathode, caused by the steady increase of pH due to cathodic evolution of hydrogen gas. Under all conditions of deposition, cathodic current efficiency (CCE) of the bath is found high. *i.e.* >85 %. A slight decrease in CCE with increasing current density as observed in Table 2, may be due to the excessive hydrogen evolution during plating.

Table 2. Effect of current density on pH, Fe content, CCE, thickness, hardness, glossiness and appearance of Zn-Fe electrodeposited from optimized bath at 303 K

<i>j</i> / A dm ⁻²	рН	Fe content, wt.%	CCE, %	Thickness, μm	Vickers hardness (HV ₂₀₀)	Glossiness	Appearance of deposit
1.0	3.0	2.64	87.6	7.2	135	109.0	Greyish white
2.0	3.0	4.71	90.5	10.6	158	117.0	Bright
3.0	3.0	5.87	93.6	15.8	181	156.1	Bright
4.0	3.0	8.19	87.0	17.9	195	138.6	Bright
5.0	3.0	9.81	85.8	21.5	199	146.8	Porous bright

Effect of temperature

Temperature is also found to play outstanding role on the composition and appearance of the deposit, as is the case of Zn-Fe alloys. As shown in Table 3, the deposit was found greyish white (due to high Fe content) at low temperature, and silver bright (due to low Fe content) at high temperature, respectively. This may be ascribed by the fact that at elevated temperature, more readily depositable metal (zinc) are favoured to be replenished at the cathode film.

Table 3. Effect of temperature on Fe content in the deposit plated at 3.0 A dm⁻² from bath having optimal composition

<i>T /</i> K	Fe content in deposit, wt.%	Appearance of deposit
283	6.02	Greyish
293	6.08	Bright
303	5.87	Bright
313	3.78	Bright
323	2.14	Porous bright

Corrosion study

Potentiodynamic polarization study

Electroplated specimens were subjected to corrosion study and corrosion data of Zn-Fe coatings corresponding to different current densities are given in Table 4. The increase of corrosion rate (CR) with current density is due to the changed phase structure caused by high Fe content in the deposit. High CR observed at very low current density is due to increased Fe content. This may be due to the tendency of bath to transit from anomalous to normal co-deposition [15].

Table 4. Corrosion parameters of Zn-Fe alloy coatings plated at different current density in potential ramp of -0.250 V to +0.250 V from OCP at scan rate of 1 mV s⁻¹ in 5 % NaCl

<i>j</i> / A dm ⁻²	i _{corr} / μA cm ⁻²	E _{corr} / V vs. Ag/AgCl	$\beta_{\rm c}$ / mV dec ⁻¹	eta_{a} / mV dec $^{ ext{-}1}$	Corrosion rate x10 ⁻² , mm year ⁻¹
1.0	12.36	-1.259	41.0	20.4	13.2
2.0	6.083	-1.240	54.6	37.8	9.42
3.0	1.666	-1.233	22.7	16.6	3.36
4.0	4.072	-1.239	29.3	20.1	6.38
5.0	9.011	-1.259	145.4	50.3	12.13

Large variation in the Tafel's slope of cathodic polarization shown in Figure 1, indicates that the corrosion rate is controlled more by the cathodic reaction. It was observed that the deposit formed at 3.0 A dm $^{-2}$ with ~5.87 wt.% Fe showed the lowest corrosion rate (3.36×10 $^{-2}$ mm year $^{-1}$). Hence it is inferred that at 3.0 A dm $^{-2}$, the added (SA+CA) combination has reduced the availability of free Fe $^{2+}$ ions in the solution by proper complexation, improving thus homogeneity of coatings and reducing the corrosion rate.

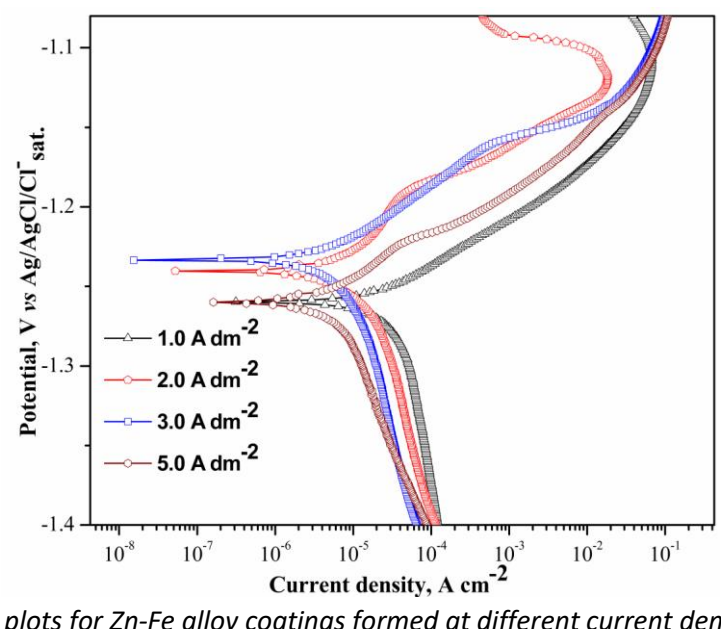


Figure 1. Tafel plots for Zn-Fe alloy coatings formed at different current densities from the optimal bath at scan rate of 1 mV s^{-1}

Electrochemical Impedance study

EIS is useful technique for ranking coatings, assessing interfacial reactions, quantifying coating breakdown, and predicting the lifetime of coating/metal systems. Advantages of this AC technique over DC techniques include the absence of any significant perturbation of the system, applicability to the assessment of low conductivity media and existence of frequency components that may provide mechanistic information. The EIS responses of Zn-Fe alloy coatings, deposited from the optimal bath at different current densities, are shown in Figure 2.

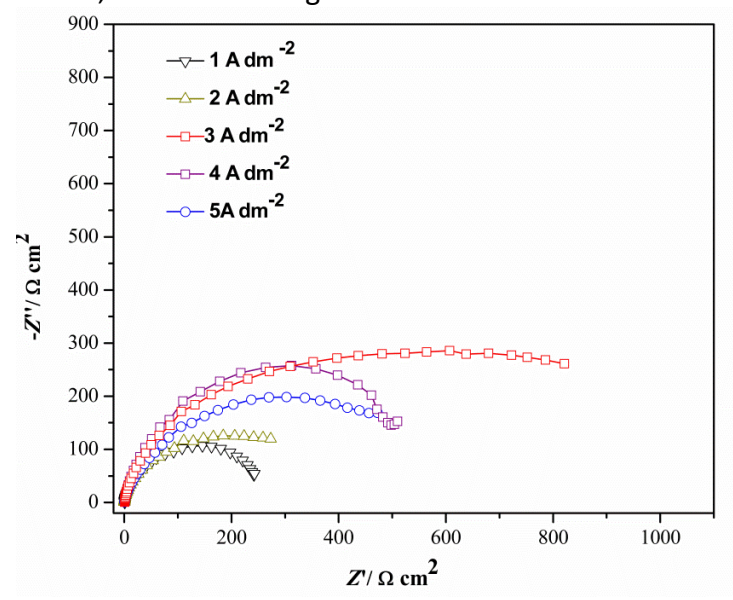


Figure 2. Electrochemical impedance spectra (100 kHz–20 mHz) of Zn-Fe coatings electrodeposited at different current densities.

Usual semicircle response due to corrosion can be noticed for each curve. The same origins of all curves are due to the solution resistance that is nearly identical in all cases, as the same bath chemistry and cell configuration were used. Since diameters of semicircles are related to the corrosion resistance, it may be noted that the highest corrosion resistance is exhibited by the coating deposited at the optimal current density, *i.e.* at 3.0 A dm⁻².

Cyclic polarization study

The cyclic polarization behavior shown in Figure 3 confirmed the formation of both air formed oxide layer and corrosion product layer. In the potential range of -0.3 V to -0.7 V, the current density of backward scanning was higher than that of the forward scanning, indicating the breakdown of the air formed oxide layer, while in the potential range from -0.7 V to -1.0 V it was lower than that of forward scanning, is due to formation of corrosion product initiated by pitting.

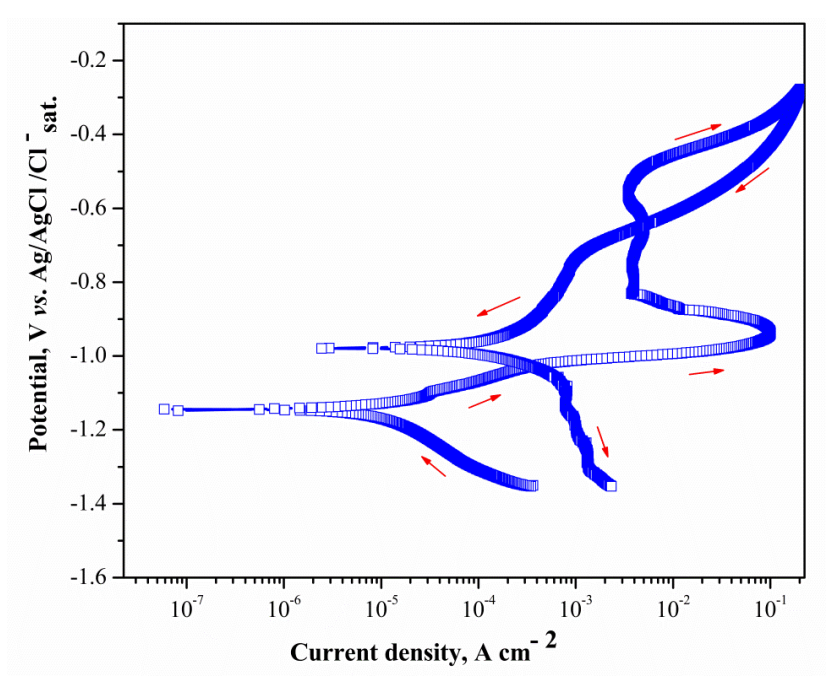


Figure 3. Cyclic polarization curve of Zn-Fe alloy electrodeposited at 3.0 A dm⁻² at scan rate of 1 mV s^{-1} in 5 % NaCl

X-ray diffraction analysis (XRD)

The phases of the electrodeposited Zn-Fe alloy are very complicated, depending on their chemical compositions [9]. XRD patterns of Zn-Fe alloys presented in Figure 4 shows the formation of coatings having different phase structures, depending on the current density at which they were deposited. The XRD peaks reveal that Zn-Fe alloys having range of compositions is formed and many phases coexist. It may be noticed that only relative intensities of few phases of zinc like (100), (101), (200) and (110) change among coatings deposited at different current densities, and hence different compositions were generated [9]. It was found that Zn-Fe alloy deposited at 3.0 A dm⁻² (with the lowest CR) exhibits two intense peaks corresponding to Zn with (100) and (101) phases.

SEM Analysis

SEM analysis showed that current density plays a significant role on the surface morphology and homogeneity of the deposit. Variation in the surface morphology with current density is shown in Figure 5. The coating was found to be very thin at 2.0 A dm⁻² (Figure. 5a) and bright at optimal current density 3.0 A dm⁻² (Figure 5b). At high current density, however, the deposit was found to be porous as shown in Figure 5c.

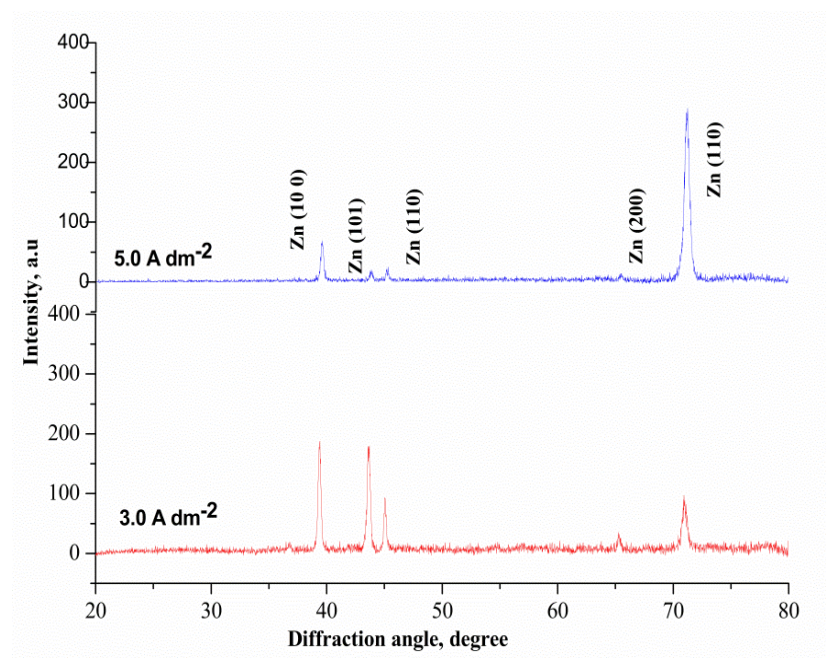


Figure 4. X-ray diffraction profiles of Zn-Fe coating electrodeposited on mild steel from optimized bath at different current densities

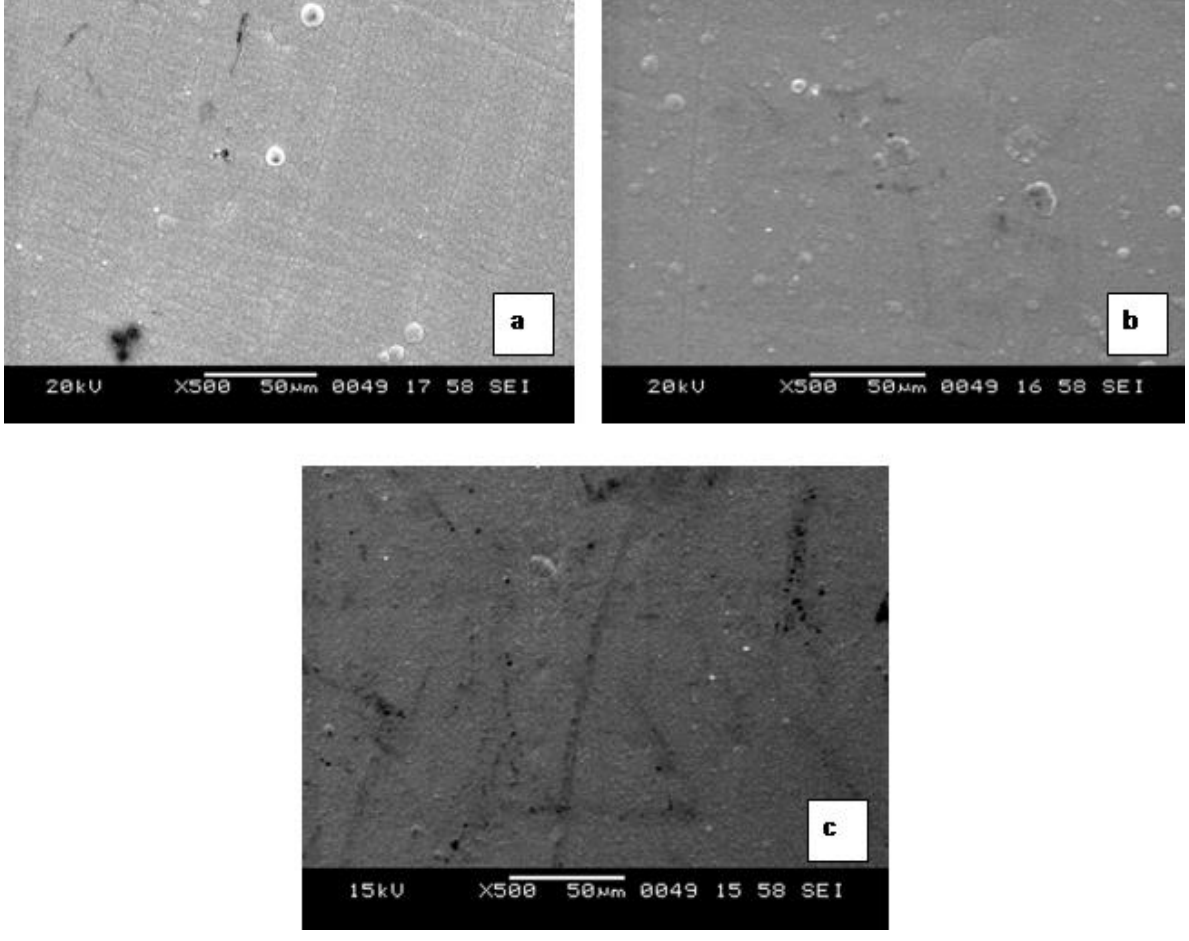


Figure 5. Scanning electron microscopy (SEM) images of Zn-Fe alloys deposited at (a) 2.0; (b) 3.0 and (c) 4.0 A dm $^{-2}$

Conclusions

• An electrolytic bath has been proposed for deposition of bright and corrosion resistive Zn-Fe alloy coatings on mild steel using SA and CA as additives. At all conditions, the electroplating

process followed the anomalous co-deposition with preferential deposition of zinc. The effect of temperature on the deposition process showed that the co-deposition of metals is diffusion controlled. The optimum condition for electroplating of Zn-Fe alloy is found at the cathode current density 3.0 A dm⁻², bath temperature 30 °C and pH 3.0.

- At the optimum bath composition and processing parameters, the Zn-Fe alloy coating showed maximal corrosion resistance and minimal corrosion rate (3.36 ×10⁻² mm year⁻¹).
- The current density was found to play an important role on the production and properties of the deposit. No transition current density at which the co-deposition behaviour changed from the anomalous to normal type was observed over the wide range of current densities (1.0-5.0 A dm⁻²).
- Increase of Fe (less readily depositable metal) content in the deposit with temperature confirmed the diffusion controlled deposition process.
- The cyclic polarization study showed that improved corrosion resistance is due to barrier effect of oxide layer and corrosion products.
- XRD study revealed that Zn-Fe alloy coating with the highest corrosion resistance corresponds to Zn with (100) and (101) phases.

References

- [1] J. B. Bajat, S. Stankovic, B. M. Jokic, Journal of Solid State Electrochemistry 13 (2009) 755
- [2] A. Brenner, Electrodeposition *of Alloys: Principles and Practice*, Academic Press, New York, 1963 p. 589.
- [3] N. R. Short, A. Abibsi, J. K. Dennis, *Transactions* of the *Institute of Metal Finishing* 67 (1984) 73-77
- [4] A. Abibsi, J. K. Dennis, N. R.Short, *Transactions* of the *Institute of Metal Finishing* **69** (1991) 145-148
- [5] R. Ramanauskas, R. Juskenas, L. Kalinicenko, F. Garfias-Mesias, *Journal of Solid State Electrochemistry* **8** (2004) 416-421
- [6] C. Q. Yang, Z. L. Long, Y. C. Zhou, Journal of Materials Science Letters 21 (2002) 1677–1680
- [7] Z. Zhang, W. H. Leng, H. B. Shao, J. M. Wang, C. N. Cao, Journal of Electroanalytical Chemistry **517** (2001) 127-138
- [8] J. D. Jensen, G. W. Crichlow, D. R. Gabe, *Transactions of the Institute of Metal Finishing* **76** (1998) 87-191
- [9] C. J. Lan, W. Y. Liu, S. T. Ke, T. S. Chin, Surface & Coatings Technology 201 (2006) 3103-3108
- [10] C. Q. Yang, Z. L. Long, Y. C. Zhou, *Transactions* of the *Institute of Metal Finishing* **80** (2002) 161-163
- [11] S. L. Diaz, O. R. Mattos, O. E. Barcia, F. Fabri Miranda, Electrochimca Acta 47 (2002) 4091
- [12] A. C. Hegde, K. Venkatakrishna, N. Eliaz, Surface & Coatings Technology 205 (2010) 2031-2041
- [13] N. Eliaz, K. Venkatakrishna, A. C. Hegde, Surface & Coatings Technology 205 (2010) 1969-1978
- [14] A. I. Vogel, Quantitative Inorganic Analysis, Longmans Green and Co, London, 1951 p. 245
- [15] Nasser Kanani, *Electroplating- Basic Principles, Processes and Practice*, Elsevier Pub. Ltd. U. K, 2006 p. 240

©2019 by the authors; licensee IAPC, Zagreb, Croatia. This article is an open-access article distributed under the terms and conditions of the Creative Commons Attribution license (http://creativecommons.org/licenses/by/4.0/)





Open Access: ISSN 1847-9286

www.jESE-online.org

Original scientific paper

Potentiometric detection of low-levels of sulfamethazine in milk and pharmaceutical formulations using novel plastic membrane sensors

Saad S. M. Hassan[⊠], Ayman H. Kamel[®], Nada H. A. Elbehery

Chemistry Department, Faculty of Science, Ain Shams University, Cairo, Egypt

Corresponding authors E-mail: [™]saadsmhassan@yahoo.com; [™]ahkamel76@sci.asu.edu.eg

Received: June13, 2018; Revised: July 29, 2018; Accepted: July 30, 2018

Abstract

Novel potentiometric sensors for selective screening of sulfamethazine (SMZ) in pharmaceutical preparations and milk samples were reported. The sensor membranes were made from PVC matrix doped with magnesium(II)-, manganese(II)- and dichlorotin (IV)-phthalocyanines as ionophores and aliquat-336 and nitron/SMZ ion-pair complex as ion exchangers. These sensors revealed fast, stable and near-Nernstian anionic response for the singly charged sulfamethazine anion over the concentration range $10^{-2} - 10^{-5}$ M. The sensors exhibited good selectivity towards SMZ over most known anions, excipients and diluents commonly added in drug preparations. Validation of the proposed methods was demonstrated via evaluating the detection limit, linear response range, accuracy, precision (within-day repeatability) and between-day-variability. The sensors were easily interfaced with a double channel flow injection system and used for continuous monitoring of SMZ in drug formulations, spiked milk samples and biological tissues. The method offers the advantages of design simplicity, results accuracy, and automation feasibility.

Keywords

Sulfamethazine; potentiometric-ion sensors; automation; method validation

Introduction

Sulphonamides are classified and managed as antimicrobials for the treatment of food-producing animals such as cattle, sheeps, pigs and poultry [1,2]. Side effects are correlated with high quantities of antibiotic residues in edible tissues such as resistance of microorganisms to antibiotic treatment, toxicological hazards, and allergenic effects [3]. For food safety, the maximum allowable quantities determined by the European community for sulfonamides in meat food products and milk is $100~\mu g/L$ [4]. Sulphamethazine (SMZ) (also known as sulfadimidine, SDM) is an example of sulphon-

amides, a broad-spectrum antibiotic used for the treatment of gastrointestinal and respiratory tract infections in livestocks. SMZ is categorized as a bacteriostatic drug which is very helpful for treatment of bacterial diseases in humans and other species caused by gram positive and gram negative bacteria [5]. It is widely used in veterinary practice for the treatment of coccidiosis in laying hens at the dose of 2 g/L for 6 consecutive days via the drinking water [6]. It is also used for therapeutic, prophylactic or as growth promoter and halt the growth of bacteria in animal production [3,7]. Meat containing residual of SMZ can result in development drug resistance and hypersensitivity [8]. It has been reported that SMZ is the major issue in testing veterinary animal's feeds. Therefore, analytical methods are needed for detecting and quantification of SMZ residues in food animal products and pharmaceutical formulations. Several methods have been reported for SMZ determination. These methods include colorimetry [9], immunoassay [1,10-13], gas chromatography [14-17], high performance liquid chromatography [18-22], thin layer chromatography [23], liquid chromatography [25-29], microbiological diffusion assay [29], microtitre plate assay [30], indirect atomic absorption spectrometry [31], ratiometric fluorescence with carbon and quantum dots [32], voltammetry [33], potentiometric sensors [34], piezoelectric sensors [35] and transmittance near infrared spectrometry [36].

Most of these methods, however, have several drawbacks due to too long time consumption, labor-intensive effort and expensive cost. Some of these methods need sophisticated instrumentation, suffer from a lack of selectivity, cover a narrow concentration range and need several manipulation steps for preparation and assessment procedures. On the other hand, potentiometric sensors are considered as viable and simple tools and have been used for the analysis of many types of pharmaceuticals [31-34]. These sensors have usually good performance characteristics and display useful analytical features [35-38]. However, little is known about their use for quantification of sulfamethazine.

In the present work, novel potentiometric sensors are proposed for determination of SMZ. Sensors are based on doping PVC membranes with ion exchangers and metal phthalocyanines. Aliquat-336 and nitron ion association complexes with SMZ and charged Mn(II), Mg(II) and Sn(IV) phthalocyanine ionophores are also used as sensing materials. These electroactive materials were dispersed in plasticized PVC membranes and used for static and hydrodynamic measurements of SMZ. The sensors were incorporated in a double channel flow injection system and used for continuous determination of SMZ in cow milk, chicken tissues and pharmaceutical formulations.

Experimental

Reagents and solutions

Analytical reagent grade chemicals were used in this work and de-ionized water (conductivity < $0.1\,\mu\text{S/cm}$) was employed for solutions preparation. High molecular weight polyvinyl chloride (PVC), o-nitrophenyloctylether (o-NPOE), magnesium (II)-, manganese (II)- and dichlorotin (IV)- phthalocyanines, aliquat-336, tridodecyl-methylammonium chloride (TDMAC) and tetrahydrofuran (THF) were obtained from Fluka (Ronkonoma, NY). Nitron was purchased from Riedel-de Haën. Pure grade of sodium sulfamethazine was obtained from Sigma Aldrich.

 10^{-2} M nitron solution was prepared by dissolving the appropriate solid amount in 20 % acetic acid solution. 20 mL of 10^{-2} M nitron solution and 10 mL of 10^{-2} M SMZ were mixed together and stirred for 15 min. A brown precipitate is formed, filtered off, washed with de-ionized water, dried at room temperature and ground to a fine powder. The elemental analysis agreed with the composition $[C_{20}H_{17}N_4^+][C_{13}H_{13}N_3S]$ that confirms (1:1) stoichiometric ratio. Stock solution of 10^{-1} M

SMZ was prepared in de-ionized water. Less concentrated SMZ standards were accurately prepared by dilution of the stock solution with a fresh $0.01 \text{ M Na}_2\text{SO}_4$ solution at pH 7. Effect of interfering species was evaluated using 10^{-2} M solutions of sodium salts of phosphate, citrate, chloride, thiocyanate, salicylate, iodide, ascorbate, oxalate, tartrate and acetate.

Apparatus

All potentiometric measurements were done with the electrochemical cell Ag/AgCl double junction reference electrode/sample test solution/SMZ selective membrane/10⁻³ M SMZ + 10⁻³ M of NaCl/AgCl/Ag. An Orion, 90-00-29, double junction electrode filled with 0.1 M lithium acetate in its outer compartment was used. Potential differences between indicator and reference electrodes were measured by an Orion digital pH/mV meter (type SA 720). The potentiometric signal output was transferred to a replacement point with six ways out; therefore, six sensors readings outplace in the same solution can be achieved. Each way represented an electrical connector that provided suitable adaptation to each sensor. The pH was measured by a Ross glass pH combination electrode (Orion 81-02). Spectrophotometric assays were carried out on a Thermo scientific UV/VIS Evolution 300.

Sensor construction and electromotive force (EMF) measurements

Three milligrams of metal-phthalocyanine ionophores were mixed with 126.4 mg of o-NPOE plasticizer, 64.5 mg PVC and 1.2 mg TDMAC and dissolved in 3 mL THF. The mixture was poured in a glass Petri dish (3 cm diameter). A membrane consisting of nitron/SMZ ion-pair complex or aliquat-336 was prepared by mixing 3 mg of the complex, 125.5 mg of o-NPOE and 65.4 mg PVC. The mixture was dissolved in 3 mL THF and also poured in a glass Petri dish. The cocktail solutions in Petri dishes were left to evaporate overnight at room temperature to form thin plastic membranes. The membranes were removed and discs were cut out and glued into PVC body using THF. A mixture of 10^{-3} M of SMZ and 10^{-3} M of NaCl was used as an internal reference solution and $^{\sim}$ 3 mm diameter Ag/AgCl coated wire was employed as an internal reference electrode. Conditioning of the sensors was performed by soaking overnight in 10^{-4} M SMZ solution. The sensors were stocked in the same solution when they are not used.

The SMZ sensors were calibrated by immersing them in conjunction with the reference electrode in a 25 mL beaker containing 10 mL of 10^{-2} M Na₂SO₄ solution of pH 7 as an ionic strength adjustor. Portions (0.5-1.0 mL) of 10^{-4} - 10^{-1} M standard SMZ solutions were successively added and the potential response of stirred solutions was measured after stabilization to ± 0.5 mV. A calibration graph was drawn by the EMF readings put against the logarithm of SMZ concentrations. From the linear part of the obtained curve, the quantification of unknown concentrations of sulfamethazine drug can be obtained.

Flow injection setup and measurements

A home-made tubular detector for SMZ was constructed as described previously [39]. The sensor was conditioned in 10^{-3} M aqueous SMZ solution for 24 h and was stored in the same solution when not used. A carrier solution consisting of 10^{-2} M Na₂SO₄ of pH 7 was propelled by means of a peristaltic pump through PTEE tubing (1.13 mm). The sample loop ($100 \mu L$) of the injection valve was filled and the valve was rotated to allow the sample to be transferred by 10^{-2} M Na₂SO₄ stream (pH 7) to the flow with rate 3.5 mL/min. The potential outputs were recorded using data acquisition (eight-channel electrode-computer interface (Nico-2000 Ltd., London, UK) controlled by Nico-2000 software).

Analytical applications

Some commercially available sulphadimidine injection solutions containing 0.333 g SMZ/mL were analyzed. The vial contents were dispersed in water by sonication and diluted with 0.01M Na₂SO₄ to bring the concentration within the linear calibration range.1.0 mL aliquots of fresh cow milk samples were spiked with 9.0 mL aliquots of 0.5-10.0 μ g SMZ/mL in 0.01M Na₂SO₄ of pH 7.0. The mixture was thoroughly homogenized in 15 mL screw capped falcon centrifuge tubes and sonicated for a period of 5 min to ensure convenient drug extraction. The potential readings were measured as previously described using SMZ sensors. The potential readings were recorded after equilibrium (10-20 s) and compared with the calibration plot.

Portions (1.0 g) of chicken muscles were homogenized and fortified with 5000 μ g/mL SMZ standard solution to give levels of 0.5, 0.75, 1.0 and 2.0 μ g/mL of SMZ. The spiked chicken samples were extracted with 3 mL of acetonitrile/water mixture (80:20, v/v) for 30 min at room temperature with continuous shaking. The sample mixture were centrifuged, filtered and dried under a steady flow of dry nitrogen gas. The residue was re-dissolved in 10 mL of 0.01 M Na₂SO₄ of pH 7.0.

Results and discussion

Sensors characteristics

Nitron, aliquat-336 and metal-phthalocyanines were utilized as sensing materials for sulfamethazine (Fig. 1). The structure of these compounds form 1:1 complexes with SMZ as confirmed by elemental analysis and infrared spectrometry.

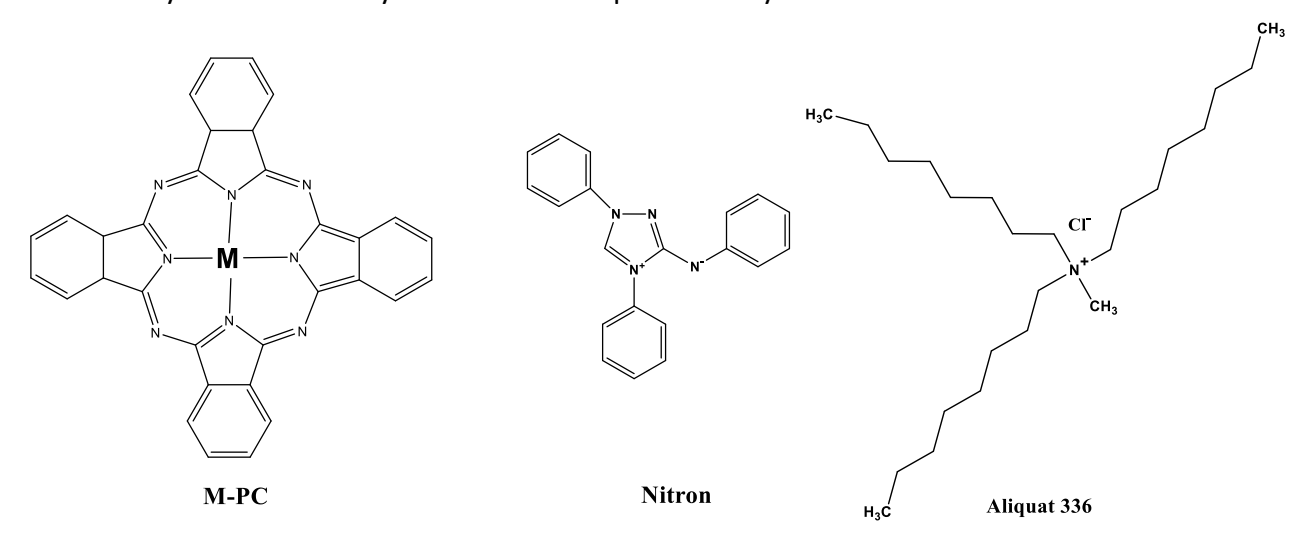


Figure 1. Structure of the proposed electroactive materials used for construction of sulfamethazine membrane sensors

Liquid-contact potentiometric sensors were constructed. The membrane sensors were prepared by incorporating 1.5 wt% of the sensing material in plasticized PVC matrix (33.6 wt% PVC and 64.4 wt% o-NPOE solvent mediator). The sensors were tested and electrochemically evaluated at 25±1 °C according to the reported recommendations of IUPAC [40]. A cationic additive consisting of 0.5 wt% TDMAC was added to membranes containing metal-phthalocyanines. The response features of these sensors are shown in Table 1. It can be noticed that sensors with a membrane incorporating nitron/SMZ and aliquat-336 show calibration slopes of -41.7±0.6 and -63.9±0.8 mV/decade over the linear concentration range 7.76×10^{-6} - 10^{-2} and 1.38×10^{-5} - 10^{-2} M with lower detection limits of 0.86 and 1.36 µg/mL, respectively. Sensors based on metal phthalocyanines (MgPC, MnPC and SnPC), in the presence of TDMAC as a cationic additive, exhibit calibration slopes of -65.3±0.4, -80.1±0.4 and

-69.9 \pm 0.6 mV/decade over the linear concentration ranges 4.8 \times 10⁻⁶-10⁻², 2.6 \times 10⁻⁶-10⁻² and 7.9 \times 10⁻⁶-10⁻² M with detection limits of 0.55,0.4 and 0.8 μ g/mL, respectively. Other performance characteristics of all investigated sensors are also presented in Table 1.

The time required for MgPC, MnPC and SnPC based membrane sensors to reach values within ± 1 mV of the final equilibrium potential after immersion in SMZ solutions, each having a 10-fold difference in concentration, varies from 10 s for >10⁻³ M to 30 s for <10⁻³ M SMZ. Nitron/SMZ and aliquat-336 based sensors showed a response time of 20-30 s for 10^{-3} - 10^{-5} M. All the membrane sensors exhibit a day-to-day reproducibility of better than 0.6 mV for 10^{-2} - 10^{-5} M SMZ solutions.

Method validation

Validation of the proposed potentiometric methods for SMZ assessment was made by systematic measuring of the response range, lower detection limit (LOD), accuracy (recovery), precision (r), within-day repeatability (CV_w), between day-variability (CV_b), linearity (correlation coefficient) and sensitivity (slope) over a period of 6 months. The results obtained on six batches (six determinations each) using the quality assurance standards [41] are depicted in Table 1. These data support the application of the proposed new sensors for quality control assessment of drug formulations.

			Sensor		
Parameter	MgPC	MnPC	SnPC	Aliquat-336	Nitron/SMZ
Slope, mV/decade	-65.3 ± 0.4	-80.1±0.4	-69.9±0.6	-63.9 ± 0.8	-4 1.7± 0.6
Correlation coefficient (r)	-0.9996	-0.999	-0.999	-0.994	-0.999
Linear range, M	4.78×10 ⁻⁶ -10 ⁻²	2.63×10 ⁻⁶ -10 ⁻²	7.94×10 ⁻⁶ -10 ⁻²	1.38×10 ⁻⁵ -10 ⁻²	7.76×10 ⁻⁶ -10 ⁻²
Detection limit, μg/mL	0.55	0.40	0.80	1.36	0.86
pH working range,	7	7	7	6.5–8	6.5–8
Response time for 10 ⁻³ M, s	ca.10	ca.10	ca.10	ca.10	ca.10
Life span, week	8	8	8	8	8
Standard deviation ($\sigma_{\rm v}$), mV	1.1	0.7	0.8	1.3	1.1
Accuracy, %	99.8	99.7	99.1	99.3	99.2
Trueness, %	98.9	98.2	98.3	99.2	99.1
Repeatability(CV _w), %	0.3	0.7	0.5	0.7	0.4
Between day-variability(CVb), %	0.8	0.7	1.2	1.3	0.4

Table 1. Performance characteristics of SMZ membrane sensors in 10⁻² M Na₂SO₄ solution at pH 7.0

Accuracy and precision

The agreement between the average concentration value obtained from 12 sets of potentiometric results for each sensor and the reference SMZ value obtained using the standard spectrophotometric method, was examined for the same SMZ solutions ($2.0\,\mu g/mL$ of SMZ in 0.01M Na₂SO₄ at pH7.0). The standard deviation and coefficient of variation were compared. A comparison between the proposed potentiometric sensors and the standard spectrophotometric method was done. Both methods were carried out using six portions of the same sample and each one in duplicate. The average mean SMZ value, standard deviation, and coefficient of variation are comparable (Table 1). This reflects the response repeatability of the sensors and confirms the accuracy of the proposed method.

Linearity, limit of detection (LOD) and limit of quantification (LOQ)

Linearity of the calibration graph, detection limit and quantification limit, were evaluated together with the linear regression analysis. The SMZ concentration was varied in the range from 10^{-6} M to 10^{-2} M. Each concentration was measured in triplicate. From the calibration curves in Figure 2, the linear ranges is $7.8 \times 10^{-6} - 10^{-2}$ (2.1-2783 µg/mL), $1.4 \times 10^{-5} - 10^{-2}$ (3.8-2783 µg/mL),

 4.8×10^{-6} - 10^{-2} ($1.3-2783\mu g/mL$), 2.6×10^{-6} - 10^{-2} ($0.7-2783~\mu g/mL$) and 7.9×10^{-6} - 10^{-2} ($2.2-2783~\mu g/mL$) for nitron/SMZ, aliquat-336, MgPC, MnPC and SnPC based membrane sensors, respectively. Detection limits calculated according to IUPAC guidelines ranged between 0.4 and $1.4~\mu g/mL$, respectively. Fixed or proportional bias of the proposed sensors was checked by a simple linear regression for the measured concentrations. The slopes of the regression lines were near the same to those of the ideal value of unity ($r^2 = 0.999$). The present potentiometric method shows no systematic difference between the assessed and expected concentrations within the test range. The statistical analysis for linearity measurements is tabulated in Table 1.

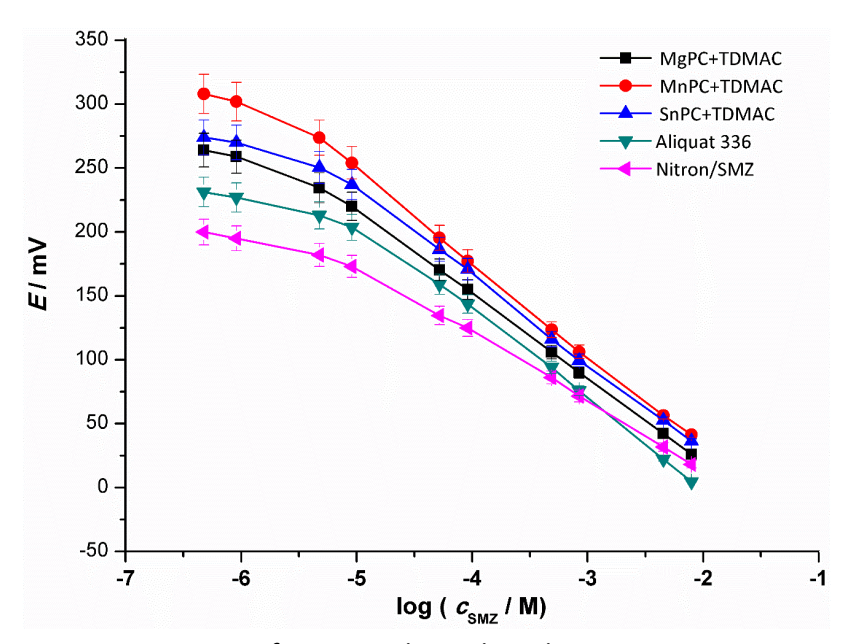


Figure 2. Potentiometric response of SMZ membrane based sensors using 0.01 M Na₂SO₄ at pH 7

Specificity

Selectivity of ion-potentiometric sensors is quantitatively related to the equilibrium at the interface between sample and sensor membrane. The impact of various common anions on the response of SMZ sensors was investigated by measuring the selectivity coefficients ($\log K^{\text{Pot}}$) of some species using the fixed solutions method [42]. The logarithmic values of $\log K^{\text{Pot}}$ were calculated by Eq. (1)

$$K^{\text{Pot}}_{A,B} = a_A/(a_B)^{Z_A/Z_B} \tag{1}$$

where α_B is 1.0×10^{-3} M of the interfering species, Z_A and Z_B are the ionic charges of main and interfering ions and α_A is the intersection of the extrapolated linear portions of the plot EMF versus the logarithm of SMZ concentration. In general, the values of log K^{Pot} showed the extent of preferential SMZ interaction over different ionic species. Compounds that are commonly present in pharmaceuticals or biological samples were considered for this purpose. Potentiometric selectivity coefficient ($K^{Pot}_{A,B}$)data are illustrated in Table 2.

As shown in Table 2, sensors based on MgPC, MnPC and SnPC ionophores have a relatively high selectivity toward SMZ compared to other hydrophobic anions such as ClO₄, salicylate, I⁻ and SCN⁻ and other several common anions. The reason for the high selectivity of this electrode for the SMZ ion is thought to be due to a possible interaction of the anions with the central metal ion in the phthalocyanine ligand.

	Potentiometric selectivity coefficient							
Interfering ion	MgPC	MnPC	SnPC	Aliquat-336	Nitron/SMZ			
PO ₄ ³⁻	-3.8	-3.9	-2.6	-2.8	-2. 8			
Cl -	-2.03	-2.04	-1.4	-1.3	-1.3			
Salicylate	-1.04	-1.29	-0.3	-0.1	-0.1			
SCN -	-1.28	-2.04	-1.1	+0.65	-1.6			
[-	-2.04	-2.32	-0.9	+0.67	-1.1			
Citrate	-3.84	-3.87	-2.7	-2.9	-2.7			
CH₃COO⁻	-1.28	-1.45	-1.2	-1.4	-0.8			
Tartarate	-2.3	-4.47	-3.4	-2.5	-3.6			
C ₂ O ₄ ²⁻	-3.33	-2.56	-1. 6	-2.1	-1.6			
Ascorbate	-1.62	-1.28	-0.5	-1.04	-0.5			

Table 2. Potentiometric selectivity coefficients (K^{Pot}_{SMZ,B}) of SMZ membrane sensors in 10⁻² M Na₂SO₄ at pH 7.0

It has already been reported that metal complexes of phthalocyanines are able tocoordinate with some analyte anions at the fifth and sixth axial positions of the carrier molecule, producing selective interaction and inducing the selectivity sequence for anions which deviates from the Hofmeister series [43]. For sensors based on aliquat-336 and nitron/SMZ as ion exchangers, their selectivity behavior depends on the lipophilicity of the ion in the aqueous solution due to ion-exchange mechanism. So, these sensors exhibited severe interferences from highly lipophlic anions such as ClO_4 , salicylate and I ions. From all said above, we can conclude that selectivity coefficient values obtained for Mg(II)-, Mn(II)-and Sn(IV)- phthalocyanines based membrane sensors apparently differ from the Hofmeister selectivity pattern observed for nitron/SMZ and aliquat-336 based sensors.

Ruggedness (Robustness)

The sensitivity of the proposed method to variations of experimental conditions (temperature, pH, and sample size) was tested. The ruggedness test was done using "Youden and Steiner partial factorial design" where eight replicate analyses were conducted, and three factors are varied and analyzed [44].

The effect of pH variation on the sensors potentials was studied for the SMZ solution of 10^{-3} mol L⁻¹. The pH was adjusted by small additions of the concentrated HCl or NaOH solution and recorded by a combined glass-pH electrode. It was noticed that potential responses of the sensors are almost stable over the range of 6.5-8.0, with small potential variations within ± 2 mV. Variation of the concentration of SMZ samples over the range 10^{-5} - 10^{-2} M did not affect the accuracy by more than 1%. Change of the temperature of the test solution from 18- 25° C slightly affected the results. The simplest form of the Nernst equation is: $E = E_0 + (0.065/n) \log c$. However, the 0.065/n part of the equation is a simplification of 2.303RT/nF. So, at 18° C, 2.303RT/F = 0.060 volts and upon increasing the temperature to 25° C, this value goes up to 0.065 volts.

Flow injection assembly

FIA is an extraordinary branch in analytical chemistry which is operating in different techniques of analysis. FIA demonstrates many advantages like small volumes of samples that are quantified, fast operating, low cost, friendly to environment, applicability in the industrial field and easily automation. Four different sensors were constructed as previously mentioned to detect SMZ concentration under hydrodynamic operation.

A linear relationship between log [SMZ] concentrations and FIA signals were obtained over the concentration range of 10^{-6} - 10^{-3} M using 0.01 M Na₂SO₄, pH 7 as shown in Fig. 3. The optimum flow rate for measuring was chosen to be 3.5 mL/min. The sensors revealed a sub-Nernstian response

with slopes of -53.7, -39, -43.2 and -37 mV/decade over a linear concentration range between 9.9×10^{-5} , 10^{-5} , 1.1×10^{-5} and 10^{-4} M to 10^{-2} M, and detection limits of 17.5, 2.78, 2.78, 13.94 µg/mL for the aliquat-336, MgPC, MnPc and Nitron/SMZ membrane-based sensors, respectively. General performance characteristics are shown in Table 3. The lower sensitivity of FIA measurements may be attributed to the small volume of the injectable sample, flow rate, and time taken for the sample to be reacted on the surface of the sensor. As shown in Table 3, the sample frequency/hour is 60, 46, 48 and 50 sample/h for aliquat-336, MgPC, MnPc and nitron/SMZ membrane-based sensors, respectively.

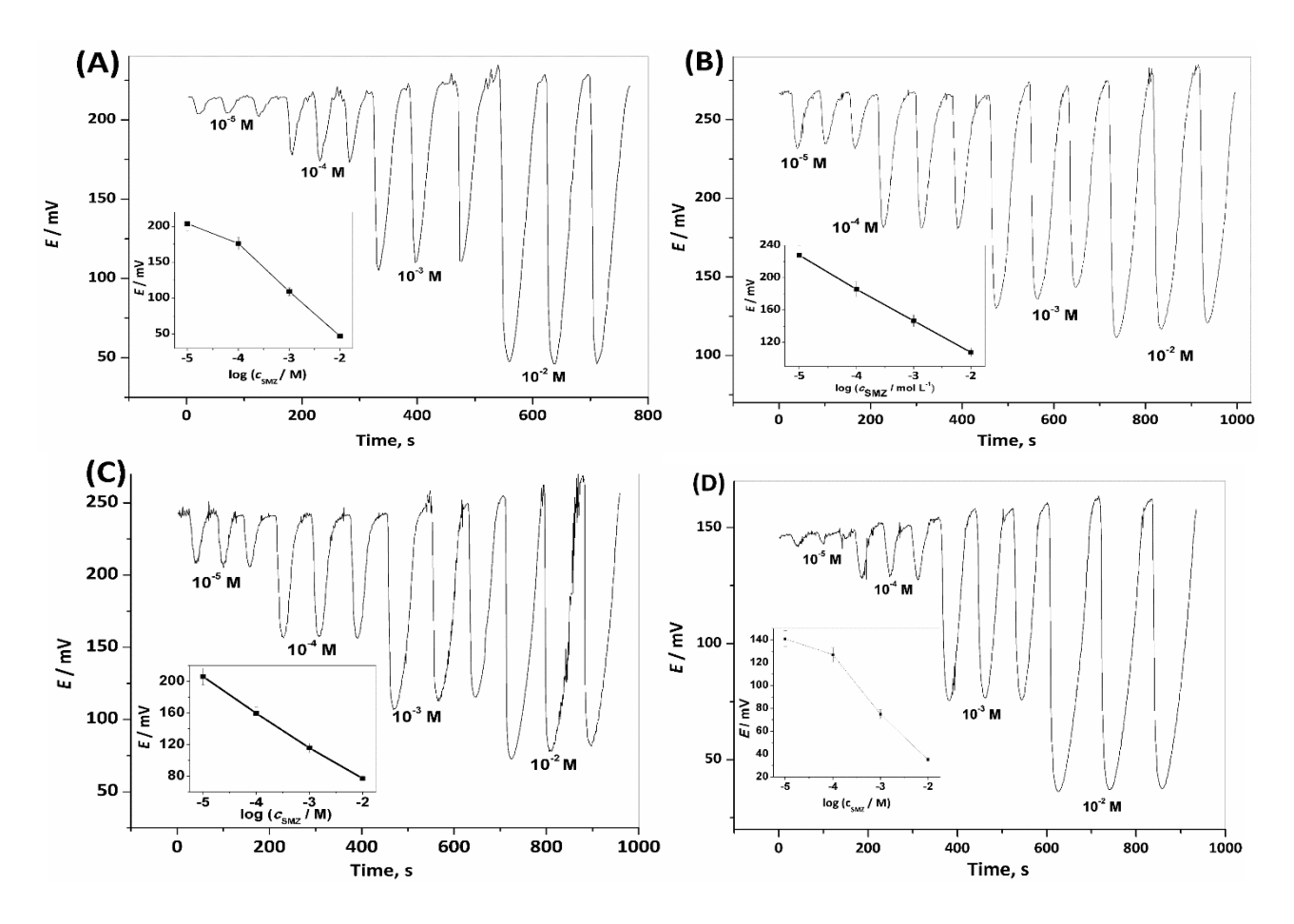


Figure 3. FIA signals for the evaluation of SMZ in 0.01 M carrier sodium sulphate solution pH 7.0, loop sample 100 μL, and flow rate 3.5 mL/min; (A) Aliquat-336; (B) MgPC; (C) MnPC; and (D) Nitron/SMZ membrane based sensors

Table 3. Performance characteristics of SMZ membrane sensors plasticized with o-NPOE under hydrodynamic mode (FIA) of operation in 10⁻²M Na₂SO₄ buffer of pH 7.0

	Sensor					
Parameter	Aliquat-336	MgPC	MnPC	Nitron/SMZ		
Slope, mV/decade	-53.7	-39	-43.2	-37		
Correlation coefficient®	-0.986	-0.988	-0.997	-0.979		
Linear range, M	9.9×10 ⁻⁵ -10 ⁻²	1.0x10 ⁻⁵ -10 ⁻²	1.1x10 ⁻⁵ -10 ⁻²	1.0x10 ⁻⁴ -10 ⁻²		
Detection limit, μg/mL	17.5	2.78	2.78	13.94		
Life span, week	8	8	8	8		
Optimum flow rate, mL/min	3.5	3.5	3.5	3.5		
Sample frequency, sample/h	60	46	48	50		

SMZ assessment

To test the applicability of the proposed method using the proposed sensors for determining SMZ, natural matrices such as drug formulations, milk or chicken muscle samples were taken. Two commercial products containing SMZ, labeled 33.3 g/100 mL were collected from local markets for veterinary treatments. Potentiometric determination of SMZ in triplicate under both static and hydrodynamic mode of operations showed results with an average recovery of 99.1 and 98.7 % and a mean standard deviation of ± 1.2 and ± 2.3 % for both static and hydrodynamic mode of operations (Table 4). These data were compared with results obtained by UV-spectrophotometry [45]. An *F*-test revealed that there is no significant difference between the means and variances of two sets of results. Quality control/quality assurance (QC/QA) of the method was tested by daily drug analysis over one month. R and X control charts [46] clearly indicated that all distribution measurements and range of assays data were under statistical control (lie between the warrant and control limits without any abnormalities).

Table 4. Potentiomeric determination of SMZ in pharmaceutical preparations using SMZ membrane sensors

					Fo	und, g/10	0mL				
Commercial	Potentiometry									Cnootro	
products*	Aliqua	at-336	MgPC/	TDMAC	MnPC/	TDMAC	SnPC/1	TDMAC	Nitro	n/SMZ	Spectro- metry [45]
	Batch	FIA	Batch	FIA	Batch	FIA	Batch	FIA	Batch	FIA	metry [45]
Sulphadimidine Injection**	32.7±1.1	31.8±0.9	32.6±1.4	31.7±1.4	33.4±0.6	31.8±0.3	31.7±1.7	33.7±0.1	31±0.2	35.9±0.9	34±0.7
Sulphadimidine Injection***	31.8±0.9	34.4±1.2	32.6±0.7	33.6±1.8	33±1.2	34.7±1.5	32.2±1.6	32.5±1.1	33.4±0.2	32.6±1.3	33.7±0.4

^{*}Labeled 33.3 g/100mL; **ADWIA, Egypt; *** UCCMA, Egypt

The method was also tested for determining SMZ in milk and chicken muscles by spiking aliquots of different samples with the known standard of SMZ. The results showed an average recovery of 99.1 % with a relative standard deviation of $\pm 0.8 \%$. Results obtained for determination of SMZ in milk and chicken muscle samples using batch and FIA are compared in Table 5.

Table 5. Assessment of SMZ in spiked samples with milk and chicken muscle using MnPC membrane-based sensor

Sample	Spikod ug/ml	*Found	d, μg/mL
Sample	Spiked, μg/mL	Batch	FIA
	0.5	0.47±0.05	-
Cow milk	5	4.2±0.2	4.1±0.5
	10	9.6±0.7	9.3±0.3
	0.5	0.42±0.04	-
Chickon muscles	0.75	0.68±0.07	-
Chicken muscles	1	0.93±0.06	-
	2	1.8±0.1	-

^{*}Average of 5 measurements

Conclusions

Novel, simple and low cost potentiometric sensors were developed, characterized and used for static and continuous quantification of sulfamethazine drug. Automatic determination of SMZ using a flow-through system coupled with a potentiometric detector proved to be an advantageous method over many other analytical methods. Determinations of SMZ can be accomplished within a wide concentration range, regardless of the samples colors and turbidity. In addition, increased sensitivity provides improved precision, high sampling rates, low consumption of sample volume and better reproducibility. The results obtained in this work suggest that this methodology could be applied for rapid and accurate analysis of SMZ in different complex matrices. The sensors were

utilized for SMZ determination in different pharmaceutical formulations in addition to chicken muscles and milk samples at an input rate of < 40 samples/hour. No interferences are caused by most anions that are normally present in these matrices. The results favorably compare with data obtained by the standard spectrophotometric method.

References

- 1. M. Franek, V. Kolar, A. P. Deng, S. Crooks, Food and Agricultural Immunology 11 (1999) 339-349.
- 2. N. T. Crosby, Determination of Veterinary Residues in Food, Ellis Horwood, NewYork, 1991.
- 3. N. A. Botsoglou, D. J. Fletouris, *Drug Residues in Foods: Pharmacology, Food Safety and Analysis*, Marcel Dekker, New York, pp.1194, 2001.
- 4. C. Hartig, T. Storm, M. Jekel, Journal of Chromatography A 854 (1999) 163-173.
- 5. Saganuwan, A. Saganuwan, Animal Research International 3 (2006) 457-460.
- 6. A. C. Tella, O. M. Olabemiwo, G. K. Obiyenwa, M. O. Salawu, African Scientist 11 (2010) 189-193.
- 7. D. D. Holland, S. E. Katz, Journal Association of Official Analytical Chemists 74 (1991) 784-789.
- 8. M. T. Combs, S. Boyd, M. Khorassani, L. T. Taylor, Agricultural and Food Chemistry 45 (1997) 1779-1783.
- 9. D. P. Schwartz, Journal Association of Official Analytical Chemists 65 (1982) 701-705.
- 10. J. H. Park, Korean Journal of Animal Science 41 (1999) 129-134.
- 11. V. Gaudin, M. L. Pavy, Journal of AOAC International 82 (1999) 1316-1320.
- 12. G. A. Baxter, M. C. O'Connor, S. A. Haughey, S. R. H. Crooks, C. T. Elliott, Analyst 124 (1999) 1315-1318.
- 13. H. Yang, West China Journal of Pharmaceutical Science 14 (1999) 238-241.
- 14. S. J. Stout, W. A. Steller, A. J. Manuel, M. O. Poeppel, A. R. daCunha, *Journal Association of Official Analytical Chemists* **67** (1984) 142-144.
- 15. V. B. Reeves, Journal of Chromatography B 723 (1999) 127-137.
- 16. B. Chiavarino, M. E.Crestoni, A. D. Marzio, S. Fornarini, *Journal of Chromatography B: Biomedical Sciences and Applications* **706** (1998) 269-277.
- 17. R. K. Munns, J. E. Roybal, Journal Association of Official Analytical Chemists 65 (1982) 1048-1053.
- 18. F. Belliardo, Journal of Apicultural Research 20 (1981) 44-48.
- 19. M. Petz, Zeitschrift Fur Lebensmittel-Untersuchung Und –Forschung 176 (1983) 289-293.
- 20. E. D. McGary, Analyst 111 (1986) 1341-1342.
- 21. G. Stoev, A. Michailova, Journal of Chromatography A 871 (2000) 37-42.
- 22. B. C. Grande, M. S. G. Falcón, M. R. Comesaña, J. S. Gándara, Journal of Agricultural Food Chemistry 49 (2001) 3145-3150.
- 23. U. R. Cieri, Journal Association of Official Analytical Chemists 59 (1976) 56-59.
- 24. R. L. Smallidge, E. J. Kentzer, K. R. Stringham, E. H. Kim, C. Lehe, R.W. Stringham, E. C. Mundell, *Journal Association of Official Analytical Chemists* **71** (1988) 710-717.
- 25. J. D. Weber, M. D. Smedley, Journal Association of Official Analytical Chemists 72 (1989) 445-447.
- 26. J. D. Weber, M. D. Smedley, Journal of AOAC International 76 (1993) 725-729.
- 27. G. Bartolucci, G. Pieraccini, F. Villanelli, G. Moneti, A. Triolo, Rapid Communication of Mass Spectrometry 14 (2000) 967-973.
- 28. P. Edder, A. Cominoli, C. Corvi, Trav. Chim. Aliment. hyg. 88 (1997) 554-569.
- 29. D. Jonas, G. Knupp, H. Pollmann, Archiv Fur Lebensmittelhygiene 34 (1983) 138-141.
- 30. R. K. Buick, N. M. Greer, C. T. Elliott, Analyst 125 (2000) 95-396.
- 31. S. S. M. Hassan, M. H. Eldesouki, Journal Association of Official Analytical Chemists 64 (1981) 1158-1163.
- 32. L. Chen, Y. Xu, L. Sun, J. Zheng, J. Dai, C. Li, Y. Yan, Analytical Letters 51(13) (2018) 2099-2113
- 33. L. Urzúa, M. Pérez-Ortiz, A. Álvarez-Lueje, Journal of the Chilean Chemical Society 63(1) (2018) 3914-3917
- 34. A. H. Kamel, S. A. A. Almeida, M. G. F. Sales, F. T. C. Moreira, Analytical Sciences 25 (2009) 365-371.
- 35. J. Yuan, S. Yao, Talanta 58 (2002) 641-648.
- 36. Q. Fu, X. He, H. Suo, J. Wang, C. Zhao, Journal of Near Infrared Spectroscopy 20 (2012) 397-406.
- 37. S. S. M. Hassan, E. M. Elnemma, W. H. Mahmoud, A. H. K. Mohamed, Journal of Applied Electrochemistry 36 (2006) 139-146.
- 38. A. H. Kamel, H. E. M. Sayour, Electroanalysis 21 (2009) 2701-2708.
- 39. S. S. M. Hassan, A. H. Kamel, H. Abd El-Naby, Journal of Chinese Chemical Society 61 (2014) 295-302.
- 40. IUPAC, Analytical Chemistry Division, Commission on Analytical Nomenclature, Pure Applied Chemistry 66 (1994) 2527-2536.
- 41. J. K. Taylor, Quality Assurance of Chemical Measurements (CRC Press, Florida, 1987).
- 42. Y. Umezawa, K. Umezawa, H. Sato, Pure Applied Chemistry 67 (1995) 507-518.
- 43. Z. L. Jun, C. W. Xiao, Y. Ruo, G. L. Hui, Q. Y. Ru, Analyst 119 (1994) 1363-1366.
- 44. L. P. van Reeuwijk, V. J. G. Houba, Guidelines for Quality Management in Soil and Plant Laboratories, *Food and Agriculture Organization of the United nations (FAO) Rome* **74** (1998) 95-97.
- 45. N. Yongnian, Q. Zhengbao, S. Kokot, Chemometrics and Intelligent Laboratory Systems 82 (2006) 241-247.
- 46. W. Funk, V. Dammann, G. Donnevert, Quality Assurance in Analytical Chemistry, VCH, New York, 1995.

©2019 by the authors; licensee IAPC, Zagreb, Croatia. This article is an open-access article distributed under the terms and conditions of the Creative Commons Attribution license (http://creativecommons.org/licenses/by/4.0/)





Open Access: ISSN 1847-9286

www.jESE-online.org

Short review

Voltammetric and amperometric sensors for determination of epinephrine: A short review (2013-2017)

Hadi Beitollahi^{1,⊠}, Mohadeseh Safaei¹, Somayeh Tajik²

¹Environment Department, Institute of Science and High Technology and Environmental Sciences, Graduate University of Advanced Technology, Kerman, Iran

²NanoBioElectrochemistry Research Center, Bam University of Medical Sciences, Bam, Iran

Corresponding authors E-mail: [™] h.beitollahi@yahoo.com; Tel.: +98 3426226613; Fax: +98 3426226617

Received: July 16, 2018; Revised: September 13, 2018; Accepted: Septrember 19, 2018

Abstract

The present review focuses on voltammetric and amperometric methods applied for determination of epinephrine (EP) in last five years (2013-2017). Occurrence, role and biological importance of EP, as well as non-electrochemical methods for its assessment, are firstly reviewed. The electrochemical behavior of EP is then illustrated, followed by a description of the voltammetric and amperometric methods for EP content estimation in various media. Different methods for development of electrochemical sensors are reviewed, starting from unmodified electrodes to different composites incorporating carbon nanotubes, ionic liquids or various mediators. From this perspective, the interaction between functional groups of the sensor material and the analyte molecule is discussed, as it is essential for analytical characteristics obtained. The analytical performances of the voltammetric or amperometric chemical and biochemical sensors (linear range of analytical response, sensitivity, precision, stability, response time, etc.) are highlighted. Numerous applications of EP electrochemical sensors in fields like pharmaceutical or clinical analysis where EP represents a key analyte, are also presented.

Keywords

Epinephrine; electrooxidation; voltammetry: amperometry

Contents

1.	Introduction	28
2.	Epinephrine determination by non-electrochemical techniques	28
3.	Voltammetric and amperometric sensors	29
3.	1. Voltammetry/amperometry at bare/unmodified electrodes	-29
3.	2. Voltammetry/amperometry at modified electrodes	-29
	3. 2. 1. Chemically modified electrodes	-29

	3. 2. 2. Modified electrodes with polymer	31
	3. 2. 3. Modified electrodes with carbon nanotubes	33
	3. 2. 4. Modified electrode with nanoparticles and nanocomposites	35
4.	Interferences from compounds present in biological media and pharmaceuticals	37
5.	Analytical performances of electrochemical epinephrine sensors	39
6.	Some applications of electrochemical epinephrine sensors in pharmaceutical and biological fluid analysis	39
7.	Conclusions	40
Αŀ	breviation	41
Re		

1. Introduction

Epinephrine (EP), also called adrenaline, is an important catecholamine neurotransmitter in the mammalian central nervous system [1]. Many life phenomena are related to the concentration of EP in blood. It also served as a chemical mediator for conveying the nerve pulse to efferent organs. Medically, EP has been used as a common emergency healthcare medicine [2,3]. EP is used to stimulate heartbeat and to treat emphysema, bronchitis, bronchial asthma and other allergic conditions, as well as the eye disease, glaucoma. Therefore, performing the research of EP has an important significance to medicine and life science [4]. EP is synthesized naturally in the body from L-tyrosine by the action of different enzymes. Almost 50 % of the secreted hormone appears in urine as free and conjugated, 3 % as vanilmandelic acid (VAM), the most abundant metabolite in urine [5]. Only small amounts of free EP are excreted. Meanwhile, EP is an electroactive compound and can be determined by electrochemical methods [6-11]. However, actual electrochemical detection of EP has two challenges. One is its low concentration level, while another challenge often encountered is the strong interference arising from electroactive compounds like norepinephrine (NE), dopamine (DA), ascorbic acid (AA) and uric acid (UA) [6]. To resolve these problems, one of the most common routes is using a modified electrode to improve the measuring sensitivity of EP and minimize the interference of AA and UA to EP determination [7-12]. Although many modified electrodes have been demonstrated to be effective for detecting EP, there is still a need to develop a new method with high efficiency and convenience for the detection of EP [13,14].

Injectable EP solutions used by emergency medical personnel and hospitals are principally degraded via oxidation. This degradation can be accelerated by heavy metals, ultraviolet light, exposure to oxygen, and increased pH. Typical preventive measures for hindering oxidative degradation use light-resistant containers, buffered solutions, and/or antioxidants [15-20]. Due to the crucial role of EP in biochemistry and industrial applications, the determination of EP still presents research interest. Quick monitoring of EP levels during production and quality control stages is important [21-24]. In this review, we investigate the latest progress in modification of electrodes and its improvement in detection of EP.

2. Epinephrine determination by non-electrochemical techniques

Several methods have been reported for the determination of EP including high performance liquid chromatography (HPLC) [25,26], HPLC-mass spectrometry [27], fluorimetry [28], HPLC optical fiber biosensor [29], capillary electrophoresis [30,31], flow injection [32,33], HPLC with fluorimetric detection [34], chemiluminescence [35,36] and spectrophotometry [37,38].



3. Voltammetric and amperometric sensors

Voltammetry is a potentiodynamic technique, based on measuring the current arising from oxidation or reduction reactions at the working electrode surface, when a controlled potential variation is imposed [39,40]. Amperometry is based on the application of a constant potential to a working electrode, and the subsequent measurement of the current generated by the oxidation/reduction of an electroactive analyte [41-43].

3. 1. Voltammetry/amperometry at bare/unmodified electrodes

Bare electrodes without functionalization represent an interesting alternative, in particular when high sensitivity is not required. This approach has been realized by use of a simpler system, resulting in reduced costs for both production and use, and long-term stability. An electrochemical biosensor for the sensitive detection of EP was introduced by Li *et al.* [44]. Their results showed that the magnitude of the oxidation peak current of EP is related to many factors, including the pH value of the supporting electrolyte in the working electrode electrolytic cell, the acidity of the supporting electrolyte in the auxiliary electrode electrolytic cell, the distribution coefficients for different EP species, the properties of electrode surface charge and the molecular configuration of electroactive component. In performing experiments, pH of PBS buffer solution was kept at 7.0 in the working electrode electrolytic cell and HCl solution maintained at 1.0 mol L⁻¹ in the auxiliary electrode electrolytic cell. The standard solutions of different amounts of EP were added to the working electrode electrolytic cell and the oxidation peak current of EP was recorded by cyclic voltammetry (CV). The range of 2.0×10^{-7} - 1.0×10^{-4} mol L⁻¹, with a detection limit of 6.2×10^{-8} mol L⁻¹ was obtained. Satisfactory results have been achieved for the determination of EP in injection. The recovery of the standard addition was in the range of 95.0-102.0 %.

Jemelkova *et al.* [45] reported the voltammetric behavior of EP investigated by differential pulse voltammetry (DPV) at a carbon paste electrodes (CPE) made with different carbon powders CR-2, glassy carbon (GC) microparticles, and single-wall carbon nanotubes (SWNT). In Briton-Robinson (BR) buffer solution (pH 6), the linear dependence was found for the determination of EP by the given method in the concentration ranges of 1×10⁻⁶-1×10⁻⁴ (CR-2), 1×10⁻⁶-1×10⁻⁴ (GC microparticles) and 4×10⁻⁶-1×10⁻⁴ (SWNT) mol L⁻¹. Limits of detection were 8× 10⁻⁷, 8×10⁻⁷ and 2×10⁻⁶ mol L⁻¹, respectively. The best results were obtained by employing the CPE containing carbon paste with 50 % (w/w) of SWNT, which showed a linear dynamic range of 4×10⁻⁷-1×10⁻⁴ mol L⁻¹ and a limit of detection 2×10⁻⁷ mol L⁻¹.

3. 2. Voltammetry/amperometry at modified electrodes

The need for over-potential diminution and fouling minimization has required the electrode modification with a view to increase sensitivity and obtain more prominent peak separation. These properties are required mainly in complex media such as biological samples particularly prone to interferences, where EP coexists with other electroactive species.

3. 2. 1. Chemically modified electrodes

Numerous electrochemical methods have been developed to determine EP on the basis of its electroactive nature. Most of these methods, however, have two major problems in EP determination which reduce accuracy and sensitivity of the results. The first is that in a natural environment, EP often coexists with a high concentration of electroactive biomolecules like UA, DA, NE, and AA that interfere with each other. The second problem of reported methods is that the product of EP oxidation (epinephrine chrome) can easily transform into polymers, which block its

further oxidation on the electrode surface. Hence, despite of considerable investigations, the preparation of a sensitive sensor with satisfactory selectivity and low detection limit with high sensitivity is still of great interest.

Development and application of L-glutamic acid functionalized graphene nanocomposite modified GCE for the determination of EP were reported by Kang *et al.* [46] Linear relationship between EP concentration and current response measured by DPV method was obtained in the range of 1×10^{-7} to 1×10^{-3} mol L⁻¹ with a limit of detection of 3×10^{-8} mol L⁻¹. The modified electrode was employed to determine EP in urine with satisfactory results.

Zhang and Wang [47] have described β -Mercaptoethanol self-assembled monolayer modified electrode, fabricated on a bare gold (ME/Au SAMs). The films accelerated the electron transfer as mediators, and showed an excellent electrocatalytic activity for the oxidation of EP. The electrochemical behavior of EP at ME/Au SAMs has been studied by CV and the electrocatalytic mechanism is explored. At potential of -0.044V (*vs.* SCE) in the aqueous buffer (pH 4.0), the first oxidation wave was observed for EP at the modified electrode (electrochemical oxidation of leucoepinephrine to epinechrome). In contrast, the first oxidation wave was not observed for NE or DA under same conditions.

Fabrication of modified GCE for determination of EP in aqueous solutions was reported by Ahmadian Yazdely *et al.* [48]. Their DPV results exhibited the linear dynamic range from 5.0×10^{-8} to 1.1×10^{-5} mol L⁻¹ and detection limit of 2.3×10^{-8} mol L⁻¹ for EP. In addition, the analytical performance of the modified electrode for quantification of EP in real samples was evaluated.

Sharath Shankar and Kumara Swamy [49] have successfully investigated tetradecyltrimethyl ammonium bromide (TTAB) surfactant immobilized at CPE which has been proposed for simultaneous investigation and determination of EP and serotonin (5-HT) in presence of AA. Voltammetric techniques in the phosphate buffer solution (PBS) (pH 7.4) were applied. The anodic peak of EP was observed at 198 mV (vs. Ag/AgCl/KCl) at the scan rate 50 mV s⁻¹. The interference studies showed that the modified electrode exhibits excellent selectivity for the determination of EP in the presence of large excess of AA and 5-HT. Differences of the oxidation peak potentials for EP-AA and EP-5-HT were about 215 and 165 mV, respectively. Detection limit of the modified electrode obtained by DPV technique was found to be 0.12 µmol L⁻¹. The developed method was applied to the determination of EP in synthetic samples with satisfactory results.

Jahanbakhshi [50] reported a synthesis of mesoporous carbon foam (MCF) with particular properties due to simplistic and template-free procedure. The synthesized MCF was characterized by transmission electron microscopy, field emission scanning electron microscopy, X-ray diffraction and BET surface area techniques. Porous MCF, with pore diameters of 5 to 10 nm resulted in extensive specific surface area that modifies the electrode surface. The obtained MCF was dispersed in the Salep solution to prepare a stable suspension (S-MCF). The resultant composite was casted on the surface of GCE to assemble the S-MCF modified GCE electrode (S-MCF/GCE). CV method was used to study electrochemical behavior and determination of EP was conducted by applying DPV method in the presence of UA. In the optimized conditions, the presented sensor was found able to detect the concentration range of 0.1-12 μ mol L⁻¹ with a limit of detection of 40 nmol L⁻¹. The presented methodology possesses a reliable reproducibility, repeatability and stability in biological samples.

Sensitive and selective determination method for EP was developed by Chandrashekar *et al.* [51] by immobilization of TX-100 surfactant on the bare CPE. The catalytic activity of the modified electrode for the oxidation of EP was determined using CVs recorded at different scan rates. The

effect of the solution pH on the voltammetric response of EP was examined using the phosphate buffer solution. The TX-100/CPE demonstrated a good performance for the determination of EP in the concentration range from 10 to 50 μ mol L⁻¹, with a detection limit of 1×10⁻⁶ mol L⁻¹. The application was conducted for the determination of EP in a human serum sample and the sensor was proven to be rapid, having excellent selectivity and repeatability.

In the research of Dehghan Tezerjani *et al.* [52], an electrochemical sensor was constructed for determination of EP. The sensor was based on the CPE modified with graphene oxide (GO) and 2-(5-ethyl-2,4- dihydroxyphenyl)-5,7-dimethyl-4 H-pyrido (2,3-d) (1,3) thiazine-4-one (EDDPT) as modifiers. The modified electrode was applied as an electrochemical sensor for oxidation of EP. Under the optimum conditions, the overpotential value for EP oxidation decreased for about 279 mV at the modified CPE more than at non-modified CPE. Also, the designed electrochemical sensor was applied to determine EP in the drug sample and for simultaneous determination of EP, ACT and DA in human serum solutions.

3. 2. 2. Modified electrodes with polymer

In recent years, electrochemically modified electrodes with conductive or redox polymers have been widely used owing to their excellent and unique physical and chemical properties. This kind of modification is established as the best approach for selective determination of some biomolecules because the surface characteristic on the electrode can be modulated by introducing various chemicals with reactive groups. The polymer-modified electrodes showed broad potential windows and can still catalyze electrochemical reactions which have high overpotential and poor selectivity.

Electropolymerization of fuchsine acid (FA) was studied by Taei *et al.* [53] on the surface of GCE in different electrolyte media. Then, a novel Au-nanoparticle poly(FA) film modified GCE (poly(FA)/AuNP/GCE) was constructed for the simultaneous determination of AA, EP and UA. In addition, for the poly(FA)/AuNP/GCE, oxidation peak potentials of AA-EP and EP-UA were found separated for 150 mV and 180 mV, respectively. At the same time, for the bare GCE, not any separation was noticed. DPV results exhibited the linear dynamic range of 0.5-792.7 μ mol L⁻¹ for EP with the detection limit of 0.01 μ mol L⁻¹. The diffusion coefficient for the oxidation reaction of EP on AuNP/poly (FA) film coated GC electrode was calculated as 2.6 (±0.10) × 10⁻⁵ cm² s⁻¹.

Li and Wang [54] have investigated an electrochemical sensor based on the poly(guanine) (PGA) modified GCE that was fabricated by electropolymerization of guanine on the bare GCE surface. This modified electrode exhibited good electrocatalytic property towards the oxidation of EP and UA in 0.1 mol L^{-1} PBS (pH 4.0), seen as enhanced peak currents and well defined peak separations. Under optimum reaction conditions, oxidation peak currents of EP and UA were proportional to their concentrations in the range of 1.0×10^{-5} to 1.0×10^{-3} mol L^{-1} and detection limit of 1.8×10^{-6} mol L^{-1} was determined for both compounds. Finally, this method was efficiently used for the determination of EP in EP injections.

Kocak and Dursun [55] used a modified electrode that was fabricated by overoxidation of polymer film after electropolymerization of p-aminophenol on a bare GCE. Higher catalytic activity was observed for electrocatalytic oxidation of AA, EP, and UA in PBS (pH 7.4) at the overoxidized poly(p-aminophenol) film modified GCE (Ox-PAP/GCE), due to enhanced peak current and well defined peak separations compared to both bare GCE and poly (p-aminophenol) film modified GCE (PAP/GCE).

Devadas et al. [56] presented for the first time, a simultaneous voltammetric determination of EP and p-acetoaminophenol (AP) on the poly(curcumin) (1,7 bis((4-hydroxy-3-methoxyphenyl)-1,6-

-heptadiene-3,5 dione) modified GCE. Curcumin (CM) was polymerized onto the GCE surface by simple electropolymerization process. Low peak to peak (ΔE_p) separation of 60 mV was observed, indicating fast electron transfer between poly(CM) and the electrode surface. Moreover, the poly(CM) modified GCE exhibited enhanced electrocatalytic activity for EP in the linear range of 4.97-230.76 μ mol L⁻¹ and very low detection limit (LOD) of 0.05 μ mol L⁻¹.

Taei and Jamshidi [57] introduced a polymerized film of Adizol Black B (ABB) on the surface of GCE for the simultaneous determination of AA, EP and UA. This new modified electrode presented an excellent electrocatalytic activity towards the oxidation of AA, EP and UA by DPV method. The separation of the oxidation peak potentials for AA-EP and EP-UA were at about 180 and 130 mV, respectively. The diffusion coefficient for the oxidation reaction of EP at the poly(ABB) film coated GCE was calculated as $1.54 (\pm 0.10) \times 10^{-4} \, \text{cm}^2 \, \text{s}^{-1}$.

Ma *et al.* [58] demonstrated an electrochemical sensor based on the silver doped poly-L-cysteine film (Ag-PLC) that has been fabricated for simultaneous determination of DA, EP and UA in the presence of AA. Although voltammetric signals of DA and EP were resolved at the bare GC electrode, the signals of DA and UA were not resolved in a mixture. However, (Ag-PLC) modified electrode does not only separate voltammetric signals of DA, EP and UA with potential difference of 390 and 135 mV between DA-EP in the cathodic peak potential and UA-(DA+EP) in the anodic peak potential respectively, but also shows higher electrocatalytic activity towards DA, UA and EP in the presence of high concentration of AA. For EP, the linear range was determined from 5.00×10⁻⁶ to 1.10×10⁻⁴ mol L⁻¹. The practical application for this modified electrode was demonstrated by determining the concentration of DA, UA and EP in human urine samples.

Li and Sun [59] introduced a novel paladium doped poly(L-arginine) modified electrode (Pd-PLA/GCE), fabricated by electrochemical immobilization of the paladium doped poly (L-arginine) on a GCE. This modified electrode was used for determination of EP by the CV method. The method was successfully applied to the determination of EP in injection with satisfactory results.

A simple and sensitive poly(L-aspartic acid)/electrochemically reduced graphene oxide modified GCE, poly(L-Asp)/ERGO/GCE, has been constructed by electrochemical reduction of GO that was drop coated on the GCE within 2 mmol L⁻¹ L-aspartic acid in PBS (pH 6). As suggested by Mekassa et al [60], this procedure gives rise to in situ polymerization of L-aspartic acid on the ERGO. Significant enhancement of the peak current response of EP was observed, accompanied with a negative shift in the peak potential value at the composite modified electrode, compared to the bare electrode. Real sample analysis was carried out in the pharmaceutical formulation of EP hydrochloride injection, which revealed good recovery results of 94–109 %.

According to Vieira da Silva [61], the polymerization of ferulic acid (FA), forming poly(FA) on MWCNTs modified GCE was performed and the modified platform applied for simultaneous determination of NADH, EP and DA. CV and CA methods were employed to investigate the electrocatalytic oxidation of NADH, EP and DA on the modified electrode in aqueous solutions. The obtained analytical curve for EP showed linear range between 73-1406 μ mol L⁻¹. The detection limit was 22.2 μ mol L⁻¹ for EP.

Poly(ionic liquids), (PILs), have been applied as the linkers between Au nanoparticles and polypyrrole nanotubes (PPyNTs) for the synthesis of Au/PILs/PPyNTs hybrids. As was reported by Mao *et al.* [62], due to the presence of PILs, high density of well dispersed AuNPs was deposited on the surface of PILs/PPyNTs by anion exchange with Au precursor and in situ reduction of metal ions. The catalytic oxidation peak current obtained by DPV method increased linearly with increasing EP concentration in the range of 35-960 μmol L⁻¹ with a detection limit of 298.9 nmol L⁻¹, according to

the criterion of a signal-to-noise ratio (S/N=3). These results suggested that this modified electrode shows excellent electrocatalytic activity towards this significant hormone in human life.

3. 2. 3. Modified electrodes with carbon nanotubes

Carbon nanotubes (CNTs) have attracted more attention in physical, chemical and material science fields due to their unique electrical conductivity, chemical stability and high mechanical strength and modulus. The subtle electronic properties of carbon nanotubes suggest that they are able to promote electron transfer when used as the electrode material in electrochemical reactions. These properties provided a new manner of electrode surface modification for designing new electrochemical sensors and novel electrocatalytic materials.

In the research performed by Apetrei [63], a biosensor comprising tyrosinase immobilized on a SWCNTs modified GCE was developed for determination of EP. Tyrosinase maintained high bioactivity on this nanomaterial by catalyzing the oxidation of EP to EP quinone, which was electrochemically reduced (-0.07 V vs. Ag/AgCl) on the biosensor surface. Under optimum conditions, the biosensor showed a linear response in the range of 10-110 μ mol L⁻¹ and a limit of detection was calculated as 2.54 μ mol L⁻¹ with a correlation coefficient of 0.977 for EP. The repeatability, expressed as the relative standard deviation for five consecutive determinations of 10^{-5} mol L⁻¹ EP solution, was 3.4 %.

Valentini *et al.* [64] used oxidized single wall carbon nanohorns (o-SWCNHs) for the first time, in order to assemble chemically modified screen printed electrode (SPE) that is selective towards the electrochemical detection of EP in the presence of serotonine-5-HT (S-5HT), DA, NE, AA, ACT and UA. EP neurotransmitter was detected by using DPV in a wide linear range of concentrations (2-2500 μ mol L⁻¹) with high sensitivity, very good reproducibility (RSD ranging from 2 to 10 % for different SPEs), short response time for each measurement (only 2 s) and low detection limit (LOD = 0.1 μ mol L⁻¹).

A simple electrochemical sensor for EP has been developed by Ghica and Brett [65]. They modified a carbon film electrode (CFE) with MWCNTs in a chitosan matrix. Under optimum conditions (pH 7.0), the MWCNT/CFE electrode showed significant electrocatalytic oxidation of EP with a decrease of overpotential value for about 200 mV and 11-fold increase of the peak current value, compared to the unmodified CFE. The sensor exhibited excellent stability over a period of 6 months and was successfully applied to the analysis of injectable adrenaline solutions.

The electrochemical behavior of a multi walled carbon nanotube paste electrode modified with 2-((7-(2,5-dihydrobenzylideneamino) heptylimino methyl) benzene-1,4-diol (DBHB) was studied by Mazloum Ardakani *et al.* [66]. CV method was used to study the electrocatalytic mechanism of EP electrooxidation at the modified electrode. Catalytic rate constant and diffusion coefficient were obtained for oxidation of EP. By using DPV method, a highly selective and simultaneous determination of EP, acetaminophen and folic acid has been obtained at the modified electrode used as an electrochemical sensor.

Wu *et al.* [67] reported a sensor for EP that is based on ITO electrode modified with MWCNTs being pre-coated with a polymerized ionic liquid (PILMWNTs). The chitosan film was electrodeposited on the ITO electrode in the presence of EP and the PILMWNTs. This film acts as an excellent recognition matrix due to excellent film forming ability and many functional groups that favor hydrogen bond formation with the target EP. The electrochemical response to EP was linear in 0.2 μ mol L⁻¹ to 0.67 mmol L⁻¹ concentration range, and detection limit was as low as 60 nmol L⁻¹ (at S/N = 3).

Wang *et al.* [68] demonstrated a modified GCE that was covered with a layer of MWCNT coated with hexadecyltrimethyl ammonium bromide (CTAB). The modified electrode showed excellent electrochemical catalytic properties for the redox reaction of EP and AA. In the presence of CTAB, the peak separation between EP and AA can be broadened to 256 mV by the CTAB.

Graphite paste electrode (GPE) modified with 1-butyl-3-methylimidazolium hexafluoro phosphate (BMIMPF₆) and MWCNTs was prepared for simultaneous voltammetric determination of EP and xanthine (XN) by Rajabi *et al.* [69]. The prepared electrode (BMIMPF₆-MWCNT/GPE) showed excellent catalytic activity in the electrochemical oxidation of EP and XN, leading to remarkable enhancement of the corresponding peak currents and lowering the peak potentials. The peak current values of linear sweep voltammograms increased linearly with EP concentrations in the range of 0.30-60 μ mol L⁻¹ in 0.1 mol L⁻¹ PBS (pH 7.0). Applicability of this modified electrode as the voltammetric biosensor was demonstrated by simultaneous determination of EP and XN in human urine, human blood serum and ampoule.

In the study of Babaei *et al.* [70], electrooxidation of EP, ACT and mefenamic acid (MEF) has been investigated by application of nickel hydroxide nanoparticles/MWCNT modified GCE (MWCNT-NHNPs/GCE) using CV and DPV methods.

In another study, Pradhan *et al.* [71] employed a composite electrode for the amperometric detection of EP. Composite electrode was developed by electropolymerizing bromothymol blue (BTB) on the CPE bulk modified with MWCNTs. Electropolymerization of BTB on the surface of CPE involved much less energy compared to a CPE surface. The modification enhanced the current sensitivity of EP by 5.5 times as compared to the bare CPE. The sensor showed the optimum current response at physiological pH and the response was linear for the concentration of EP in the ranges $0.8-9.0~\mu$ mol L⁻¹ and $10.0-100~\mu$ mol L⁻¹, respectively. The detection limit was $8\times10^{-7}~m$ ol L⁻¹. The amperometric response of EP remained unaltered even in the presence of 50-fold excess of UA, AA and 100-fold excess of L-Tryptophan, L-Tyrosine, L-cysteine and nicotinamide adenine dinucleotide. This sensor showed stability, reproducibility, antifouling effects and was successfully applied for the determination of EP in blood serum and adrenaline injection.

Thomas *et al.* [72] developed an amperometric sensor for the determination of EP which was fabricated by modifying the CPE with pristine multi walled carbon nanotubes (pMWCNTs). Bulk modification, followed by a drop casting of sodium dodecyl sulfate (SDS) onto the surface for its optimal potential application was performed. Analytical applications of the modified electrode were demonstrated by determining EP in spiked blood serum and adrenaline tartrate injection.

Filho *et al.* [73] developed an electrochemical method for the single and simultaneous determination of DA and EP in human body fluids, using a GCE modified with nickel oxide nanoparticles and carbon nanotubes within a dihexadecyl phosphate film. SWV and DPV methods were applied. By using DPV with the proposed electrode, a separation of ca. 360 mV between the peak reduction potentials of DA and EP was present in binary mixtures. The detection limit of EP was determined as 8.2×10^{-8} mol L⁻¹.

Koteshwara Reddy *et al.* [74] checked out an efficient electrochemical sensor for selective detection of EP. It was fabricated with the aid of a functionalized MWCNT-chitosan biopolymer nanocomposite (Chit-f CNT) electrode. MWCNTs were successfully functionalized with the aid of nitric acid and confirmed by the Raman spectral data. Functionalized carbon nanotubes (f CNT) were dispersed in chitosan solution and the resulting bio nanocomposite was used for the fabrication of sensor surface by drop and cast method. Electrochemical characteristics of the fabricated sensor were understood using CV and DPV analysis for the detection of EP in PBS (pH 7.4).

3. 2. 4. Modified electrode with nanoparticles and nanocomposites

Nanotechnology and nanoscience represent new and enabling platforms that promise to provide a broad range of novel uses and improved technologies for environmental, biological and other scientific applications. One of the reasons staying behind the intense interest is that nanotechnology permits the controlled synthesis of materials, where at least one dimension of a structure is less than 100 nm. Nanostructured materials have also been incorporated into electrochemical sensors for biological and pharmaceutical analyses. While they offer unique advantages, including enhanced electron transfer, large edge plane/basal plane ratios and rapid kinetics of the electrode processes.

In a study of Sadeghi *et al.* [75], CPE was modified with zinc oxide (ZnO) nanoparticles and 1,3-dipropylimidazolium bromide was used as a binder. It was found that the oxidation of EP at the surface of modified electrode occurs at about 80 mV less positive potential than at unmodified CPE. DPV peak current values showed a linear relationship with concentration of EP in the range of 0.09-800 μ mol L⁻¹, with a detection limit of 0.06 μ mol L⁻¹. The proposed sensor was successfully applied for the determination of EP in real samples.

As suggested by Babaei *et al.* [76], simultaneous determination of EP and ACT can be performed using a GCE modified with a MWCNTs, nickel hydroxide nanoparticles (NHNPs) and Mg-Al layered double hydroxide (LDH) composite (MWCNTs-NHNPs-LDH/GCE). Based on DPV method, the oxidation of EP exhibited a dynamic range between 0.04-60 μ mol L⁻¹ and detection limit (3 σ) of 11 nmol L⁻¹. This method was used for the determination of EP in real samples, using the standard addition method.

Gold nanoparticles/polyaniline nanocomposite thin film was deposited on to the surface of GCE by Langmuir-Blodgett (LB) technology to fabricate a new voltammetric sensor (GNPs/PAn-LBGCE) for EP and UA detection, as was reported by Zou *et al.* [77]. Electrochemical behavior of EP and UA at the modified electrode was investigated in PBS (pH 6.6).

Silai *et al.* [78] have reported a modified electrode that was prepared by immobilizing Pt-nanoparticles into a chitosan film. The investigation of the influence of experimental conditions (scan rate, frequency, pH) on the electrochemical behavior of EP was realized by the CV method.

Novel MCM/ZrO₂ nanoparticles modified CPE was fabricated and used by Mazloum-Ardakani *et al.* [79], in order to study the electrooxidation of EP and ACT and their mixtures. The modified electrode showed electrocatalytic activity toward EP and ACT oxidation with a decrease of the overpotential value by 173 mV for EP at the surface of the MZ-CPE and an increase in peak current at pH 7.0.

Jin and Zhang [80] used the nanogold modified GCE obtained by electrodeposition, which can catalytically oxidize and accumulate EP. In this research, effects of changes of pH and concentration of PBS on the electrochemical behavior of EP were studied. This modified electrode could be applied for determination of EP in the presence of AA. DPV data showed that under optimal conditions, the obtained anodic peak currents were linearly dependent on the EP concentration in the range of 1.0×10^{-4} - 1.0×10^{-6} mol L⁻¹.

Razavian *et al.* [81] employed electrochemical sensor that was developed and tested for detection of L-tyrosine in the presence of EP. The electrode was prepared by surface modification of a GCE with nafion and cerium dioxide nanoparticles. The modified electrode exhibited a significant electrochemical oxidation effect of EP in a 0.2 mol L^{-1} Britton-Robinson (BR) buffer solution (pH 2). The electro-oxidation peak current increased linearly with the EP concentration in the molar concentration range of 5 to 220 μ mol L^{-1} . By employing DPV method for simultaneous

measurements, two reproducible peaks for L-tyrosine and EP in the same solution with a peak separation of about 443 mV were detected.

Nitrogen doped three dimensional porous graphene (NG) modified electrode was fabricated by Yang et~al.~ [82]. The obtained data showed that electrooxidation of EP at the modified electrode is greatly facilitated, which was ascribed to the excellent properties of NG. The modified electrode was used for simultaneous determination of EP and metanephrine (MEP). DPV peak currents of EP increased linearly with their concentration within the range of 1.0 μ µmol L⁻¹ to 1.0 mmol L⁻¹, with a sensitivity of 0.021 μ A / (μ mol L⁻¹) for EP. The detection limit for EP was ascertained to be 0.67 μ mol L¹. Additionally, the detection of EP and MEP was found possible in the presence of AA and UA. The modified electrode was applied to the detection of EP and MEP in human plasma samples with recoveries from 98.9 % to 100.9 %, and EP hydrochloride injections with recoveries from 100.3 % to 104.6 %.

Chen and Ma [83] used a graphene modified GCE obtained *via* drop casting method and applied it to the simultaneous detection of EP, UA, and AA by CV method in a PBS solution (pH 3.0). The oxidation potentials of EP, UA, and AA at the graphene modified GCE were 0.484, 0.650, and 0.184 V (*vs.* Ag/AgCl), respectively. Peak separations between EP and UA, EP and AA, and UA and AA were about 166, 300, and 466 mV, respectively.

A hybrid membrane, consisting of aminated graphene and Ag nanoparticles, (AgNPs), was prepared on the surface of GCE by the CV method, where aminated graphene (GR-NH₂) acted as a matrix for immobilizing AgNPs. The morphology and electrochemical properties of this hybrid membrane were characterized together with the voltammetric behavior of EP in a study of Huanhuanin *et al.* [84]. The membrane exhibited excellent eletrocatalytic activity for the redox reaction of EP and resolved the electrochemical response of EP and UA into two oxidation peaks.

According to Mak *et al.* [85], organic electrochemical transistors (OECTs) were found to be excellent transducers for various types of biosensors. It was highly sensitive EP sensor based on OECTs prepared on glass substrates by solution process. The device performance was optimized by immobilizing Nafion and carbon based nanomaterials on the gate electrodes of the OECTs. The detection limit of the sensors was as low as 0.1 nmol L⁻¹, which could cover the concentration level of EP in medical detections.

In a study performed by Beitollahi *et al.* [86], CPE modified with vinyl ferrocene (VF) and CNTs was used for the sensitive and selective voltammetric determination of EP, which could be related to the strong electrocatalytic effect of the VF and CNT towards this compound. The mediated oxidation of EP at the modified electrode was investigated by CV. SWV method of EP at the modified electrode exhibited linear dynamic ranges with a detection limit of 3.0×10⁻⁸ mol L⁻¹. SWV was also used for simultaneous determination of EP and tryptophan at the modified electrode. Quantification of EP and tryptophan in some real samples was performed by the standard addition method.

Zhang et al. [87] described a facile preparation of polydopamine (PDA)-nanogold composite modified GCE used for the sensitive determination of EP, DA, AA and UA simultaneously. Under mild spontaneous reaction condition, DA as a reducing agent and monomer and HAuCl₄ as an oxidant trigger for DA polymerization were mixed together with the source of gold nanoparticles to yield a composite of DA polymer and gold nanoparticles. These composite particles were then anchored on GCE by electropolymerization of the remaining DA monomer. The resultant electrode exhibited excellent electrocatalytic redox activities toward EP, DA, AA and UA. Furthermore, although the oxidation peaks of EP and DA at the modified electrode appeared at the same potential of 230 mV

(vs. Ag/AgCl), three well defined oxidation peaks were generally obtained for AA, EP, DA and UA (50, 230, 380 mV vs. Ag/AgCl).

In a study of Redin el al. [88], a green approach for the preparation of carbon black (CB) and electrochemically reduced graphene oxide composite (ERGO) was described. Electrochemical sensors were based on screen printed carbon electrodes (SPCEs), fabricated on poly (ethylene terephthalate) (PET). The SPCE/CB-ERGO sensor was tested with DA, EP and paracetamol (PCM), exhibiting an enhanced electrocatalytic performance compared to the bare SPCE.

In another study, Gupta *et al.* [89] have synthesized NiO/CNTs nanocomposite and applied it for fabrication of NiO/CNTs nanocomposite modified CPE (CPE/NiO/CNTs) as SWV sensor for the determination of EP. The electrooxidation signal of EP showed an irreversible response at 0.3 V (*vs.* Ag/AgCl). The oxidation current of EP was doubled compared to a CPE. At the best electrochemical conditions, the voltammetric oxidation signal of EP showed linear dynamic range $(0.08-900.0 \ \mu mol \ L^{-1})$, with detection limit of 0.01 $\mu mol \ L^{-1}$.

Electrochemical sensor developed by Anithaa *et al.* [90] for the simultaneous determination of EP and xanthine is based on the gamma irradiated SDS-WO3 NPs. The fabricated sensor exhibited wide linear range (0.009-1000 μ mol L⁻¹) with low detection limit (1.8 nmol L⁻¹) for EP.

Tsele *et al.* [91] studied electrochemical properties of functionalized MWCNT/polyaniline (PANI) doped with metal oxide (TiO₂, RuO₂) nanoparticles. Successful syntheses of MWCNT, TiO₂, RuO₂, PANI, MWCNT-PANI-TiO₂ and MWCNT-PANI-RuO₂ nanomaterials were confirmed using suitable characterization techniques. Au-MWCNT-PANI-TiO₂ and Au-MWCNT-PANI-RuO₂ modified electrodes showed the best electron transport properties towards the oxidation of EP, compared with other electrodes investigated. The Tafel values obtained in the presence of EP as 0.448 and 0.442 V/decade for Au-MWCNT-PANI-TiO₂ and Au-MWCNT-PANI-RuO₂ electrodes respectively, suggested adsorption due to analyte oxidation intermediates products. The linear calibration plot for EP was obtained in the concentration range of 4.9 to 76.9 μ mol L⁻¹, while a limit of detection for Au-MWCNT-PANI-TiO₂ electrode was 0.16 μ mol L⁻¹.

4. Interferences from compounds present in biological media and pharmaceuticals

Interference studies were carried out with several chemical substances prior to the application of the proposed method for the assay of EP in urine samples and the injection solution. The potential interfering substances were chosen from the group of substances commonly found with EP in pharmaceuticals and biological fluids. In biological environments, AA is commonly present with EP and may be oxidized at similar potential as EP.

In the research performed by Kang *et al.* [46], CVs of EP and AA were respectively recorded at the L-glutamic acid-graphene/GCE. The results showed that the oxidation peak of EP is not affected by presence of AA. This means that the modified electrode is able to distinguish EP from AA.

The influence of various foreign species on the determination of 50.0 μmol L⁻¹ EP, 100.0 μmol L⁻¹ AA and 50.0 μmol L⁻¹ UA was investigated by Taei *et al.* [53]. The tolerance limit was taken as the maximum concentration of the foreign substance(s) which caused an approximately ±5 % relative error in the determination. It was also found that Mg⁺², Ca⁺², SO₄⁻², Br⁻, K⁺, NO⁻³, ClO₄⁻ glycine, glucose, sucrose, lactose, fructose, valine, aspartic acid, urea, and saturation of starch solution did not interfere with the determination of these compounds. However, greater amounts of cysteine (40-fold), oxalate ion (100-fold), and citric acid (30-fold) did cause interference in the simultaneous determination of EP, AA and UA by poly(fuchsine acid) modified GCE.

As was reported by Ahmadian Yazdely *et al.* [48], the maximal tolerable concentration of foreign substances was, by using the thiourea modified GCE, determined as 5.0×10^{-5} mol L⁻¹ for glucose, uric acid, ascorbic acid, citric acid, dopamine, and Na⁺, K⁺, Cu²⁺, Mg²⁺, NO₃⁻ and SO₄²⁻ ions.

In their study, Li and Wang [54] have illustrated that K⁺, Na⁺, Ca²⁺, Mg²⁺, sucrose and glucose do not interfere significantly, while L-glutamic acid, Cu²⁺ and Fe²⁺ ions showed a certain effect on the examinations of EP and UA.

Sadeghi *et al.* [75] studied the influence of various substances as potential interfering compounds on the determination of EP by the SWV method under optimum conditions. A study was performed by a novel biosensor based on ZnO nanoparticle/1,3-dipropylimidazolium bromide ionic liquid modified CPE. The tolerance limit was defined as the maximum concentration of the interfering substance like glucose, fructose, lactose, sucrose tryptophan, histidine, glycine, valine, methionine, lucine, alanine, phenylalanine, Ca²⁺, Li⁺, ClO₄⁻, SO₄²⁻, SCN⁻, Na⁺, Mg²⁺, K⁺, AA, urea, cysteine and UA that caused an error less than 5 % for the determination of EP. The results showed that the peak current of EP was not affected by all conventional cations, anions and organic substances.

As stated by Babaei *et al.* [70], interferences of AA, L-glutamic, L-alanin, aspartic acid and aspirin in determination of EP were significant only at relatively high concentrations, confirming that the proposed nickel hydroxide nanoparticles/MWCNTs modified GCE (MWCNT-NHNPs/GCE) was likely to be free from interferences from common components of biological samples.

Wang *et al.* [68] have illustrated the influence of some metal ions and anions that usually exist in biological fluid on the determination of 5.0×10^{-5} mol/L EP. If the ±5 % error was allowed, 5.0×10^{-3} mol/L of K⁺, Na⁺, Fe²⁺, Mg²⁺, Cl⁻, SO₄²⁻ did not show obvious interference on a modified GCE, fabricated by covering with a layer of MWCNTs coated with hexadecyl trimethyl ammonium bromide (CTAB).

In another work, Apetrei *et al.* [63] investigated the influence of various interfering agents on determination of EP. The interfering substances Na⁺, S₂O₅²⁻, Cl⁻, urea, tartaric acid, hydrochloric acid, glucose and glycine did not show any influence on the biosensor response when detecting EP. An absence of significant modification of the peak current recorded in the presence of interfering species was demonstrated. Therefore, tyrosinase immobilized on a single-walled carbon nanotube modified GCE (tyrosinase/SWCNT-GCE) can be considered to be a good biosensor for recognition of EP.

Mazloum Ardakani *et al.* [66] studied the electrochemical behavior of a MWCNT paste electrode modified with 2-((7-(2,5-dihydrobenzylideneamino) heptylimino) methyl) benzene-1, 4-diol (DBHB). Influence of various foreign species like AA, DA, UA, levodopa, N-acetyl and captopril at concentrations 5 times higher than EP did not show any interference in the determination of EP.

The influence of various foreign species on the determination of 50 μ M EP was investigated by Mekassa *et al.* [60] under optimum experimental conditions. Potentially interfering substances were chosen from the group of substances commonly found with EP in pharmaceutical formulations and biological fluids. The tolerance limit was defined as the maximum concentration of the foreign substance(s) that caused an approximately ± 5 % relative error in the determination of EP. According to the obtained results, AA, citric acid, D-glucose, lactose, glycine, Mg²⁺, Ca²⁺, Na⁺, and K⁺ did not show any interference effect in the determination of EP.

Study of Vieira da Silva [61] showed that influence of interference on the electrode response can be useful to set up the sample preparation with the goal to minimize their effects. Interference from electroactive compounds typically present in a physiological sample (e.g., serotonin (SER), AA and

UA) commonly hinders the accurate determination of EP. The selectivity of the sensor was examined in the presence of SER, AA and UA.

5. Analytical performances of electrochemical epinephrine sensors

The analytical performances of electrochemical methods depend on the sensor's construction and some of the most illustrative examples are extensively reviewed in Table 1.

Table 1. Some analytical performances attained in electrochemical determination of EP.

Type of detection	Transducer	Linear response	Detection limit	Relative stand. dev.	Ref.
Voltammetry (CV, DPV)	L-glutamic acid functionalized graphene nanocomposite, modified glassy carbon electrode	10 ⁻⁷ - 10 ⁻³ mol L ⁻¹	3×10 ⁻⁸ mol L ⁻¹	≤ 3.4 %	[46]
Voltammetry (DPV)	β-Mercaptoethanol self-assembled monolayer modified gold electrode	10 ⁻⁷ -10 ⁻⁴ mol L ⁻¹	3.3×10 ⁻⁸ mol L ⁻¹		[47]
Voltammetry (CV, DPV)	Glassy carbon electrode modified with thiourea	5.0×10 ⁻⁸ -1.1×10 ⁻⁵ mol L ⁻¹	2.3×10 ⁻⁸ mol L ⁻¹	1.2 %	[48]
Voltammetry (CV, DPV)	Tetradecyltrimethyl ammonium bromide (TTAB) surfactant immobilized carbon paste electrode	0.15 - 30 μmol L ⁻¹	0.12 μmol L ⁻¹	2.4 %	[49]
Voltammetry (CV, DPV)	Mesoporous carbon foam modified glassy carbon electrode	0.1-12.0 μmol L ⁻¹	40 nmol L ⁻¹		[50]
Voltammetry (CV, DPV)	Au-nanoparticle poly-fuchsine acid film modified glassy carbon electrode (poly(FA)/AuNP/GCE)	0.5–792.7 μmol L ⁻¹	0.01 μmol L ⁻¹	0.37 %	[53]
Voltammetry (CV, SWV)	Poly (guanine) modified glassy carbon electrode (PGA/GCE)	10 ⁻⁵ - 10 ⁻³ mol L ⁻¹	1.8 × 10 ⁻⁶ mol L ⁻¹		[54]
Voltammetry (CV)	Single-walled carbon nanotube-modified glassy carbon electrode	10-110 μmol L ⁻¹	2.54 μmol L ⁻¹	3.4 %	[63]
Voltammetry (SWV)	ZnO nanoparticle/1,3-dipropylimidazo- lium bromide ionic liquid-modified carbon paste electrode	0.09-800 μmol L ⁻¹	0.06 μmol L ⁻¹	3.2 %	[75]
Voltammetry (CV, DPV)	Glassy carbon electrode coated with a novel Mg–Al layered double hydroxide–nickel hydroxide nanoparticles–multiwalled carbon nanotubes composite	0.04-60 μmol L ⁻¹	11.0 nmol L ⁻¹	≤3.1 %	[76]
Voltammetry (CV)	Gold nanoparticles/polyaniline Langmuir-modified glassy carbonelectrode	4×10 ⁻⁷ - 10 ⁻⁵ mol L ⁻¹	8×10 ⁻⁸ mol L ⁻¹	1.97 %	[77]
Voltammetry (DPAS)	MCM/ZrO ₂ nanoparticles modified carbon paste electrode	10 ⁻⁶ -2.5×10 ⁻³ mol L ⁻¹	5.0×10 ⁻⁷ mol L ⁻¹		[79]
Voltammetry (CV)	A graphene-modified glassy carbon electrode	0.20-100 μmol L ⁻¹	0.001 μmol L ⁻¹		[83]
Voltammetry (CV, DPV)	Aminatedgraphene and Ag nanoparticles modified GCE	0.916-184 μmol/L	2.0 nmol L ⁻¹		[84]
Voltammetry (CV, SWV)	Vinylferrocene and carbon nanotubes (CNTs)-modified carbon paste electrode	0.1-1000.0 μmol L ⁻¹	3.0 × 10 ⁻⁸ mol L ⁻¹	≤ 2.5 %	[86]

6. Some applications of electrochemical epinephrine sensors in pharmaceutical and biological fluid analysis

Electrochemical EP sensors have widespread application in pharmaceutical and biomedical analysis, as shown in Table 2.

Table 2. Numerical data on EP content determined in various analysed systems.

Method	Electrode type	Analysed medium	Recovery, %	Reference
CV, DPV	L-glutamic acid functionalized graphenenano- composite, modified glassy carbon electrode	EP Injection	100.4	[46]
DPAS	β-Mercaptoethanol self-assembled monolayer modified gold electrode	EP Injection	100.9	[47]
CV	Glassy carbon electrode modified with thiourea	EP Injection	101.2	[48]
DPV	Tetradecyltrimethyl ammonium bromide (TTAB) surfactant immobilized carbon paste electrode	EP Injection	96.3	[49]
DPV	Glassy carbon, electrode coated with a novel Mg–Al layered, double hydroxide–nickel	Blood	97.6	[76]
	hydroxide nanoparticles, multi-walled carbon nanotubes composite	Urine	98.2	.2 [76]
DPV	Gold nanoparticles/polyanilineLangmuir— modified glassy carbonelectrode	Serum	98.36	[77]
DPV	MCM/ZrO ₂ nanoparticles modified, carbon paste electrode	EP Injection	101.7	[79]
DPV	Graphene-modified glassy carbon electrode	Urine	99.7	[83]
DPV	GCE, modified by aminatedgraphene and Ag nanoparticles	Serum	100.24	[84]
DPV	Vinylferrocene and carbon nanotubes (CNTs)- Modified Carbon Paste Electrode	EP Injection Ampoule	101.0 102.0	[86]

7. Conclusions

In past five years, utilization of electroanalytical methods for pharmaceutical analysis has significantly increased, especially for EP assessments. However, there is a limited number of publications concerning a combination of pre-concentration and electrochemical detection of EP. Electrochemical techniques are often preferred to laborious instrumental methods for EP determination, which is due to the simplicity of procedure and instrumentation, minimum requirements with respect to sample pretreatment, as well as fast response, sensitivity and low cost. Also, accurate results can be obtained in real time and complex media. Different modalities of sensor development already described in the literature are presented, starting from bare to chemically modified sensors. Recent advances imply the use of carbon nanotubes and various composites, for which large surface area and electrocatalytic activity greatly enhance the analytical signal, diminishes the peak potential corresponding to EP oxidation and solves peak overlapping problems in complex samples. Provided that adequate pretreatment and cleaning steps are included, several examples of viable EP determination in various media performed by bare electrodes, even in the presence of interfering compounds are also presented. Method performances and application areas depend on the chosen electrochemical technique. It can be generally concluded that different ways of construction and expected performances of sensor electrodes are adequate and tuned to the nature of the analysed compound and respective matrix. The nature of the electrode material and surface groups formed, as well as their interaction with analyte molecules, greatly influence the electrooxidation rate, as well as pH value of the analysed matrix, electrolyte type, and the peak potential and height. The mechanism and rate of electrooxidation are strongly dependent on the following factors: electrode nature and modifiers, electrode pre-treatment, surface groups, pH, electrolyte and presence of other compounds. The interaction between the respective form of analyte molecule present at some pH value (range) and the functional groups of the electrode/modifier layer is found essential for determining electrooxidation rate and electrode performance. In complex media where interference is expected, modifiers enhance the catalytic peak current of the analyte of interest, allowing better peak separation from interfering compounds.

Abbreviation

AA Ascorbic acid

CFE Carbon film electrode
CPE Carbon paste electrodes

CV Cyclic voltammetry

DA Dopamine

DPV Differential pulse voltammetry

EP Epinephrine

GCE Glassy carbon electrode

MWCNT Multi walled carbon nanotube

NE Norepinephrine

SWV Square wave voltammetry
SWNT Single-walled carbon nanotube

UA Uric acid

VAM Vanilmandelic acid

References

- [1] W. Ge Yun, Chinese Journal of Chemistry **23** (2005) 297-302.
- [2] M. Mazloum Ardakani, H. Beitollahi, M. A. Sheikh Mohseni, A. Benvidi, H. Naeimi, M. Nejati-Barzoki, N. Taghavinia, *Colloids and Surfaces B: Biointerfaces* **76** (2010) 82-87.
- [3] F. Ni, Y. Wang, D. Zhang, M. Li, Electroanalysis 22 (2010) 1130-1135.
- [4] J. X. Qiao, H. Q. Luo, N. B. Li, Colloids and Surfaces B: Biointerfaces 62 (2008) 31-35.
- [5] W. Ren, H. Q. Luo, N. B. Li, Sensors 6 (2006) 80-89.
- [6] T. Łuczak, *Electroanalysis* **21** (2009) 2557-2562.
- [7] X. H Zhang, Sh. F. Wang, *Analytical Letters* **35** (2002) 995-1006.
- [8] A. A. Ensafi, M. Taei, T. Khayamian, Colloids and Surfaces B: Biointerfaces 79 (2010) 480-487.
- [9] M. Taei, M. Jamshidi, Journal of Solid State Electrochemistry 18 (2014) 673-683.
- [10] S. Y. Ly, Analytical Letters **45** (2012) 1197-1203.
- [11] M. Taei, H. Hadadzadeh, F. Hasanpour, N. Tavakkoli, M. Hadadi Dolatabadi, *Ionics* 21 (2015) 3267-3278.
- [12] N. B. Li, L. M. Niu, H. Q. Luo, *Microchimica Acta* **153** (2006) 37-44.
- [13] M. Mazloum-Ardakani, H. Beitollahi, M. K. Amini, B. F. Mirjalili, F. Mirkhalaf, *Journal of Electroanalytical chemistry* **651** (2011) 243-249.
- [14] Y. X. Sun, S. Fu Wang, X. H. Zhang, Y. F. Huang, Sensors and Actuators B: Chemical 113 (2006) 156-161.
- [15] H. Beitollahi, H. Karimi-Maleh, H. Khabazzadeh, Analytical Chemistry 80 (2008) 9848-9851.
- [16] H. Beitollahi, M. Mazloum Ardakani, B. Ganjipour, H. Naeimi, *Biosensors and Bioelectronics* **24** (2008) 362-368.
- [17] T. Tavana, M. A. Khalilzadeh, H. Karimi-Maleh, A. A. Ensafi, H. Beitollahi, D. Zareyee, *Journal of Molecular Liquids* **168** (2012) 69-74.
- [18] H. Beitollahi, I. Sheikhshoaie, Analytical Methods 3 (2011) 1810-1814.
- [19] M. Mazloum-Ardakani, H. Beitollahi, M. K. Amini, F. Mirkhalaf, M. Abdollahi-Alibeik, *Analytical Methods* **3** (2011) 673-677.
- [20] H. Mahmoudi Moghaddam, H. Beitollahi, S. Tajik, H. Soltani, Electroanalysis 27 (2015) 2620-2628.
- [21] F. Wang, Y. Xu, L. Wang, K. Lu, B. Ye, Journal of Solid State Electrochemistry 16 (2012) 2127-2133.
- [22] W. Ma, D. M. Sun, Chinese Journal of Analytical Chemistry 35 (2007): 66-70.
- [23] S. Shahrokhian, R. S. Saberi, Electrochimica Acta 57 (2011) 132-138.
- [24] F. Cui, X. Zhang, Journal of Electroanalytical Chemistry 669 (2012) 35-41.
- [25] M. A. Fotopoulou, P. C. Ioannou, *Analytica Chimica Acta* **462** (2002) 179-185.

- [26] S. Shelkovnikov, H. C. Gonick, *Life sciences* **75** (2004) 2765-2773.
- [27] V. Carrera, E. Sabater, E. Vilanova, M. A. Sogorb, Journal of Chromatography B 847 (2007) 88-94.
- [28] X. Zhu, P. N. Shaw, D. A. Barrett, *Analytica Chimica Acta* **478** (2003) 259.
- [29] F. DP. Ferreira, L. IB Silva, A. C. Freitas, T. AP Rocha-Santos, A. C. Duarte, *Journal of Chromatography A* **1216** (2009) 7049-7054.
- [30] L. IB Silva, F. DP. Ferreira, A. C. Freitas, T. AP. Rocha-Santos, A. C. Duarte, *Talanta* 80 (2009) 853-857.
- [31] L. Zhang, S. Qv, Z. Wang, J. Cheng, Journal of Chromatography B 792 (2003) 381-385.
- [32] Sh. Wei, G. Song, J.M. Lin, Journal of Chromatography A 1098 (2005) 166-171.
- [33] E. M. Garrido, J. LFC. Lima, C. Delerue-Matos, *Journal of Pharmaceutical and Biomedical Analysis* **15** (1997) 845-849.
- [34] J. J. Willemsen, H. A. Ross, M. C. Jacobs, J. W. Lenders, T. H. Thien, L. M. Swinkels, T. J. Benraad, *Clinical Chemistry* **41** (1995) 1455-1460.
- [35] Y. Su, J. Wang, G. Chen, *Talanta* **65** (2005) 531-536.
- [36] J. Michałowski, P. Hałaburda, *Talanta* **55** (2001) 1165-1171.
- [37] M. H. Sorouraddin, J. L. Manzoori, E. Kargarzadeh, A. M. Haji Shabani, *Journal of Pharmaceutical and Biomedical Analysis* **18** (1998) 877-881.
- [38] M. Zhu, X. Huang, J. Li, H. Shen, *Analytica Chimica Acta* **357** (1997) 261-267.
- [39] X. Ma, M. Chao, Z. Wang. Analytical Methods 4 (2012) 1687-1692.
- [40] X. Ma, M. Chen, X. Li, A. Purushothaman, F. Li, *International Journal of Electrochemical Science* **7** (2012) 991-1000.
- [41] Y. Zhang, W. Ren, Sh. Zhang, International Journal of Electrochemical Science 8 (2013) 6839-6844.
- [42] H. Beitollahi, S. Nekooei, M. Torkzadeh-Mahani, *Talanta* **188** (2018) 701-707.
- [43] H. Beitollahi, S. Ghofrani Ivari, M. Torkzadeh-Mahani, *Biosensors and Bioelectronics* **110** (2018) 97-102.
- [44] J. Li, E. Shangguan, D. Guo, F. Gao, Q. Li, X. Z. Yuan, H. Wang, Electrochimica Acta 186 (2015) 209-215.
- [45] Z. Jemelkova, J. Barek, J. Zima, *Analytical Letters* **43** (2010) 1367-1376.
- [46] H. Kang, Y. Jin, Q. Han, Analytical Letters 47 (2014) 1552-1563.
- [47] Z. Xiu-Hua, Sh. F. Wang, Analytical Letters **35** (2013) 995-1006.
- [48] M. A. Yazdely, M. A. Taher, S. Tajik, Analytical & Bioanalytical Electrochemistry 5 (2013) 517-522.
- [49] S. Shankar, B. E. Kumara Swamy, *International Journal of Electrochemical Science* **9** (2014) 1321-1339.
- [50] M. Jahanbakhshi, Materials Science and Engineering C 70 (2017) 544-551.
- [51] B. N. Chendrashekar, B. E. Kumara Swamy, K. J. Gururaj, C. Cheng, *Journal of Molecular Liquids* **231** (2017) 379-385.
- [52] M. D. Tezerjani, A. Benvidi, A. Dehghani Firouzabadi, M. Mazloum-Ardakani, A. Akbari, *Measurement* **101** (2017) 183-189.
- [53] M. Taei, F. Hasanpour, N. Tavakkoli, M. Bahrameian, Journal of Molecular Liquids 211 (2015) 353-362.
- [54] Li. I. Hongying, W. A. N. G. Xueliang, *Electrochemistry* **83** (2015) 434-439.
- [55] Ç. Koçak, Z. Dursun, *Journal of Electroanalytical Chemistry* **694** (2013) 94-103.
- [56] B. Devadas, M. Rajkumar, Sh. M. Chen, Colloids and Surfaces B: Biointerfaces 116 (2014) 674-680.
- [57] M. Taei, M. Jamshidi, Journal of Solid State Electrochemistry 18 (2014) 673-683.
- [58] W. Ma, X. Yao, D. Sun, Asian Journal of Chemistry 25 (2013) 6625-6632.
- [59] H. Li, D. Sun, *Asian Journal of Chemistry* **27** (2015) 2539-2542.
- [60] B. Mekassa, M. Tessema, B. S. Chandravanshi, P. GL Baker, F. N. Muya. *Journal of Electroanalytical Chemistry* **807** (2017) 145-153.
- [61] S. da, L. Vieira, C. Bezerra Lopes, W. Ceciliano d. Silva, Y. Galdino d. Paiva, F. de Assis dos Santos Silva, P. Rodrigues Lima, L. Tatsuo Kubota, M. Oliveira Fonseca Goulart. *Microchemical Journal* 133 (2017) 460-467.
- [62] H. Mao, H. Zhang, W. Jiang, J. Liang, Y. Sun, Y. Zhang, Q. Wu, G. Zhang, X. M. Song. *Materials Science and Engineering: C* **75** (2017) 495-502.
- [63] I. M. Apetrei, C. Apetrei, International Journal of Nanomedicine 8 (2013) 4391-4399.
- [64] F. Valentini, E. Ciambella, V. Conte, L. Sabatini, N. Ditaranto, F. Cataldo, G. Palleschi, *Biosensors and Bioelectronics* **59** (2014) 94-106.
- [65] M. E. Ghica, Ch. M. A. Brett, *Analytical Letters* **46** (2013) 1379-1393.
- [66] M. Mazloum-Ardakani, F. Sabbaghian, B. F. Mirjalili, M. A. Sheikh-Mohseni, *Analytical and Bioanalytical Electrochemistry* **6** (2014) 106-119.

- [67] Y. Wu, X. Feng, Sh. Zhou, H. Shi, H. Wu, Sh. Zhao, W. Song, *Microchimica Acta* **180** (2013) 1325-1332.
- [68] X. Wang, J. Li, Z. Yu, International Journal of Electrochemical Science 10 (2015) 93-101.
- [69] H. Rajabi, M. Noroozifar, M. Khorasani-Motlagh, *Analytical & Bioanalytical Electrochemistry* **8** (2016) 522-531.
- [70] A. Babaei, E. Rezaei, M. Sohrabi, O. Karbalaei Hasani, *Analytical & Bioanalytical Electrochemistry* **7** (2015) 302-311.
- [71] P. Pradhan, R. J. Mascarenhas, T. Thomas, I. N. N. Namboothiri, O. J. D'Souza, Z. Mekhalif, *Journal of Electroanalytical Chemistry* **732** (2014) 30-37.
- [72] T. Thomas, R. J. Mascarenhas, O. J. D'Souza, S. Detriche, Z. Mekhalif, P. Martis, *Talanta* **125** (2014) 352-360.
- [73] F. Figueiredo, L.CS. Tiago, A. Silva, F. C. Vicentini, O. Fatibello-Filho, Analyst 139 (2014) 2842-2849.
- [74] K. K Reddy, M. Satyanarayana, K. Yugender Goud, K. Vengatajalabathy Gobi, *Materials Science and Engineering C* **79** (2017) 93-99.
- [75] R. Sadeghi, H. Karimi-Maleh, A. Bahari, M. Taghavi. *Physics and Chemistry of Liquids* **51** (2013) 704-714.
- [76] A. Babaei, M. Afrasiabi, Gh. Azimi, *Analytical Methods* **7** (2015) 2469-2478.
- [77] L. Zou, Y. Li, Sh. Cao, B. Ye, Talanta 117 (2013) 333-337.
- [78] I. E. Silai, I. C. Fort, D. Casoni, G. L. Turdean, Revue Roumane de Chimie 60 (2015) 689-696.
- [79] M. Mazloum-Ardakani, A. Dehghani-Firouzabadi, N. Rajabzade, M. A. Sheikh-Mohseni, A. Benvidi, M. Abdollahi-Alibeik, *Journal of the Iranian Chemical Society* **10** (2013) 1-5.
- [80] B. Jin, H. Zhang. *Analytical Letters* **35** (2014) 1907-1918.
- [81] A. S.Razaviansra, S. M. Ghoreishi, A. S. Esmaeily, M. Behpour, L. MA Monzon, J. M. D. Coey, *Microchimica Acta* **181** (2014) 1947-1955.
- [82] Q. Yang, Y. Zhao, J. Bai, L. Wu, H.M. Zhang, L. Qu, Analytical Methods 7 (2015) 10394-10402.
- [83] M. F. Chen, X. Y. Ma, Russian Journal of Applied Chemistry 87 (2014) 200-206.
- [84] H. Xu, X. Wang, R. Chen, Z. Yu, Chemical Research in Chinese Universities 30 (2014) 205-210.
- [85] Ch. H. Mak, C. Liao, Y. Fu, M. Zhang, Ch. Y. Tang, Y. H. Tsang, H. LW Chan, F. Yan, *Journal of Materials Chemistry C* **3** (2015) 6532-6538.
- [86] H. Beitollahi, M. A. Taher, A. Hosseini, *Measurement* **51** (2014) 156-163.
- [87] Kang, Hongzhe, Yan Jin, Qian Han, *Analytical Letters* **47** (2014) 1552-1563.
- [88] G. Ibáñez-Redín, D. Wilson, D. Gonçalves, O. N. Oliveira, *Journal of Colloid and Interface Science* (2017). https://doi.org/10.1016/j.jcis.2017.12.085
- [89] V. K. Gupta, H. Mahmoody, F. Karimi, Sh. Agarwal, M. Abbasghorbani. *International Journal of Electrochemical Science* **12** (2017) 248-257.
- [90] A. C. Anithaa, K. Asokan, C. Sekar. *Electrochimica Acta* **237** (2017) 44-53.
- [91] T. P Tsele, A. S. Adekunle, E. F. Omolola, E. E. Eno, *Electrochimica Acta* 243 (2017) 331-348.

©2019 by the authors; licensee IAPC, Zagreb, Croatia. This article is an open-access article distributed under the terms and conditions of the Creative Commons Attribution license (http://creativecommons.org/licenses/by/4.0/)



Open Access: ISSN 1847-9286

www.jESE-online.org

Original scientific paper

Application of Fe₃O₄@SiO₂/GO nanocomposite for sensitive and selective electrochemical sensing of tryptophan

Hadi Beitollahi^{1,⊠}, Mohadeseh Safaei², Masoud Reza Shishehbore², Somayeh Tajik³

¹Environment Department, Institute of Science and High Technology and Environmental Sciences, Graduate University of Advanced Technology, Kerman, Iran

²Department of Chemistry, Faculty of Sciences, Islamic Azad University, Yazd Branch, Yazd, Iran ³NanoBioElectrochemistry Center, Bam University of Medical Sciences, Bam, Iran

[™]Corresponding author: E-mail h.beitollahi@yahoo.com; Tel. +98 3426226613

Received: June 6, 2018; Revised: July 30, 2018; Accepted: July 30, 2018

Abstract

A simple strategy for determination of tryptophan (TRP) based on Fe₃O₄@SiO₂/GO nanocomposite modified graphite screen printed electrode (Fe₃O₄@SiO₂/GO/SPE) is reported. Cyclic voltammetry (CV) and differential pulse voltammetry (DPV) were used to characterize the performance of the sensor. The Fe₃O₄@SiO₂/GO/SPE displayed excellent electrochemical catalytic activities. The oxidation overpotentials of tryptophan decreased significantly and its oxidation peak current increased dramatically at Fe₃O₄@SiO₂/GO/SPE. Under the optimized experimental conditions tryptophan showed linear response over the range of 1.0-400.0 μ M. The lower detection limit was found to be 0.2 μ M for tryptophan. The practical application of the modified electrode was demonstrated by measuring the concentration of tryptophan in real samples.

Keywords

Tryptophan; Fe3O4@SiO2/GO nanocomposite; graphite screen printed electrodes; voltammetry

Introduction

Tryptophan (Trp) is a vital amino acid for humans and herbivores as the precursor of hormones, neurotransmitters and other relevant biomolecules. Tryptophan is also a precursor of the neurotransmitter serotonin [1-4]. It has been implicated as a possible cause of schizophrenia in people who cannot metabolize it properly. When improperly metabolized, it creates a waste product in the brain that is toxic, causing hallucination, delusions depression, Alzheimer's and Parkinson's diseases. Therefore, determination of tryptophan is very important in blood and urine sample in these disease. This compound is sometimes added to dietary, food products, pharmaceutical formulas due

to the scarcely presence in vegetables [5-8]. Hence, a simple, fast, selective, sensitive and accurate method for the determination of this analyte is very important. Methods for the determination of tryptophan are mainly based on HPLC [9] and spectrophotometric procedures [10]. Most of these methods involve laborious and slow procedures with the modification of tryptophan by numerous reagents.

The electroanalytical methods, with respect to their sensitivity, accuracy, less expensive and simplicity have been more intentioned in recent years for analytes determination [11-14].

Screen printed electrodes (SPEs) allowing the mass production of reproducible, economical and disposable devices. Other substantial features of these SPEs which make them suitable for on-site analysis are related to their capability to be connected to portable instrumentation and its miniaturized size [15-18]. In order to improve the efficiency of usual electrodes for sensor applications, a conventional modification method is applied. Modified electrodes not only render better electrocatalytic activity, higher sensitivity and selectivity, but also lower detection limit in comparison with traditional electrodes [19-26].

Nano materials are recognized as engineered particles with considerable surface to volume ratio and dimension less than 100 nm [27-30]. Application of nanoparticles in the construction of electrochemical sensors has increased recently [31-35].

Graphene is a two dimensional (2-D) sheet of carbon atoms in a hexagonal configuration with atoms bonded by $\rm sp^2$ bonds. These bonds and this electron configuration provide this arterial with extraordinary properties, such as large surface area, theoretically 2630 m²/g for a single layer, and double that of single walled carbon nanotubes (SWCNTs). It also shows excellent thermal and electrical conductivity. Due to its unique electronic properties, large surface area, rich edge defects, a tunable band gap, room temperature Hall effect, strong mechanical strength, high elasticity and thermal conductivity; it exhibits remarkable conductivity, and sensing capability [36-38]. Magnetic iron oxide nanoparticles such as maghemite (γ -Fe₂O₃) or magnetite (Fe₃O₄), are used in decoration of graphene to obtain improved magnetic, optical, and electrochemical properties in graphene. This combination which leads to improve the properties of graphene, make it a great option for the modification of electrodes [39].

By showing advantageous properties of superparamagnetism, low toxicity and reusability, Fe_3O_4 nanoparticles (Fe_3O_4NPs) have played a major role among the most widely used magnetic sorbents. Application of bare Fe_3O_4 NPs, however, is limited owing to its oxidation characteristics and lack of target selectivity. Thus, the bare Fe_3O_4NPs is required to be functionalized in order to protect them from oxidation and raise selectivity and adsorption efficiency of a target analyte. In addition, the silica (SiO_2) has been widely used as catalysis, electronic device and amorphous materials. It should be noted that SiO_2 has attracted much attention as sensing material in the design of biosensors [40-42].

The most promising and favourable coating material proved to be silica, as it not only protects magnetic nanoparticles against oxidation and agglomeration at wide pH range, but also improves their chemical stability. Moreover, the surface of silica is often finished with a silanol group, which can react with various chemicals and silane coupling agents to conjugate with a variety of biomolecules and specific ligands. Thus, SiO₂ layers have good compatibility and hydrophilicity and indispensable properties for the use of these materials in biomedical applications [43].

The present work aims to employ the electrochemical method for determination of tryptophan at the newly synthesized $Fe_3O_4@SiO_2/GO$ nanocomposite modified screen printed electrode. The modified electrode was used successfully as an electrochemical sensor for determination of tryptophan in the real sample as a sensitive, selective, simple and rapid method.

Experimental

Apparatus and chemicals

The electrochemical measurements were performed with an Autolab potentiostat/galvanostat (PGSTAT 302N, Eco Chemie, the Netherlands). The experimental conditions were controlled with the General Purpose Electrochemical System (GPES) software. The screen-printed electrode (DropSens, DRP-110, Spain) consists of three main parts which are a graphite counter electrode, a silver pseudo-reference electrode and a graphite working electrode (diameter: 1 mm). A Metrohm 710 pH meter was used for pH measurements.

Tryptophan and all other reagents were of the analytical grade, and they were obtained from Merck (Darmstadt, Germany). The buffer solutions were prepared from orthophosphoric acid and its salts over the pH range of 2.0-9.0.

Synthesis of Fe₃O₄@SiO₂/GO nanocomposite

Graphene oxide nano sheets were synthesized from natural graphite flakes based on the modified Hummers and Offeman's method. The reduced graphene oxide (0.096 g) was dispersed in 40 ml of water, and the solution was kept in ultrasonic bath for 1 h. The mixture was further stirred vigorously for 30 min at 60 °C. Next, 177 mg of FeCl₃·6H₂O was added under the stirring. After the mixture was stirred vigorously for 30 min under the N_2 atmosphere, 95 mg of FeSO₄·7H₂O was added and stirred under the N_2 atmosphere for 30 min. Finally, 30 mL of the 6 % NH₄OH aqueous solution was added into the mixture, drop by drop, at 60 °C for 1 h and then reacted for another 2 h. The N_2 atmosphere was used during the reaction to prevent critical oxidation. The reaction mixture was then centrifuged, washed with double distilled water, and then dried. The obtained black precipitate was Fe₃O₄/GO nanoparticles and was ready for use. Core—shell Fe₃O₄@SiO₂/GO nanocomposites were prepared by growing silica layers onto the surface of Fe₃O₄/GO, as described by Lu *et al.* [43]. Twenty-five millilitres of ethanol, 1 mL of water, 1 mL of ammonium hydroxide, and 150 µL of tetraethyl orthosilicate (TEOS) were added in a 250 mL three-neck flask in a 40 °C water bath. Fe₃O₄/GO was added to the abovementioned solution under mechanical stirring. Aliquots of the mixture were taken out after 12 h by

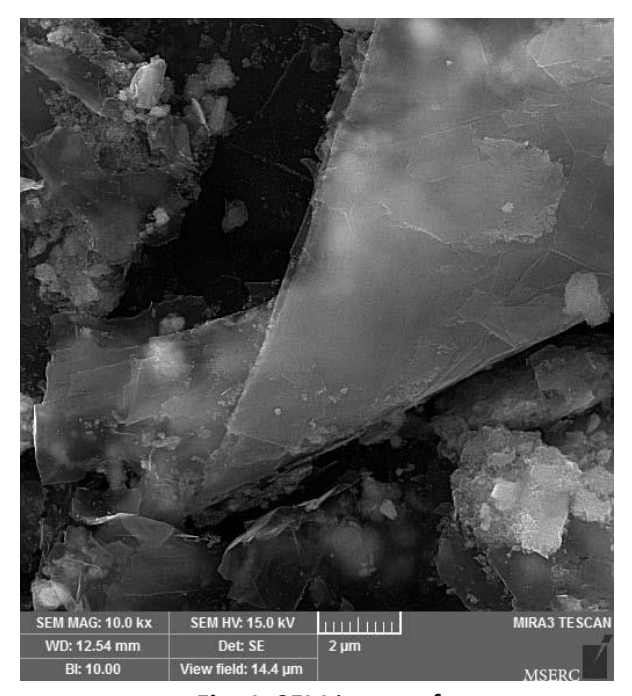


Fig. 1. SEM image of Fe₃O₄@SiO₂/GO nanocomosite

centrifugation, and then washed with water and vacuum-dried at 60 °C overnight. The morphology of the product was examined by SEM. Fig. 1 depicts the SEM pictures of $Fe_3O_4@SiO_2/GO$ nanocomposites.

Preparation of the electrode

The bare screen printed electrode was coated with Fe $_3O_4$ @SiO $_2$ /GO, as shown in the following. A stock solution of Fe $_3O_4$ @SiO $_2$ /GO in 1 mL of the aqueous solution was prepared by dispersing 1 mg of Fe $_3O_4$ @SiO $_2$ /GO with ultrasonication for 1 h, while 2 μ l of aliquots of the Fe $_3O_4$ @SiO $_2$ /GO/H $_2$ O suspension solution was cast on the carbon working electrodes, followed by waiting until the solvent was evaporated at room temperature.

Preparation of real samples

Urine samples were stored in a refrigerator immediately after collection. Ten millilitres of the samples were centrifuged for 15 min at 2,000 rpm. The supernatant was filtered out by using a 0.45 μ m filter. Next, different volumes of the solution was transferred into a 25 mL volumetric flask and diluted to the mark with phosphate buffer saline (PBS) (pH 7.0). The diluted urine samples were spiked with different amounts of tryptophan. The tryptophan contents was analysed by the proposed method by using the standard addition method.

The serum sample was centrifuged, and after filtering, diluted with PBS (pH 7.0) without any further treatment. The diluted serum sample was spiked with different amounts of tryptophan. The tryptophan contents was analysed by the proposed method by using the standard addition method.

Discussion

Electrochemical behaviour of tryptophan at the surface of various electrodes

The electrochemical behaviour of tryptophan depends on the pH value of the aqueous solution. Therefore, the pH optimization of the solution seems to be necessary in order to obtain the best results for the electrooxidation of tryptophan. Thus, the electrochemical behaviour of tryptophan was studied in 0.1 M PBS at different pH values (2.0-9.0) at the surface of $Fe_3O_4@SiO_2/GO/SPE$ by voltammetry. The peak current of tryptophan is increased with the increase of pH and reached the highest value when the pH of PBS is 7.0. Thus, the subsequent determination experiment was performed in 0.1 M pH 7.0 PBS (Fig. 2).

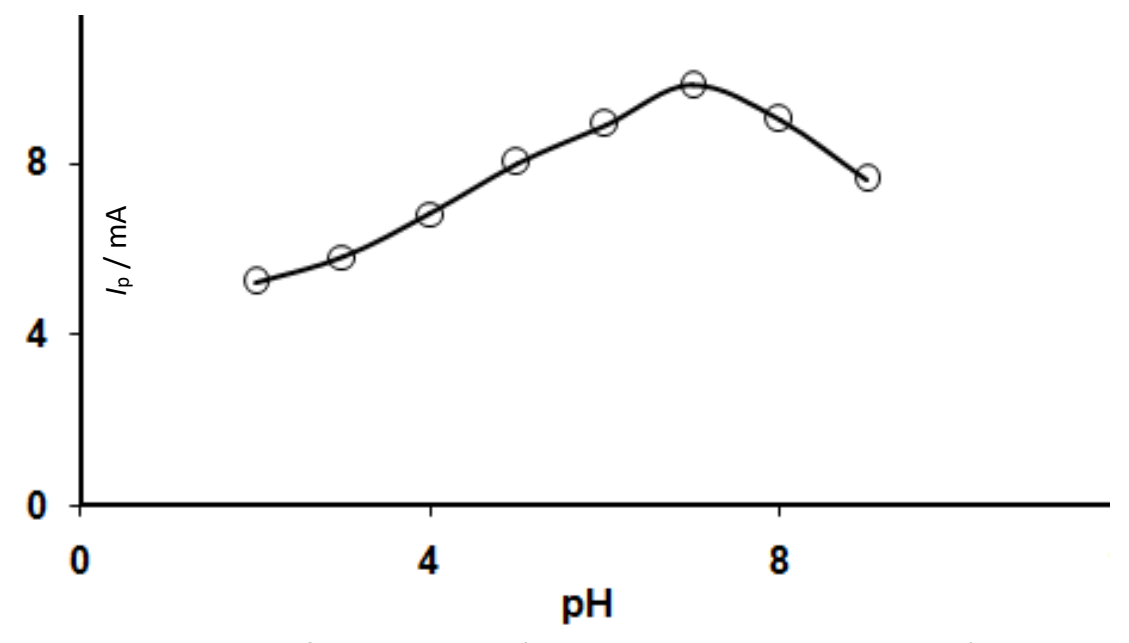


Fig. 2. Plot of Ip vs. various pH (2.0, 3.0, 4.0, 5.0, 6.0, 7.0, 8.0 and 9.0)

Fig. 3 depicts the CV responses for electrooxidation of 100.0 μ M tryptophan at the and unmodified SPE (Curve a), GO/SPE (Curve b), SiO₂/GO/SPE (Curve c) and Fe₃O₄@SiO₂/GO/SPE (Curve d) The peak potential occurs at 725 mV due to the oxidation of tryptophan, which is about 145 mV more negative than the unmodified SPE. Also, Fe₃O₄@SiO₂/GO/SPE shows much higher anodic peak current for the oxidation of tryptophan compared to the other electrodes, indicating that the modification of the unmodified SPE with Fe₃O₄@SiO₂/GO nanocomposite has significantly improved the performance of the electrode towards tryptophan oxidation.

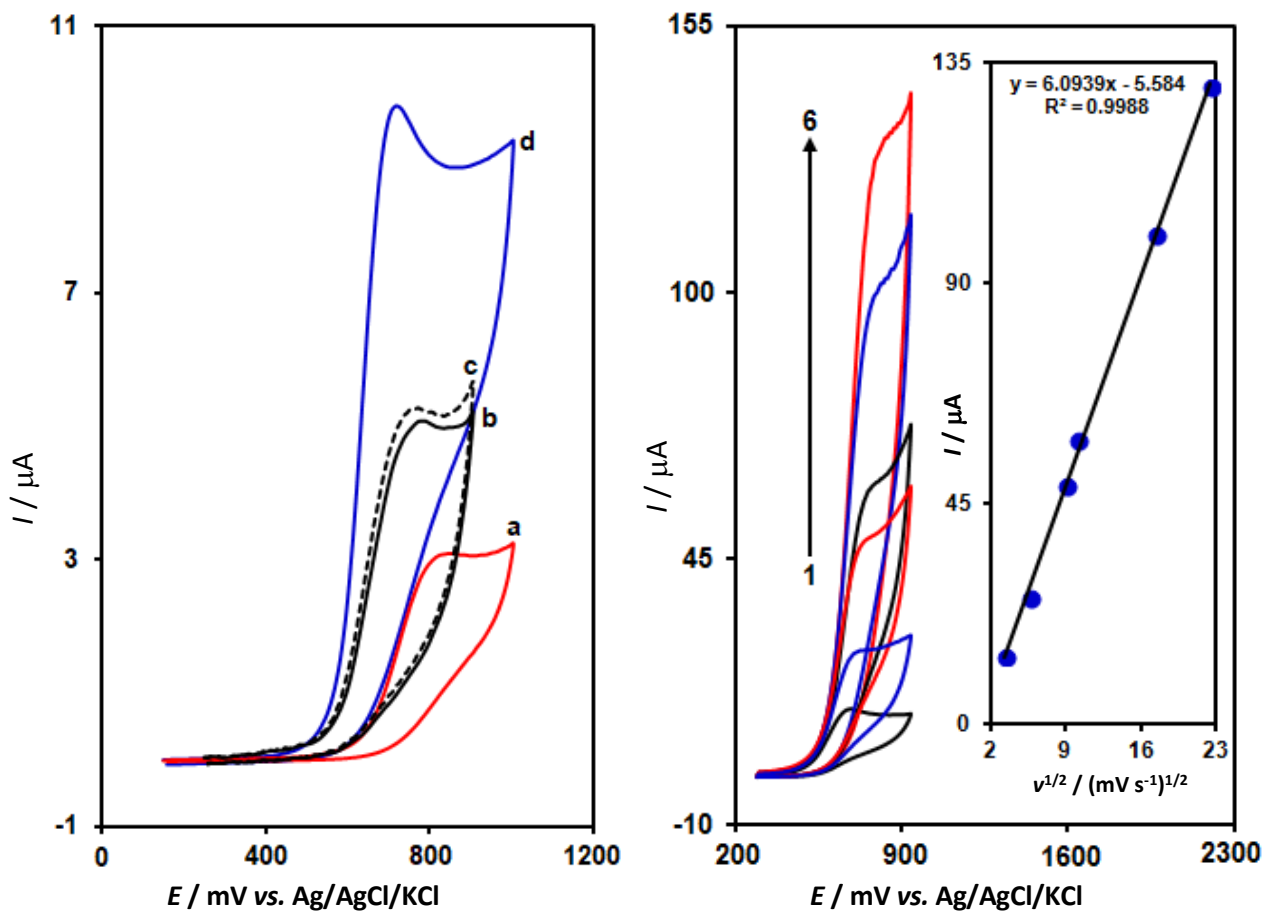


Fig. 3. CVs of a) Fe $_3O_4$ @SiO $_2$ /GO/SPE and b) unmodified SPE in the presence of 100.0 μ M tryptophan at pH 7.0. In all cases, the scan rate was 50 mV s⁻¹

Fig. 4. CVs of Fe₃O₄@SiO₂/GO/SPE in 0.1 M PBS (pH 7.0) containing 200.0 μ M of tryptophan at various scan rates; numbers 1–6 correspond to 10, 30, 80, 100, 300 and 500 mV s⁻¹, respectively. Inset: Variation of anodic peak current vs. square root of scan rate

Effect of scan rate

The effect of potential scan rates on the oxidation current of tryptophan has been studied (Fig. 4). The results showed that increasing the potential scan rate induced an increase in the peak current. In addition, the oxidation processes are diffusion controlled, as deduced from the linear dependence of the anodic peak current (I_D) on the square root of the potential scan rate ($V^{1/2}$) for tryptophan.

Tafel plot was drawn from the data of the rising part of the current–voltage curves recorded at a scan rate of 10 mV s⁻¹ for tryptophan. This part of voltammogram, known as the Tafel region is affected by electron transfer kinetics between substrate (tryptophan) and Fe₃O₄@SiO₂/GO/SPE. Tafel slope of 0.1528 V/decade was obtained, which agree well with the involvement of one electron at the rate determining step of the electrode process [44], assuming charge transfer coefficients $\alpha = 0.61$ for tryptophan.

Chronoamperometric measurements

Chronoamperometric measurements of tryptophan at Fe₃O₄@SiO₂/GO/SPE was carried out by setting the working electrode potential at 0.75 V vs. Ag/AgCl/KCl (3.0 M) for various concentrations of tryptophan (Fig. 5) in PBS (pH 7.0). For electroactive materials (tryptophan in this case) with a diffusion coefficient of D, the current observed for the electrochemical reaction at the mass transport limited condition is described by the Cottrell equation [44]:

 $I = nFAD^{1/2}C_{b}\pi^{-1/2}t^{-1/2}$

where D and C_b are the diffusion coefficient (cm² s⁻¹) and the bulk concentration (mol cm⁻³), respectively. Experimental plot of I vs. $t^{-1/2}$ was employed with the best fits for different concentrations of tryptophan (Fig. 5A). The slopes of the resultant straight lines were then plotted against tryptophan concentrations (Fig. 5B). From the resultant slope and the Cottrell equation, the mean value of D was found to be 2.5×10^{-5} cm²/s for tryptophan.

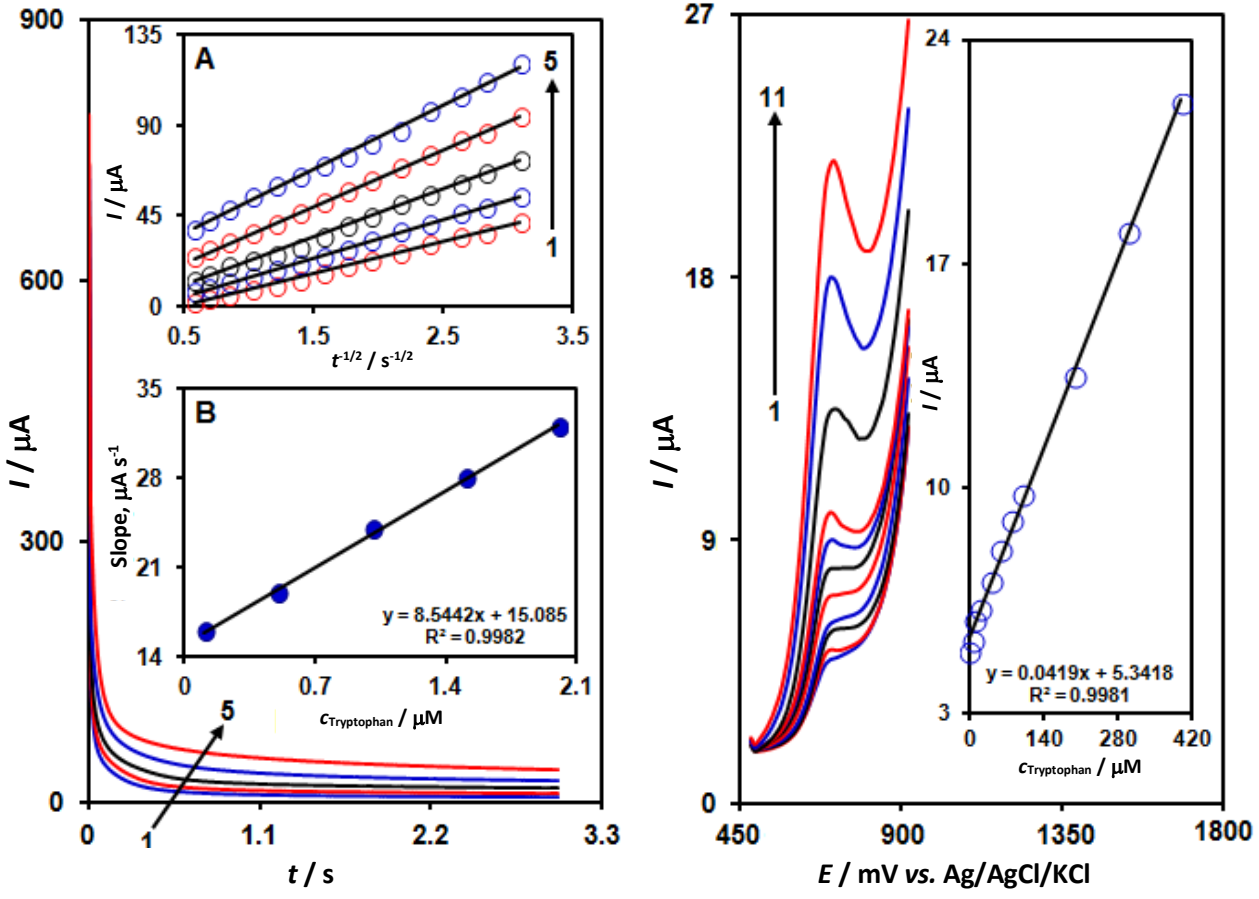


Fig. 5. Chronoamperograms obtained at Fe₃O₄@SiO₂/GO/SPE in 0. 1 M PBS (pH 7.0) for different concentrations of tryptophan. The numbers 1−5 correspond to 0.1, 0.5, 1.0, 1.5 and 2.0 mM of tryptophan. Insets: (A) Plots of I vs. t^{-1/2} obtained from chronoamperograms 1−5. (B) Plot of the slope of the straight lines against tryptophan concentrations.

Fig. 6. DPVs of Fe₃O₄@SiO₂/GO/SPE in 0.1 M PBS (pH 7.0) containing different concentrations of tryptophan. Numbers 1–11 correspond to 1.0, 5.0, 10.0, 20.0, 40.0, 60.0, 80.0, 100.0, 200.0, 300.0 and 400.0 μM of tryptophan. The inset shows the plot of the peak current as a function of the tryptophan concentration in the range of 1.0–400.0 μM.

Calibration plots and limits of detection

The electrooxidation peak currents of tryptophan at the surface of Fe₃O₄@SiO₂/GO/SPE can be used to determine tryptophan in the solution. Since differential pulse voltammetry (DPV) has the advantage of having an increase in sensitivity and better characteristics for analytical applications, DPV experiments were performed by using Fe₃O₄@SiO₂/GO/SPE in 0.1 M PBS containing various concentrations of tryptophan (Fig. 6). The results show that the electrocatalytic peak currents of tryptophan oxidation at the surface of Fe₃O₄@SiO₂/GO/SPE were linearly dependent on tryptophan concentrations over the range of 1.0-400.0 μ M (with a correlation coefficient of 0.9981) while the detection limit (3 σ) was obtained as 0.2 μ M. These values are comparable with values reported by other research groups for determination of tryptophan (Table 1).

1.0-400.0

This work

3.3

0.2

100.7

Electrode Modifier LOD, µM LDR, µM Ref. Silver nanoparticles-decorated reduced graphene Glassy 7.5 10.0-800.0 [45] carbon oxide Cu-nanoparticles incorporated overoxidized-poly Glassy 0.16 4.0-144.0 [46] carbon (3-amino-5-mercapto-1, 2, 4-triazole) Carbon Carbon nanoparticles and reduced graphene oxide 65.0 80.0-1000.0 [47] paste Poly (9-aminoacridine) functionalized multi-walled Glassy 1.0-500.0 8.0 [48]

carbon nanotubes

Fe₃O₄@SiO₂/GR Nanocomposite

Table 1. Comparison of the efficiency of some modified electrodes used in the electro-oxidation of tryptophan

Real sample analysis

carbon

Screen

printed

The new $Fe_3O_4@SiO_2/GO$ nanocomposite modified screen printed electrode was also applied for the determination of tryptophan in human blood serum and urine samples by using the standard addition method. Differential pulse voltammetry (DPV) experiments were done for different real samples. The results for the determination of the tryptophan in real samples are given in Table 2. Satisfactory recoveries of the experimental results were found for tryptophan. The reproducibility of the method was demonstrated by the mean relative standard deviation (RSD).

 $c / \mu M (n=5)$. RSD, % Sample Recovery, % Spiked **Found** 0 7.5 7.6 101.3 3.2 **Human blood serum** 12.5 12.2 97.6 2.8 17.5 17.9 102.3 1.8 27.5 27.3 99.3 2.4 0 9.7 10.0 97.0 1.9 Urine 20.0 20.5 102.5 2.8 30.0 2.2 30.4 101.3

40.3

Table 2. Determination of tryptophan in human blood serum and urine samples.

The repeatability and stability of Fe₃O₄@SiO₂/GO/SPE

40.0

The long-term stability of the Fe $_3O_4$ @SiO $_2$ /GO/SPE was tested over a 3-week period. When CVs were recorded after the modified electrode was stored in atmosphere at room temperature, the peak potential for tryptophan oxidation was unchanged and the current signals showed less than 2.6 % decrease relative to the initial response. The antifouling properties of the modified electrode toward tryptophan oxidation and its oxidation products were investigated by recording the cyclic voltammograms of the modified electrode before and after use in the presence of tryptophan. Cyclic voltammograms were recorded in the presence of tryptophan after having cycled the potential 20 times at a scan rate of 50 mV s $^{-1}$. The peak potentials were unchanged and the currents decreased by less than 2.4 %. Therefore, at the surface of Fe $_3O_4$ @SiO $_2$ /GO/SPE, not only the sensitivity increase, but the fouling effect of the analyte and its oxidation product also decreases.

Conclusion

The present study demonstrates the construction of Fe $_3O_4@SiO_2/GO/SPE$ and its application for the determination of tryptophan. The tryptophan oxidation was catalyzed at pH 7.0 and its peak potential were shifted to a less positive potential at the tryptophan surface. This modified electrode offers a considerable improvement in voltammetric sensitivity toward tryptophan, compared to the bare electrode. Differential pulse voltammetry (DPV) exhibits a linear dynamic range from 1.0-400.0 μ M and a detection limit of 0.2 μ M for tryptophan. The modified electrode showed high stability, good reproducibility and fast response for the detection of tryptophan concentrations. Moreover, the proposed method was applied to determination of tryptophan in real sample with satisfactory results.

References

- [1] J. Tashkhourian, M. Daneshi, S.F. Nami-Ana, Analytica Chimica Acta 902 (2016) 89-96.
- [2] X. Ba, L. Luo, Y. Ding, X. Liu, Sensors and Actuators B **187** (2013) 27-32.
- [3] B. Kaur, T. Pandiyan, B. Satpati, R. Srivastava, Colloids and Surface B 111 (2013) 97-106.
- [4] Q. Wang, A. Vasilescu, P. Subramanian, A. Vezeanu, V. Andrei, Y. Coffinier, S. Szunerits, *Electrochemistry Communcations* **35** (2013) 84-87.
- [5] K. Rajalakshmi, S.A. John, *Journal of Electroanalytical Chemistry* **734** (2014) 31-37.
- [6] C. Wang, X. Zou, X. Zhao, Q. Wang, J. Tan, R. Yuan, *Journal of Electroanalytical Chemistry* **741** (2015) 36-41.
- [7] H. Filik, A. A. Avan, S. Aydar, Arabian Journal of Chemistry 9 (2016) 471-480.
- [8] S. Güney, G. Yildiz, *Electrochimica Acta* **57** (2011) 290-296.
- [9] S. Hanaoka, J. Lin, M. Yamada, Analytica Chimica Acta 409 (2000) 65-73.
- [10] M.I. Evgen'ev, I.I. Evgen'eva, *Journal of Analytical Chemistry* **55** (2000) 741-745.
- [11] M. Mazloum-Ardakani, B. Ganjipour, H. Beitollahi, M.K. Amini, F. Mirkhalaf, H. Naeimi, M. Nejati-Barzoki, *Electrochimica Acta* **56** (2011) 9113-9120.
- [12] H. Beitollahi, A. Gholami, M.R. Ganjali, *Material Sciences and Engineering C* **57** (2015) 107-112.
- [13] J. T. Mehrabad, M. Aghazadeh, M.R. Ganjali, P. Norouzi, *Material Letters* **184** (2016) 223-226.
- [14] S. Tajik, M.A. Taher, H. Beitollahi, *Electroanalysis* **26** (2014) 796-806.
- [15] A. Hajializadeh, Sh. Jahani, S. Tajik, H. Beitollahi, *Analytical and Bioanalytical Electrochemistry* **10** (2018) 404-413.
- [16] H. Mahmoudi Moghaddam, H. Beitollahi, S. Tajik, Sh. Jahani, H. Khabazzadeh, R. Alizadeh, *Russian Journal of Electrochemistry* **53** (2017) 452-460.
- [17] A. Hajializadeh, S. Tajik, Sh. Jahani, H. Beitollahi, *Analytical and Bioanalytical Electrochemistry* **10** (2018) 292-301.
- [18] M. Baniasadi, Sh. Jahani, H. Maaref, R. Alizadeh, *Analytical and Bioanalytical Electrochemistry* **9** (2017) 718-728.
- [19] E. Molaakbari, A. Mostafavi, H. Beitollahi, Sensors and Actuators B 208 (2015) 195-203.
- [20] H. Beitollahi, S. Tajik, M. Malakootian, H. Karimi-Maleh, R. Hosseinzadeh, *Applied Organometallic Chemistry* **27** (2013) 444-450.
- [21] K. Roja, P.R. Prasad, P. Sandhya, N.Y. Sreedhar, *Journal of Electrochemical Science and Engineering* **6** (2016) 253-263.
- [22] T. Alizadeh, M.R. Ganjali, M. Akhoundian, P. Norouzi, *Microchimica Acta* **183** (2016) 1123-1130.
- [23] Sh. Jahani, H. Beitollahi, *Analytical and Bioanalytical Electrochemistry* **8** (2016) 158-168.
- [24] H. Beitollahi, S. Nekooei, *Electroanalysis* **28** (2016) 645-653.
- [25] M.P. Deepak, M.P. Rajeeva, G.P. Mamatha, *Analytical and Bioanalytical Electrochemistry* **8** (2016) 931-947.
- [26] M. Khatami, S. Kharazi, Z. Kishani Farahani, H. Azizi, M.A. Lima Nobre, *Tehran University Medicine Journal* **75** (2017) 72-76.
- [27] G. Zhu, Z. Azizi, S. Pourseyedi, M. Khatami, H. Mohammadi, *Journal of Cluster Science* **27** (2016) 1613-1628.

- [28] M. Khatami, R. Mehnipor, M.H. Sobhani Poor, G. Salehi Jouzani, *Journal of Cluster Science* **27** (2016) 1067-1080.
- [29] E. Zare, S. Pourseyedi, M. Khatami, E. Darezereshki, *Journal of Molecular Structure* **1146** (2017) 96-103.
- [30] H. Beitollahi, Sh. Jahani, *Electroanalysis* **28** (2016) 2022-2028.
- [31] H. Beitollahi, I. Sheikhshoaie, *International journal of Electrochemical Science* **7** (2012) 7684-7698.
- [32] H. Beitollahi, F. Garkani Nejad, *Electroanalysis* **28** (2016) 2237-2244.
- [33] H. Beitollahi, H. Karimi-Maleh, H. Khabazzadeh, *Analytical Chemistry* **80** (2008) 9948-9851.
- [34] H. Beitollahi, S. Nekooei, M. Torkzadeh Mahani, *Talanta* 188 (2018) 701-707.
- [35] N. Y. Sreedhar, K. Sunil, Analytical and Bioanalytical Electrochemistry 6 (2014) 151-158.
- [36] H. Beitollahi, S. Ghofrani Ivari, M. Torkzadeh Mahani, *Biosensors and Bioelectronics* **110** (2018) 97-102.
- [37] H. Karimi-Maleh, M. Moazampour, H. Ahmar, H. Beitollahi, A.A. Ensafi, *Measurement* **51** (2014) 91-99.
- [38] A.C. Faucett, J.N. Flournoy, J.S. Mehta, J.M. Mativetsky, Flat Chemistry 1 (2017) 42-51.
- [39] B. Nigović, A. Mornar, M. Sertić, *Microchimica Acta* **183** (2016) 1459-1467.
- [40] M.A. Farghali, T.A. S. El-Din, A.M. Al-Enizi, R.M.E Bahnasawy, *Journal of Electrochemical Science and Engineering* **10** (2015) 529-537.
- [41] N.N. Liao, Z.S. Liu, W.J. Zhang, S.G. Gong, D.M. Ren, L.J. Ke, K. Lin, H. Yang, F. He, H.L. Jiang, *Journal of Macromolecule Science A* **53** (2016) 276-281.
- [42] S.Q. Chen, X.X. Qin, W.X. Gu, X.S. Zhu, *Talanta* **161** (2016) 325-332.
- [43] Y. Lu, Y. Yin, B.T. Mayers, Y. Xia, Nano Letters 2 (2002) 183-6.
- [44] Bard, A.J., Faulkner, L.R., Electrochemical Methods Fundamentals and Applications, 2001, second ed, (Wiley, New York).
- [45] B. Kaur, T. Pandiyan, B. Satpati, R. Srivastava, *Colloids and Surface B* **111** (2013) 97-106.
- [46] C. Wang, X. Zou, X. Zhao, Q. Wang, J. Tan, R. Yuan, *Journal of Electroanalytical Chemistry* **741** (2015) 36-41.
- [47] M. Mazloum-Ardakani, N. Rajabzadeh, A. Dehghani-Firouzabadi, A. Benvidi, B. B. F. Mirjalili, L. Zamani, *Journal of Electroanalytical Chemistry* **760** (2016) 151-157.
- [48] S. Güney, G. Yıldız, *Electrochimica Acta* **57** (2011) 290-296.

©2019 by the authors; licensee IAPC, Zagreb, Croatia. This article is an open-access article distributed under the terms and conditions of the Creative Commons Attribution license (http://creativecommons.org/licenses/by/4.0/)



Open Access: ISSN 1847-9286

www.jESE-online.org

Original scientific paper

In-situ synthesis of mesoporous carbon/iron sulfide nanocomposite for supercapacitors

Xiaolong Yu, Bogang Li[™]

College of Materials Science and Engineering, Sichuan University, Chengdu 610065, China

[™]Corresponding author: E-mail <u>libogang@scu.edu.cn</u>

Received: August 7, 2018; Revised: October 20, 2018; Accepted: October 21, 2018

Abstract

Mesoporous $C@Fe_xS_y$ composite as a negative electrode for supercapacitors was synthesized via a one-step hydrothermal treatment followed by an electrodeposition process and its electrochemical properties were studied. Compared with bare carbon sphere, the electrochemical performance of $C@Fe_xS_y$ composite was significantly improved, with a high specific capacitance (267.45 F/g), good rate performance (201.08 F/g at 2.5 A/g), and superior cycling stability (almost no capacitance degradation after 1000 cycles). The results show that the obtained $C@Fe_xS_y$ composite is a promising negative electrode material for supercapacitors.

Keywords

Carbonaceous materials; porous structure; hydrothermal treatment; electrochemical properties; energy storage

Introduction

Supercapacitors have attracted tremendous attention in recent years owing to their high power density, short charging time, and good stability [1–3]. Carbonaceous materials have been widely adopted as negative electrode materials for supercapacitors because of their low cost, good electrical conductivity, and long cycle lifetime. However, carbonaceous materials exhibit limited double-layer capacitance, which limits further development of high energy density supercapacitors [4,5]. One of the effective approaches to enhance the energy density of supercapacitors is to improve the specific capacitance of carbonaceous materials [6–8].

Carbon spheres (CS) with their large surface area, high porosity, and fine pore size is a promising carbonaceous material for supercapacitors. Nevertheless, the low capacitance of CS limits its practical applications [9,10]. To improve the capacitance, researchers have recently focused on developing new negative electrode materials by activation pretreatment, doping modification, and loading of metal-base materials [5,11–13]. Among the metal-base materials, Fe-based materials are

promising candidates because of their suitable working window in negative potential, abundance, low cost, large theoretical capacitance, and nontoxicity [14–17]. Fe-based materials are combined with carbonaceous materials to explore an effective method to prepare composites; this not only could improve the rate performance of Fe-based materials, but also enhance the specific capacitance of carbonaceous materials.

In this work, CS was grown in situ on nickel foam (NF) using a one-step hydrothermal process, and iron sulfide was selected as Fe-based material. A new approach was found to synthesize $C@Fe_xS_y$ composite by using the cyclic voltammetry (CV) electrochemical deposition method to introduce iron sulfide onto CS. The electrical performance of $C@Fe_xS_y$ was investigated, and the results indicated that the $C@Fe_xS_y$ composite exhibited a significantly improved electrochemical performance than bare CS. The findings of this study would open up new possibilities for the design of carbon-based composites for high-performance supercapacitors.

Experimental

Materials

Commercial NF was used as the current collector. Anhydrous dextrose, FeCl₃·6H₂O, thiourea, and the other reagents in this experiment were used without further purification. Deionized water was used to prepare solutions.

Synthesis of carbon spheres

The CS was prepared by hydrothermal treatment. NF ($2\times4~cm^2$) was treated with hydrochloric acid (3~mol/L), acetone, and absolute ethanol in an ultrasound bath for 10 min, respectively, and then washed with deionized (DI) water. Anhydrous dextrose (10.8~g) was dispersed in 60 ml of DI water and stirred at 25 °C until a clear solution was obtained. The solution was transferred into a 100~ml Teflon-lined autoclave. A piece of NF was placed vertically in the Teflon-lined stainless-steel autoclave, soaked in the solution, at 180~c for 4 h. Subsequently, CS precursors were formed on the NF. Then, the product was washed with DI water followed by vacuum drying at 60~c for 12~h and heat treatment at 800~c for 11~h in a 11~h0 must be remove oxygen-containing groups on the surface of the CS.

Synthesis of C@Fe_xS_v composite

C@Fe_xS_y was obtained through an electrochemical deposition method. The experiment was carried out using an electrochemical workstation with a three-electrode cell. CS grown on NF was used as the working electrode, and a platinum plate and a saturated calomel electrode (SCE) were used as the counter electrode and the reference electrode, respectively. FeCl₃·6H₂O (1, 1.5, 2, 2.5, and 3 mmol) and thiourea (5 mmol) dissolved in 100 ml DI water was used as the deposition bath. The deposition process was carried out via CV at 5 mV/s for 6 cycles in the voltage range of -1.2 to 0.2 V. The as-prepared C@Fe_xS_y composites with 1, 1.5, 2, 2.5, and 3 mmol of FeCl₃·6H₂O are henceforth referred to as C@Fe_xS_y-1, C@Fe_xS_y-1.5, C@Fe_xS_y-2, C@Fe_xS_y-2.5, and C@Fe_xS_y-3, respectively. The as-prepared C@Fe_xS_y-n (n = 1, 1.5, 2, 2.5, and 3) was then carefully rinsed with DI water and dried in a vacuum oven at 60 °C for 12 h.

Characterization and electrochemical measurements

The morphology and the microstructure were observed by scanning electron microscopy (SEM, Hitachi, S-4800). The crystal structure was characterized using an X-ray diffraction (XRD, Rigaku) system with Cu K α irradiation. The chemical composition of the sample was investigated by X-ray



photoelectron spectroscopy (XPS, ESCALAB 250Xi, Thermo Scientific). The structure of $C@Fe_xS_y$ -2 was further explored by Raman spectroscopy (Renishaw Invia RM200). The Brunauer-Emmett-Teller (BET; Gemini VII) specific surface areas of the samples were determined from N_2 adsorption data in the relative pressure ranging from 0.1 to 1.0.

Electrochemical characterization was carried out using a CHI 660D electrochemical workstation (Chenhua, Shanghai) at 25 °C. The electrochemical characterization includes CV, galvanostatic charge-discharge (GCD), and electrochemical impedance spectroscopy (EIS), using a three-electrode cell with 3.0 M KOH as the electrolyte, materials grown on NF (1×1 cm²) as the working electrode, Hg/HgO as the reference electrode, and Pt foil as the counter electrode. CV was performed in the voltage window from -1 V to 0 V at scan rates of 5, 10, 20, 30, and 50 mV/s. GCD was carried out between -0.95-0 V at current densities of 0.25, 0.5, 1.0, 1.5, 2.0, and 2.5 A/g. EIS was evaluated in the frequency range of 10^5 to 0.01 Hz. The DC potential and the AC amplitude for EIS measurements are -0.01 V and 5 mV, respectively.

Results and discussion

Morphology and structural analysis

The SEM images of CS and C@Fe_xS_y-2 are presented in Figure 1. Highly dense CSs are distributed on the NF substrate (Figure 1a). These CSs exhibit smooth surfaces and they are connected with each other. This provides high volumetric specific surface area and good mass transport property, which are useful for supercapacitor application. The size distribution of the carbon particles is within the range of 1-2 μ m. Figure 1b shows that the C@Fe_xS_y-2 composite maintains the spherical structure, and many Fe_xS_y nanoparticles are dispersed on the surface of the carbon particles. This provides a large surface area for easy diffusion of the electrolyte toward the electrode surface and contributes to the enhancement of specific capacitance.

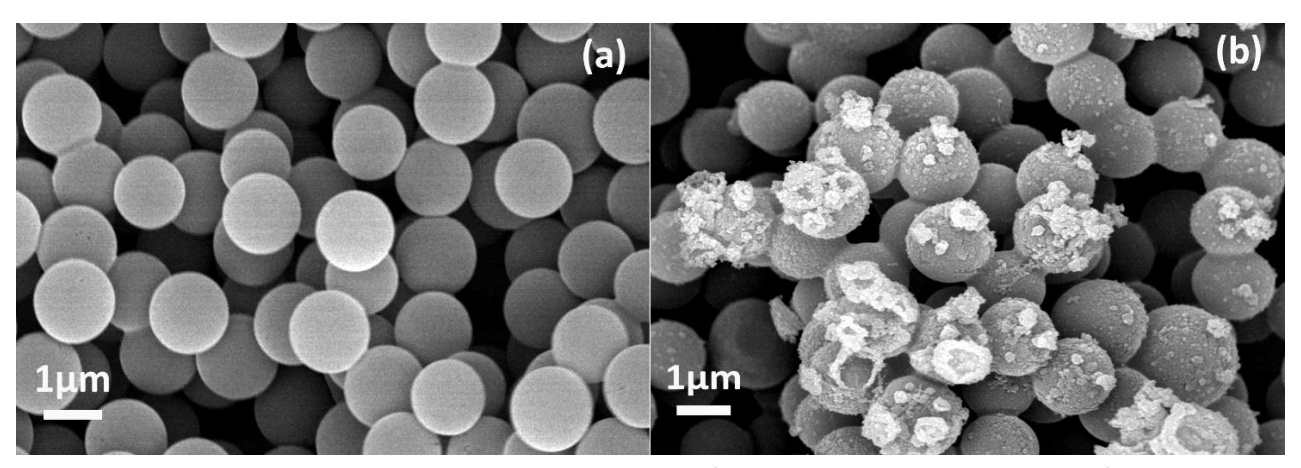


Figure 1. (a) SEM image of the carbon spheres/NF. **(b)** SEM image of $C@Fe_xS_y$ -2/NF.

The XRD patterns of CS and C@Fe_xS_y-2 (Figure 2a) showed similar characteristics. A broad diffraction peak is observed at approximately $2\theta = 23^{\circ}$ besides peaks of Ni, corresponding to (002) plane of graphitic structure. The decreased peaks for C@FexSy-2 indicate the amorphous nature of Fe_xS_y. Figure 2b shows the Raman spectrum of the CS and C@Fe_xS_y-2 samples. Both of them exhibit two characteristic peaks at 1345 and 1597 cm⁻¹, corresponding to D peak from amorphous structure of carbon and G peak from graphitic structure of carbon, respectively[18,19]. The I_D/I_G ratio of C@Fe_xS_y-2 is 0.97, a little higher than 0.90 of CS, which indicates the C@Fe_xS_y-2 has a small number of defects. The XPS data of C@Fe_xS_y-2 are shown in Figure 2c-d. The peaks at approximately 723 eV

(Fe $2p_{1/2}$), 713 eV (Fe $2p_{3/2}$) and 164 eV in the Fe 2p spectra and the S 2p spectra are assigned to amorphous iron sulfide [20,21]. These results are in good agreement with the SEM observations and further confirm the presence of C@Fe_xS_y-2 on the composite electrode.

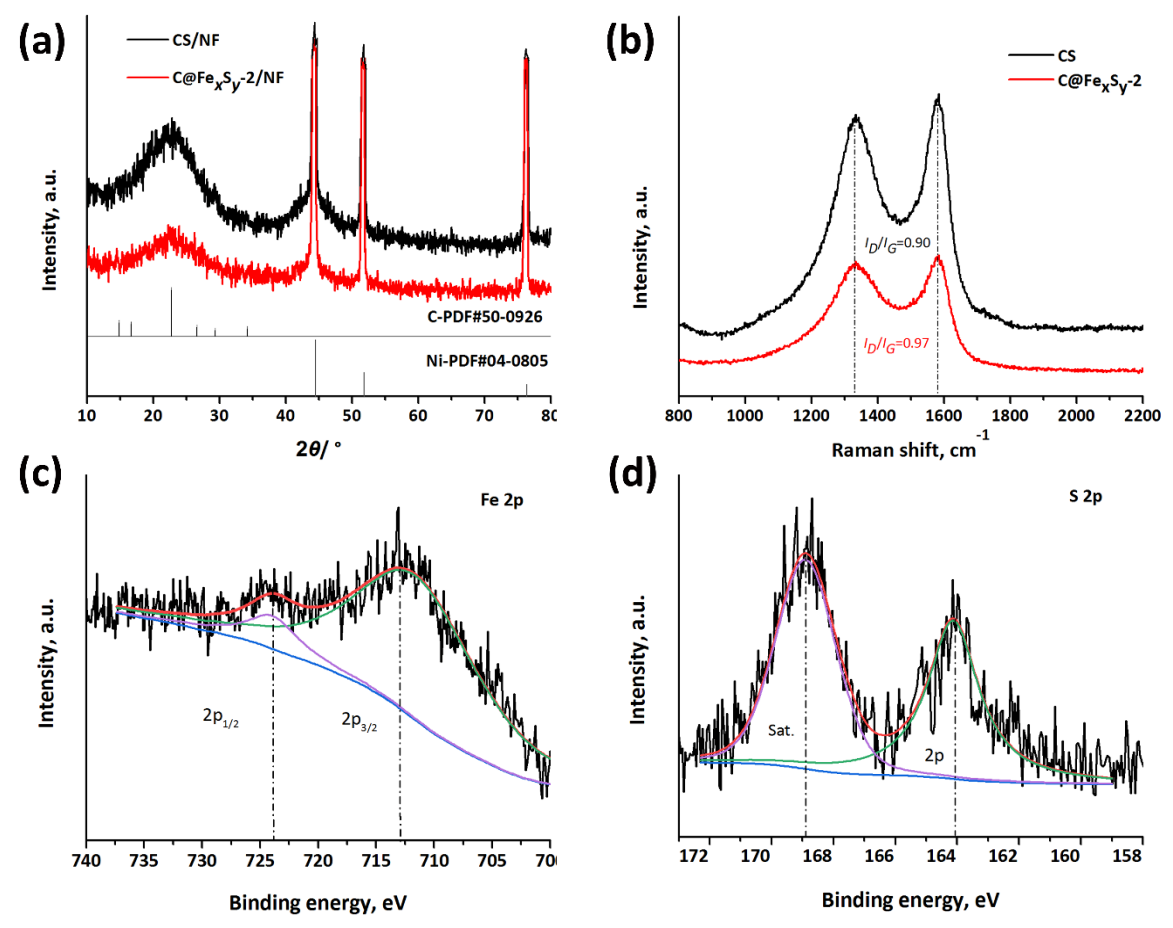


Figure 2. (a) XRD patterns of CS/NF and C@Fe_xS_y-2/NF electrode. (b) Raman spectra of CS and C@Fe_xS_y-2. (c)-(d) Fe 2p and S 2p XPS spectra of C@Fe_xS_y-2, respectively.

The nitrogen adsorption-desorption isotherms and Brunauer-Joyner-Halenda (BJH) pore diameter distribution of $C@Fe_xS_y$ -2 are shown in Figure 3. The sample exhibits a typical type IV isotherm and shows a hysteresis loop at medium relative pressure (Figure 3a), which reveals the existence of relatively mesoporous pores. The hysteresis loop exhibits H2 type characteristics, indicating that the sample has a wide pore size distribution. The BET surface area of $C@Fe_xS_y$ -2 is 117.74 m²/g. The BJH pore diameter distribution of $C@Fe_xS_y$ -2 (Figure 3b) shows that the pore diameter distribution is within the range of 5-10 nm, which further demonstrates that the sample has a mesoporous structure. From the above results, it is evident that the $C@Fe_xS_y$ -2 electrode material has a high specific surface area, and the mesoporous structure could facilitate infiltration of the electrolyte and shorten electron and ion transport distances during energy storage. This would increase the surface utilization of the active material and improve the capacitance of the electrode material.

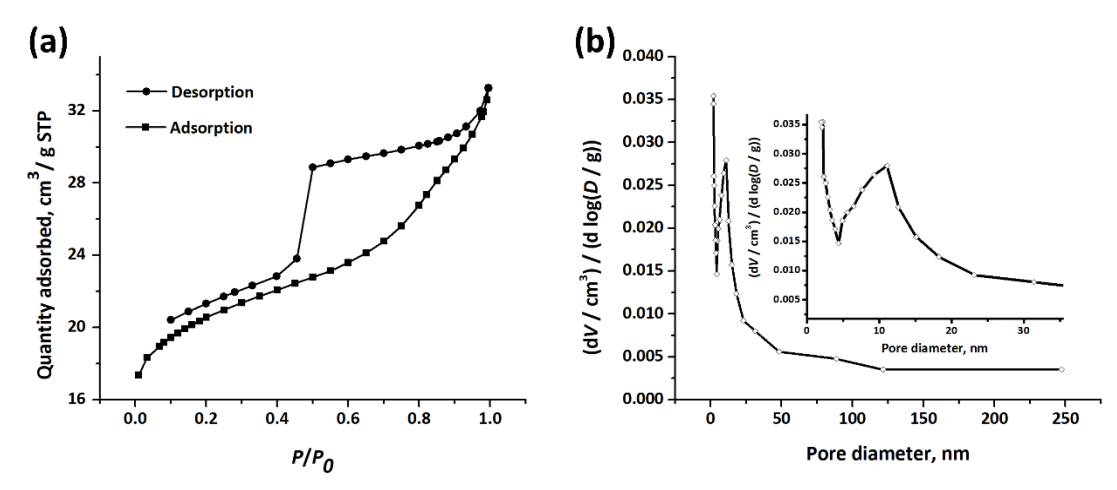


Figure 3. (a) BET of C@Fe_xS_v-2. (b) Pore diameter distribution of C@Fe_xS_v-2.

Electrochemical performance analysis

The electrochemical performance of the composites was estimated by CV and GCD measurements. Figure 4a shows the GCD curves of CS and C@Fe_xS_y-n (n = 1, 1.5, 2, 2.5, and 3) at a current density of 0.25 A/g. The charge/discharge curves are nearly linear in shape, indicating ideal electrical double-layer capacitive behavior. The symmetric triangle characteristics reveal the excellent electrochemical reversibility of the samples with high Coulombic efficiency. The C@Fe_xS_y-2 sample exhibited the longest charge-discharge time, and hence, the largest specific capacitance. The specific capacitance derived from galvanostatic tests can be determined using the following equation [22]:

$$C = \frac{I\Delta t}{m\Delta V} \tag{1}$$

where C is the specific capacitance, I is the discharge current (A), Δt is the discharge time, m is the mass of active materials loaded on the working electrode, and ΔV is the potential window.

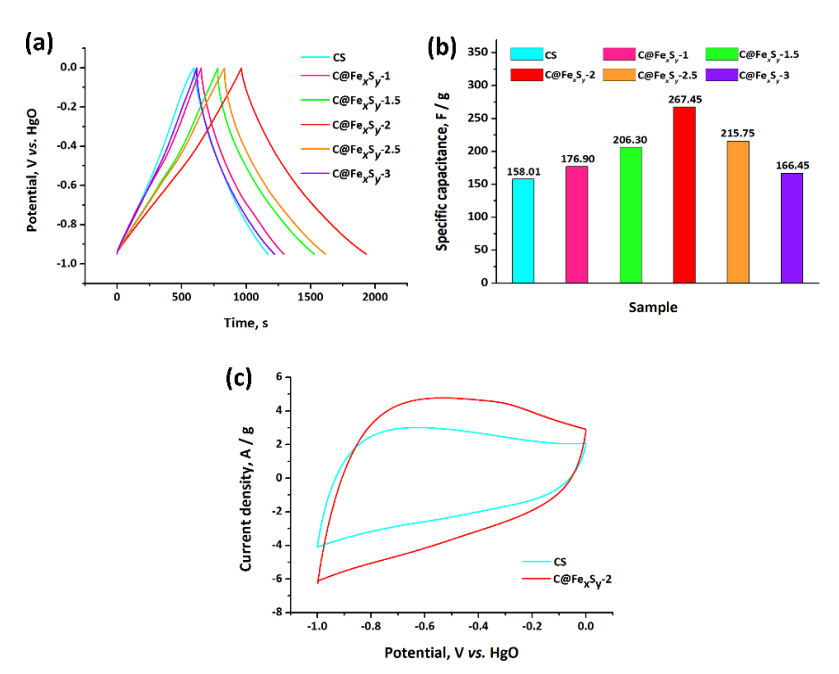


Figure 4. (a) GCD curves of CS and C@Fe_xS_y-n (n = 1, 1.5, 2, 2.5, and 3) at a current density of 0.25 A/g. **(b)** Specific capacitances of CS and C@Fe_xS_y-n based on the GCD curves. **(c)** CV curves of CS and C@Fe_xS_y-2 at a scan rate of 20 mV/s.

As plotted in Figure 4b, all the $C@Fe_xS_y$ samples exhibit a higher specific capacitance than the CS electrode (158.01 F/g); $C@Fe_xS_y$ -2 has the highest specific capacitance of 267.45 F/g at 0.25 A/g. It is considered that the loading mass of Fe_xS_y affected the capacitance, and $C@Fe_xS_y$ -2 has the optimum loading mass. The reason might be that Fe_xS_y deposited on the surface of CS provides a porous structure, which further increases the specific surface area of the electrode material and thus enhances the capacitance. However, owing to the poor conductivity of Fe-base materials, when the loading mass of Fe_xS_y further increases, the capacitance of the electrode material decreases. Figure 4c shows the CV curves of CS and $C@Fe_xS_y$ -2 at a scan rate of 20 mV/s. As expected, the $C@Fe_xS_y$ -2 composite shows a much higher capacitance than CS.

The electrochemical performance of $C@Fe_xS_y$ -2 for supercapacitor applications was investigated in KOH solution with a three-electrode system. As shown in Figure 5a, CV test was carried out at various scan rates of 5-50 mV/s. The quasi-rectangular shape of the CV curves with an obvious hump shape indicates the effect of electrical double-layer capacitance. Moreover, the rectangular shape of the curve even at a high scan rate of 50 mV/s suggests the outstanding capacitive behavior and high ionic conductivity of $C@Fe_xS_y$ -2. The inconspicuous redox peaks may be induced by Fe_xS_y . These results demonstrate that $C@Fe_xS_y$ -2 provides numerous accessible pores and paths for ion transfer. Figure 5b-c show the discharge curves of $C@Fe_xS_y$ -2 and CS at different current densities. All the curves exhibited excellent linear response, implying the ideal electric double-layer capacitive behavior of the samples. It is evident from Figure 5d that $C@Fe_xS_y$ -2 has a much higher capacitance than CS at all current densities. Remarkably, the $C@Fe_xS_y$ -2 electrode exhibited capacitance retention of 75 % when the current density was increased from 0.25 to 2.5 A/g, indicating its outstanding rate capability.

The cycling stability of $C@Fe_xS_y$ -2 was evaluated for 1000 cycles at a high charging-discharging current density of 2.5 A/g. As shown in Figure 5e, the $C@Fe_xS_y$ -2 electrode does not show capacitance degradation, and the charge/discharge curves in the last ten cycles are almost identical to those in the first ten cycles. After 1000 cycles, the capacitance retention of the $C@Fe_xS_y$ -2 electrode is even 103 % of the initial capacitance, indicating its superior cyclic performance. The reason for the slight increase in the capacitance may be the gradual entry of the electrolyte into the inner micropores of the $C@Fe_xS_y$ -2 electrode after several cycles, which increases the contact area of the electrode and electrolyte, thus enhancing the capacitance.

EIS was used to gain a deep understanding of the rate capability of the C@Fe_xS_y-2 electrode. Figure 5f shows the Nyquist plots of C@Fe_xS_y-2 and CS. It can be seen that the Nyquist plot is mainly composed of two parts: a semicircle in the high frequency range and a vertical line in the low frequency region. The inset in Figure 5f shows the magnified portion of the Nyquist plot near the origin, providing more details on the electrode impedance behavior. The *x*-intercept of the high frequency semicircle provides the value of equivalent series resistance (R_s) of the electrochemical system [23,24]. It is observed that the R_s values of C@Fe_xS_y-2 and CS are 0.60 and 0.71 Ω , respectively. The diameter of the high frequency semicircle corresponds to the charge transfer resistance (R_{ct}). The R_{ct} of C@Fe_xS_y-2 and CS was calculated to be 0.12 and 0.50 Ω , respectively. As for C@Fe_xS_y-2, the low resistances are associated with Fe_xS_y nanoparticles on the carbon substrate, which provide a larger electrolyte/electrode interface, facilitating the electrode material wetting and the ion transfer. The Nyquist plot of C@Fe_xS_y-2 exhibits an obvious Warburg 45° line region, corresponding to the semi-infinite ion diffusion resistance, which reflects a lower ion diffusion rate within the porous C@Fe_xS_y-2 electrode [25,26]. In the low-frequency region, the straight line represents the good capacitive behavior of the electrode and the more parallel to the virtual axis,

the closer to the double-layer capacitance [27]. The Nyquist plot in the low frequency range of $C@Fe_xS_y$ -2 shows a less vertical line, which is an indication that $C@Fe_xS_y$ -2 has diffusion-controlled faradaic processes due to the higher contribution of Warburg impedance [28-30].

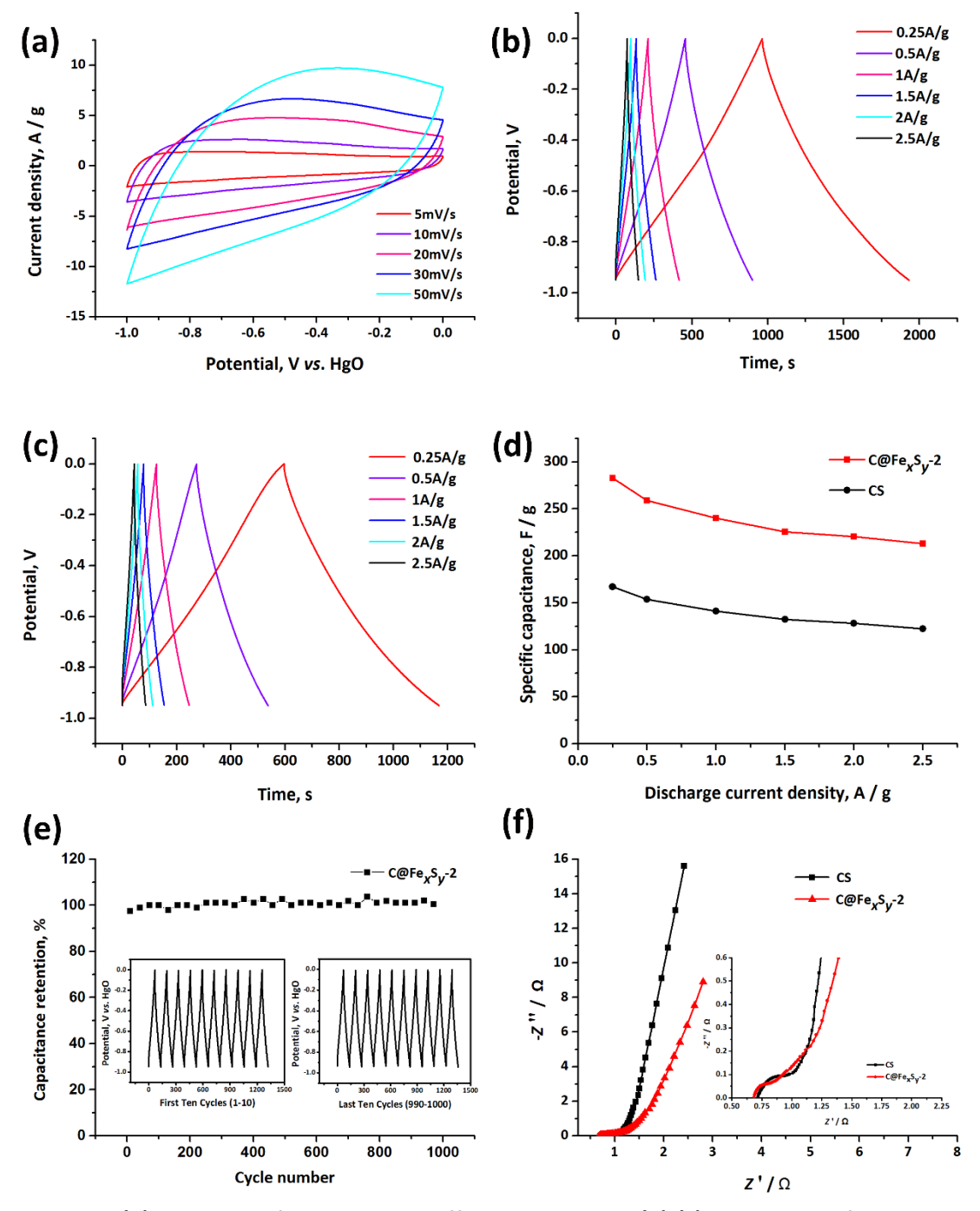


Figure 5. (a) CV curves of $C@Fe_xS_y$ -2 at different scan rates. (b)-(c) GCD curves of $C@Fe_xS_y$ -2 and CS at different current densities, respectively. (d) Specific capacitance of $C@Fe_xS_y$ -2 and CS at different discharge current densities. (e) Cycling performance of the $C@Fe_xS_y$ -2 electrode at a current density of 2.5 A/q. (f) Electrochemical impedance spectra of $C@Fe_xS_y$ -2 and CS.

Conclusions

In this study, a mesoporous negative electrode $C@Fe_xS_y$ composite was successfully fabricated on NF using a hydrothermal method followed by an electrodeposition treatment. The electrochemical performance of the $C@Fe_xS_y$ -2 electrode was significantly higher than that of bare

CS. The hybrid electrode demonstrated a high specific capacitance (up to 267.45 F/g), good rate performance (201.08 F/g at 2.5 A/g), and superior cycling stability (almost no capacitance degradation after 1000 cycles). The excellent electrochemical behavior could be attributed to the unique hybrid electrode design and the enhancement in the surface area. The present study provides an adaptable method for novel design of negative electrode materials for supercapacitors, extending the potential applications of carbon-based devices.

Acknowledgements: The authors greatly appreciate the support of Xinyue Huang, Xingye Tong, and Xiaoming Tu.

References

- [1] X. Yuan, B. Tang, Y. Sui, S. Huang, J. Qi, Y. Pu, F. Wei, Y. He, Q. Meng, P. Cao, *Journal of Materials Science: Materials in Electronics* **3** (2018) 1-13.
- [2] P. Simon, Y. Gogotsi, *Nature Materials* **7** (2008) 845-854.
- [3] S. Liu, L. Wang, C. Zheng, C. Qidi, M. Feng, Y. Yu, ACS Sustainable Chemistry & Engineering 5 (2017) 9903-9913
- [4] B. Lv, P. Li, Y. Liu, S. Lin, B. Gao, B.-Z. Lin, Applied Surface Science 437 (2017) 169-175.
- [5] N. Syarif, IA. Tribidasari, W. Wibowo, *Journal of Electrochemical Science & Engineering* **3(2)** (2013) 37-45.
- [6] H. Zhang, X. Zhang, Y. Ma, Electrochimica Acta 184 (2015) 347-355.
- [7] X. Yang, H. Ma, G. Zhang, Langmuir: The ACS Journal of Surfaces and Colloids 33 (2017) 3975-3981.
- [8] J. Pang, W. Zhang, H. Zhang, H. Zhang, G. Cao, M. Han, Y. Yang, *Carbon* **132** (2018) 280-293.
- [9] T. Liu, L. Zhang, W. You, J. Yu, Small 14 (2018) 1702407.
- [10] J.-G. Wang, H. Liu, H. Sun, W. Hua, H. Wang, X. Liu, B. Wei, *Carbon* **127** (2017) 85-92.
- [11] D. Iglesias, E. Senokos, B. Aleman, L. Cabana, C. Navío, R. Marcilla, M. Prato, J. J. Vilatela, S. Marchesan, *ACS Applied Materials & Interfaces* **10** (2018) 5760-5770.
- [12] X. Xia, Y. Zhang, Z. Fan, D. Chao, Q. Xiong, J. Tu, H. Zhang, H. Jin Fan, Y. X Xia, D. Zhang, J. Chao, Fan, Q. X Xia, J. Xiong, Tu, Z. H Fan, Zhang, *Advanced Energy Materials* **5** (2014) 1-9.
- [13] J. Tang, J. Wang, L. Shrestha, S. Hossain, Z. Alothman, Y. Yamauchi, K. Ariga, *ACS Applied Materials & Interfaces* **9** (2017) 18986-18993.
- [14] J. Ma, X. Guo, Y. Yan, H. Xue, H. Pang, Advanced Science 5 (2018) 1700986.
- [15] Y. Zhang, R. Lin, Y. Fu, X. Wang, X. Yu, J. Li, Y. Zhu, S. Tan, Z. Wang, *Materials Letters* (2018) 9-12.
- [16] Y. Zhong, J. Liu, Z. Lu, H. Xia, *Materials Letters* **166** (2015) 223-226.
- [17] M.A. Azam, R.N.A.R. Seman, M.A. Mohamed, *Advances in Natural Sciences: Nanoscience and Nanotechnology* **7(4)** (2017) 1-10.
- [18] J. Wu, H. Xu, J. Zhang, *Acta Chimica Sinica* **72(3)** (2014) 301-318.
- [19] T. Jawhari, A. Roid, J. Casado, *Carbon* **33(11)** (1995) 1561-1565.
- [20] J. Feng, L.T. Peckler, A.J. Muscat, Crystal Growth & Design 15 (2015) 3565-3572.
- [21] V. Sridhar, H. Park, *Journal of Alloys and Compounds* **732** (2017) 799-805.
- [22] N. Zhang, C. Fu, D. Liu, Y. Li, H. Zhou, Y. Kuang, *Electrochimica Acta* **210** (2016) 804-811.
- [23] J.-G. Wang, Y. Yang, Z.-H. Huang, F. Kang, *Carbon* **61** (2013) 190-199.
- [24] H. Yoo, J. Hyun Jang, J. Heon Ryu, Y. Park, S. M. Oh, Journal of Power Sources 267 (2014) 411-420.
- [25] J.-G. Wang, Z. Zhang, X. Zhang, X. Yin, X. Li, X. Liu, F. Kang, B. Wei, *Nano Energy* **39** (2017) 647-653.
- [26] J. Gao, X. Wang, Y. Zhang, J. Liu, Q. Lu, M. Liu, *Electrochimica Acta* **207** (2016) 266-274.
- [27] W. Zhang, C. Xu, C. Ma, G. Li, Y. Wang, K. Zhang, F. Li, C. Liu, *Advanced Materials* **29(36)** (2017) 1701677.
- [28] M.R. Lukatskaya, B. Dunn, Y. Gogotsi, Nature Communications 7 (2016) 12647.
- [29] J. Liu, J. Wang, C. Xu, H. Jiang, C. Li, L. Zhang, Advanced Science **5(1)** (2018) 1700322.
- [30] X. Du, C. Wang, M. Chen, Y. Jiao, *The Journal of Physical Chemistry C* **113(6)** (2009) 2643-2646.

©2019 by the authors; licensee IAPC, Zagreb, Croatia. This article is an open-access article distributed under the terms and conditions of the Creative Commons Attribution license (http://creativecommons.org/licenses/by/4.0/)





Open Access: ISSN 1847-9286

www.jESE-online.org

Original scientific paper

Remediation of clay soil contaminated with lead nitrate using washing-enhanced electrokinetic technique

Mahdi Karkush[⊠], Shahad Ali

College of Engineering, University of Baghdad, Iraq

[™]Corresponding author: E-mail mahdi karkush@coeng.uobaghdad.edu.iq; Tel.: +9647801058893

Received: July 23, 2018; Revised: October 8, 2018; Accepted: November 13, 2018

Abstract

The remediation of clay soil contaminated with lead nitrate has been investigated in details by using the electrokinetic technique enhanced by using purging solutions, mid compartment, and washing technique. The intact soil samples are obtained from Al-Ahdab oil field located in the southeast of Iraq. The soil samples are contaminated synthetically with two different percentages of lead nitrate (6.67 and 20 g/kg) and kept for 30 days. The mid compartment is used to reduce the existing paths of contaminants from the soil. Purging solutions in the anode, mid, and cathode compartments are used to control the pH value, while the activated carbon is used to prevent the reverse electroosmotic flow from cathode to anode. The main results of electrokinetic experiments, such as variations of electrical current and pH with time, and the accumulated volume of electroosmotic flow are presented and discussed. It was shown that increasing of the concentration of lead causes increase of the electrical current generated during the remediation process. As a consequence, the intensity of chemical reactions occurring in the anode, mid, and cathode compartments are also increased. The removal efficiency of lead from soil samples ranged between 12.4 and 21 %. The washing process is found beneficial in reducing the period of remediation but does not affect the removal efficiency.

Keywords

Heavy metals; lead; contaminated soil; soil remediation; washing; electrokinetic

Introduction

The contamination of soil is a significant problem that was increased in recent years because of development of industrial, agricultural, and military activities. Heavy metals (HMs) are considered as the major contaminants which have diverse effects on geotechnical properties of soil. The effects of contaminants depend on several factors such as their mobility and chemical activity in the soil, especially when the content of contaminants is above certain levels [1,2]. HMs usually adhere to the

soil particles and thus become immobile. This process is called sorption and describes the distribution of HMs between the solid and pores solution. Contamination of soil with HMs causes reduction of shear strength parameters of soil. Also, contamination of soil with HMs leads to increased compressibility and maximum dry density, but decreased optimum moisture content and permeability of soil [1]. Costs and removal efficiency are the major factors in selection of the remediation technique for removing contaminants from the soil. Also, sites contaminated with more than one type of contaminants require more than one type of remediation technique that should be applied simultaneously or in a sequence. Generally, the process of removing HMs from the soil is considered difficult, because the metals are not biodegradable or soluble in water, except mercury and selenium which could degrade and volatilize by microorganisms. The electrokinetic method (EK) has already been found suitable for the remediation of low permeability contaminated soils through applying DC current between two electrodes installed in the medium. There are generally three phenomena occurring during the EK process: electroosmosis, electromigration and electrophoresis [3].

The removal efficiency of HMs from a soil depends on several factors such as the type and composition of HM in the soil matrix and the type of soil [4,5]. During the EK process, the electrolysis occurs at the electrodes, generating hydrogen ions at the anode and hydroxide ions at the cathode [6,7]. The hydrogen ions move from the anode toward cathode while hydroxide ions move from the cathode toward anode. The advance of the acid fronts is faster than advance of the basic front migration, because the mobility of H⁺ is greater than OH⁻ for about 1.76 times [8]. Only few studies, however, investigated effects of HMs on geotechnical properties of the soil. Li et al. [9] studied the removal efficiency of cadmium (II), lead (II), and chromium (III) from a sandy soil. They used a conductive solution to separate the soil and cathode compartments, in order to enhance the removal efficiency which can be higher than 90 %. Reddy and Chinthamreddy [4] studied the effects of different purging solutions on removal efficiency of HMs from the soil contaminated with different percentages of Cr, Ni, and Cd. The removal efficiency of contaminants was found very low when the tap water was used as a purging solution, but increased when 1 M of acetic acid and 0.1 M of ethylene diamine tetraacetic acid were used as the purging solution in the cathode compartment. The maximum removal efficiency was obtained when water was used as a purging solution at the beginning of the test in anode and cathode compartments, being followed by using acetic acid as the purging solution in the cathode and NaOH solution in the anode compartments. Jensen et al. [10] demonstrated that soils with high content of carbonate compounds produced negative effects on the removal efficiency of lead from the soil. Karkush and Altaher [7] studied the remediation of the clayey soil contaminated with several concentrations of total petroleum hydrocarbons by using washing-enhanced electrokinetic technique. The purging solution used to enhance EK consisted of 30 % of ethanol and 70 % of deionized water. The results of tests demonstrated the removal efficiency of 15 % after 10 days of remediation.

In the present study, the washing-enhanced EK technique was used in the remediation of a fine-grained soil contaminated with two different percentages of lead nitrate. The EK technique was enhanced by using purging solutions and the mid compartment to increase the removal efficiency of lead from soil. Also, the activated carbon was used to prevent the reverse electroosmotic flow.

Experimental

Soil sampling and materials

The intact soil samples were obtained from an open pit excavated to a depth of 3 m below the existing ground level (EGL) in the site of Al-Ahdab oil field located in the southeast of Iraq. Depending

on the unified soil classification system (USCS), the intact soil was classified as silty clay of high plasticity (CH). The fine-grained soil is highly affected by contaminants, due to its large specific surface area, dynamic crystalline structure and charged particles [11,12]. Two quantities of Pb(NO₃)₂ (100 and 300 g) were added to soil samples in order to study the impact of lead nitrate on the chemical and physical properties of soil and measure the removal efficiency of the washing-electrokinetic remediation technique. The EK process was enhanced with purging solutions, activated carbon, and mid compartment. Lead nitrate is soluble in water, having solubility of 565 g/l. Nitric acid (HNO₃) and sodium hydroxide (NaOH) were used as purging solutions to control the pH value in the cathode and anode compartments, respectively. After several electrokinetic tests, activated carbon was used for preventing reverse electroosmotic flow occurring from anode to cathode. The physical and chemical properties of contaminant and purging solutions used in the compartments of electrokinetic cell are given in Table 1.

Chemical Molar weight, Density, Electrical conductivity Concentration рН compound g/mol g/cm³ μS/cm $Pb(NO_3)_2$ 331.2 4.53 6.67, 20 g/kg 11150 NaOH 39.99 2.13 0.1mol/l 12.3 63.01 0.001mol/l 2.5 664 HNO₃ 1.51

Table 1. Properties of contaminant and purging solutions.

Preparation of contaminated soil samples

Two disturbed soil samples were placed in plastic containers and soaked with contamination solutions, covered with tightened covers and left for one month to ensure chemical reactions between the contaminant and solid skeletons of the soil. The soil sample of 15 kg weight was put in each container and covered with the contamination solution consisted from lead nitrate and distilled water. Two quantities (100 and 300 g) of lead nitrate were mixed with 10 liters of distilled water. The distilled water was necessary for dissolution of $Pb(NO_3)_2$ and the final contaminant solution had to have sufficient volume to cover the soil sample and provide an adequate column (about 3 cm) above the soil surface. In such a way, contaminant could penetrate deeper in the soil [1,13]. The soil samples used in this study were designated with the symbols given in Table 2.

Symbol	Definition	Concentration of lead nitrate in soil, g/kg			
M0	Intact soil sample	0			
M1	Soil sample contaminated with 100 g of Pb(NO ₃) ₂	6.67			
M2	Soil sample contaminated with 300 g of Pb(NO ₃) ₂	20			

Table 2. Designation of soil samples.

Chemical and physical properties of soil samples

The chemical and physical properties of intact and contaminated soil samples were measured according to ASTM standards [14]. The chemical properties of soil samples were important for analysis of chemical reactions between the contaminant and mineral composition of soil. The measured chemical properties were the contents of trioxide sulfate (SO_3), chloride ions (CI^-), silicon dioxide (SiO_2), calcium oxide (CaO_3), organic matter (CaO_3), gypsum, total soluble salts (CaO_3), and pH value. As shown in Table 3, the results of chemical tests showed significant changes in contents of these components, resulting from the impacts of lead nitrate.

Soil Content, % На Clsample SO_3 SiO₂ CaO OMC Gypsum TSS M0 0.036 0.5442 32.37 18.31 0.04 0.620 3.60 7.6 M1 0.221 0.2650 32.63 16.61 0.513 1.081 3.45 8.4 M2 0.346 0.3290 33.54 18.24 0.682 3.65 3.00 8.2

Table 3.Chemical properties of tested soil samples.

The physical properties of soil samples listed in Table 4 involve the particle-size distribution, Atterberg's limits (LL and PL), specific gravity (GS), maximum dry density (ρ_{dmax}), optimum moisture content (ω_{opt}), and permeability of soil (k). Also, the results demonstrated that presence of lead in soil samples tended to increase the percentage of particles that had size higher than 0.005 mm [1]. CaCO₃ and OMC were the main compounds in the cementation between the particles of soil and are responsible for both, the sticking and stability of soil particles [15]. The lead has a greater adsorption ability on the surfaces of clay particles than other HMs, and formation of cation bridges among the particles of clayey soil resulted in increased stability of aggregate matrix.

k×10⁻⁸ / Content, % $\omega_{\rm opt}/$ $ho_{\mathsf{dmax}}/$ Soil sample PL, % LL, % GS g cm⁻³ Sand Silt Clay % cm sec⁻¹ M0 0.020 25.98 74 55 27 2.74 1.678 21.6 3.22 M1 0.102 29.898 70 45 26 2.78 1.720 18.5 2.60 43.373 M2 56 2.83 1.760 17.0 1.86 0.273 43 21

Table 4. Physical properties of tested soil samples.

Washing-enhanced electrokinetic remediation technique

Electrokinetic remediation technology has great capability for treatment of low permeability soils contaminated with HMs and/or organic compounds [16]. Several studies showed that using water as an electrolyte is not effective to give high removal percentage, especially when the soil is contaminated with more than one type of contaminant. The EK technique, however, can be improved by different ways, such as increasing of treatment duration, increasing electric potential gradient, and using solvents or surfactants. It has also been found that the use of purging solutions is the most promising strategy for obtaining high removal efficiency [17]. The selection of enhancing agent depends on the type and concentration of contaminant and the type of soil.

Soil washing is one of technologies that has been used in remediation of contaminated soils, and is based on isolating and extracting the most contaminated fraction of the soil. In the soil washing process, several extracting fluids containing a chemical reagent (acid/base, surfactant, chelating agent, salt, or redox agent) is used to transfer metals from the soil into an aqueous solution. Soil washing can be used alone or linked with other treatment techniques. In this study, the soil washing was linked with the EK technique to enhance the removal efficiency of contaminant from the soil. The components and dimension of the EK test set up is shown in Figure 1. In the present study, the EK technique was enhanced by four ways. The first was installing of the mid-compartment to reduce the travel path required for exit of the contaminant particles from the soil. The second way is use of the activated carbon (AC) to keep the flow from anode to cathode and prevent reverse electroosmotic flow. The AC compartment is 5 cm in length, 10 cm in width and 10 cm in height. The third way was use of purging solution (0.001 M HNO₃ in anode compartment put at initial state and followed by

addition of 0.1 M NaOH and 0.001 M HNO₃ in mid and cathode compartments, respectively). The fourth way of enhancement was utilization of the washing process.

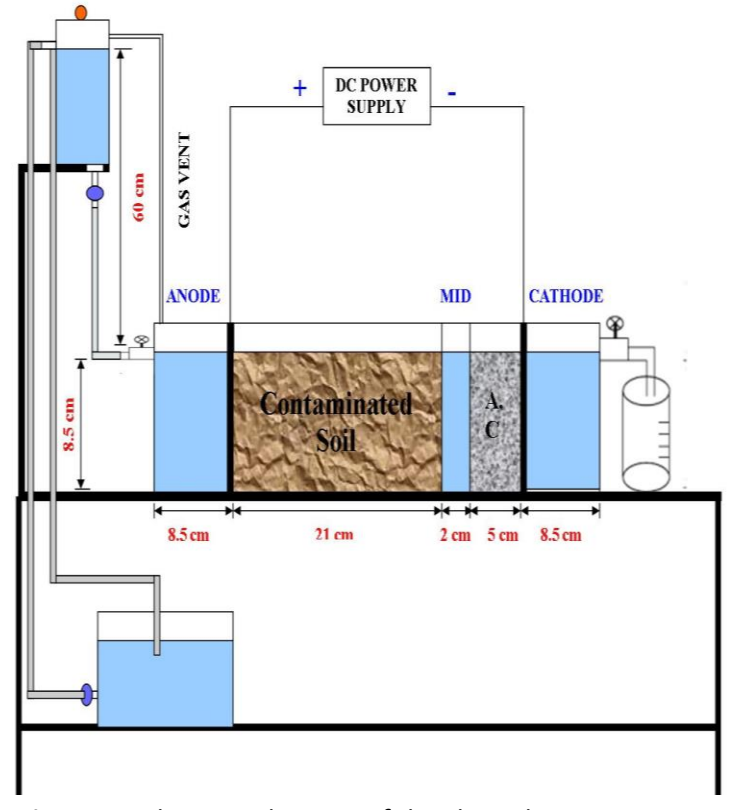


Figure 1. Schematic diagram of the electrokinetictest setup.

The major components of the system were power supply, pump station, and electrokinetic rectangular cell of dimensions 50 cm in length, 10 cm in width and 10 cm in height. The EK cell consisted of five compartments, for the soil sample, for the activated carbon, the mid compartment between soil and AC and two others for electrodes (anode and cathode). Each electrode compartment comprised a valve to manage the flow into the cell, a graphite electrode, filter paper and porous stone. The filter paper and porous stone were used to prevent soil particles from entrance into anode or cathode reservoirs. Gas vent tubes were provided in electrode compartments to release gases resulting from the electrolysis reactions and collect any liquid that was removed with the gases. A pH meter was used to measure changes in pH of the solution in the cathode, mid, and anode compartments and soil after remediation. The effluent from cathode compartment was collected to determine the accumulated volume of electroosmotic flow (EOF). The size, shape, and arrangement of electrodes and the distance between them affect also the removal efficiency. Only few researches have been conducted to select the optimum values for these parameters. The dimensions of electrodes used in the present study were 2 cm in thickness × 10 cm in width and 10.5 cm in height. Also, the voltage gradient through the soil sample will affect the movement of ions between opposite charged electrodes and the transport of charge by electroosmosis. A number of studies reported the voltage gradient in the range of 1-3 V_{DC}/cm [18,19]. The choice of the most suitable voltage gradient relies on soil properties and contamination type, where soils of high electrical conductivity need more charge than soils of low electrical conductivity. Increase of the voltage gradient will increase transport rates, i.e. ionic migration and electroosmosis rates. At the other side, increase of the voltage gradient results in increase of the electric current, the cost of the process, and the produced heat. Therefore, the voltage gradient used in this study was set to 1.3 V_{DC}/cm.

Testing procedure

The testing procedure can be described by the following steps:

- 1) preparing the EK cell (electrodes, purging solutions, a device used to control the hydraulic gradient).
- 2) Preparing the contaminated soil sample in the EK cell according to the field unit weight and natural moisture content. In front of the electrodes, the filter paper and porous stone were placed.
- 3) The electrodes compartments were filled with purging solutions. The anode reservoir was filled with 0.001 M HNO₃ at the beginning of test, and then 0.1 M NaOH was added to maintain the pH higher than 2. The cathode and mid reservoirs were filled with 0.001 M HNO₃ from the beginning of the experiment.
- 4) The graphite electrodes (anode and cathode) were linked to the power supply with a voltage gradient equal to 1.3 V_{DC} /cm.
- 5) The electric current, the volume of electroosmosis flow (EOF) and pH in the anode, mid, and cathode compartments were measured every hour during the testing period.
- 6) The test was stopped when the electrical current became constant or no change in EOF was observed.
- 7) At the end of each test, the soil specimen and AC are extruded from the cell by hands. The soil specimen was sectioned into five parts and each part was weighed and subsequently preserved in a glass container. For each soil section, pH was measured according to ASTM (D4972) and the residual concentration of lead was measured using AAS.

Results and discussion

The results of EK experiments measured with time involve: (1) the variation of electric current; (2) the rate of EOF; (3) pH values determined in compartments and soil sample, and (4) the lead content in the remediated soil samples.

Electrical current

The electrical current in the soil sample M2 was equal to zero at the first 30 hours of the EK test, then started to increase steadily, reached its maximum value and then decreased until a constant value was reached. For the soil sample M1, however, the electric current rose rapidly in the first hour of testing, reached its maximum and then continued steadily to the end of test. Increasing the concentration of ionic species in each experiment caused rising of the electrical current due to generation of H⁺ and OH⁻ ions at anode and cathode respectively. Increasing the mobility of soil solids due to the presence of ions causes rising of the electrical current produced during treatment process. The migration of these ions towards the electrodes during the treatment reduces the electric current [9,20,21]. Generally, the values of electrical current reached a peak value because dissolved salts that are connected with dry soil particles increased the quantity of ions in the pore solution [13,20]. The time required to get a stable current or reach the maximum value was variable and depended on migration rates of ions from solution to the soil column [23]. The profiles of electrical current vs. time are shown in Figure 2.

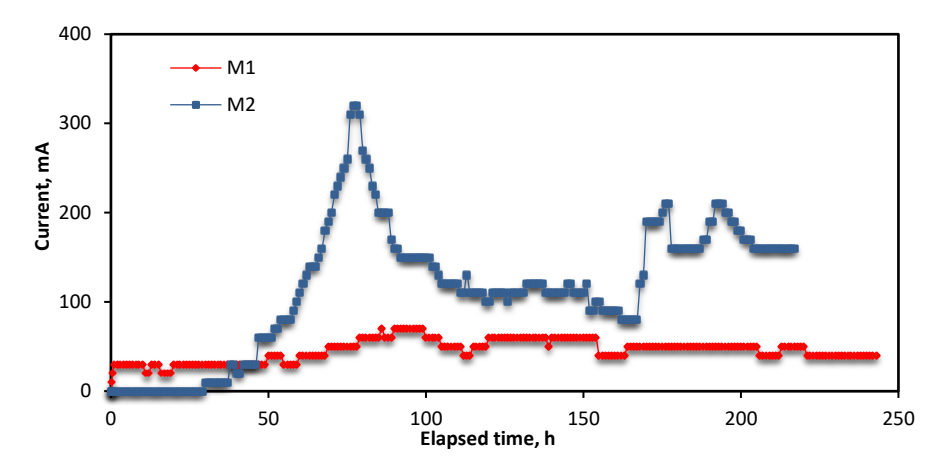


Figure 2. Variation of electrical current with time.

pH value

The values of pH measured in anode, mid, and cathode compartments during the period of testing and their variations with time are shown in Figure 3.

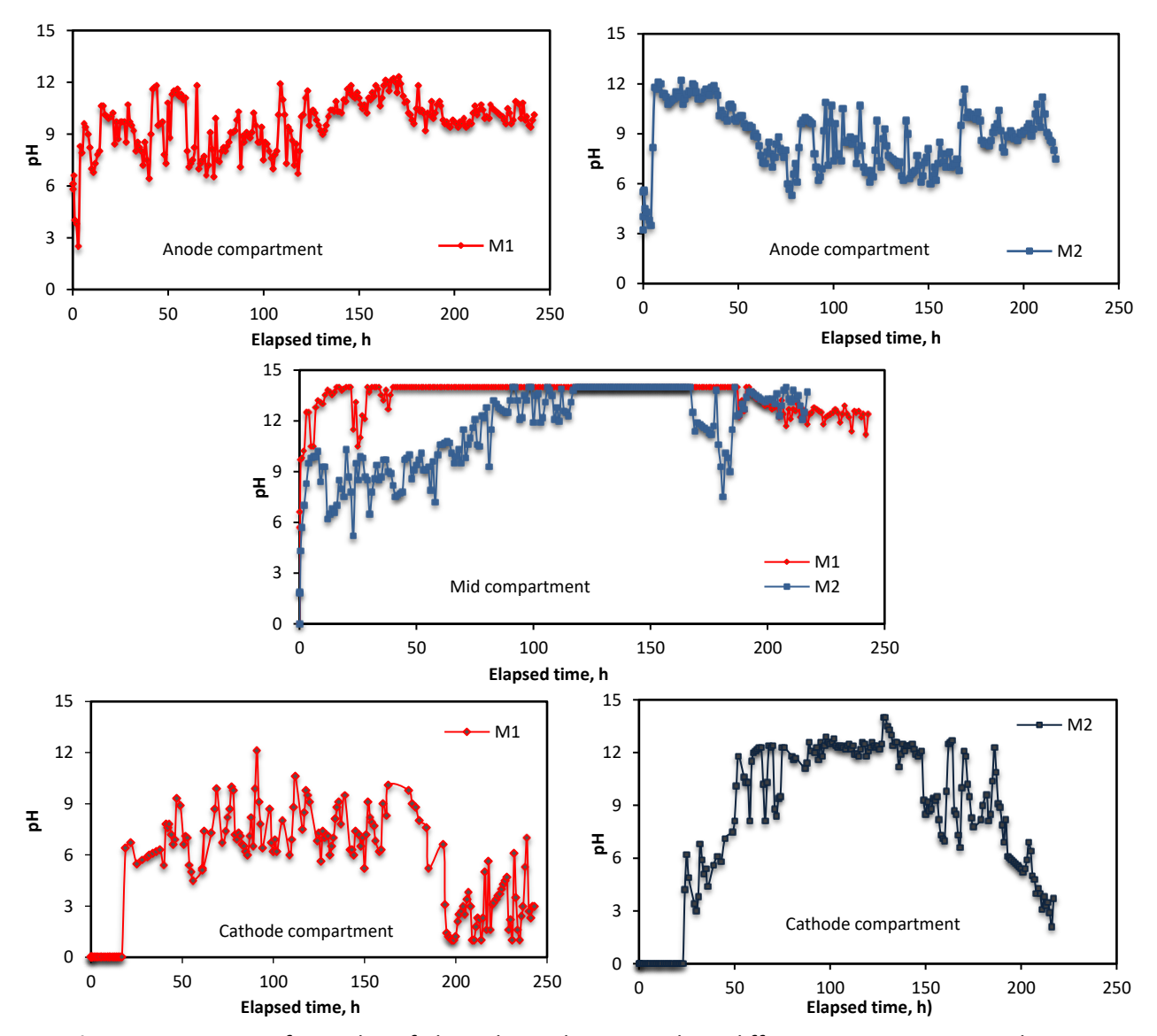


Figure 3. Variation of pH value of electrolyte solutions at three different compartments with time.

Application of voltage gradient to the soil specimen that produced low DC current leads to the production of hydrogen and hydroxyl ions at electrodes. Consequently, an acidic medium at the anode and alkaline medium at the cathode were generated [24,25]. When pH reached the value about 2, NaOH was added to the solution in the anode compartment, so the value of pH increased. The values of pH in the mid compartment were inversely proportional to the concentration of contaminant in the soil. pH value in the mid compartment depended on the quantity of accumulated salts which was higher in the soil sample M2 than M1. Increasing the sediment of salts in the compartment led to the lowering of the pH value.

In general, the pH value at anode during the test should have decreased, but in the present study, the value of pH sometimes increased and oscillated between 6-12, what may be attributed to the applied hydraulic gradient (washing process). In the cathode compartment, the value of pH was equal to zero at the beginning of testing what was due to the effect of AC which prevented the rapid change of pH value. After that, pH value began to increase and reached its maximum value due to the generation of hydroxide ions (OH⁻). The increase of electroosmotic flow towards the cathode led to lowering of pH value near the cathode because of the opposite migration of ions [26,27].

The lowering of pH value at the anode and rising at the cathode were accompanied by propagation of an acid front into the soil pores from the anode and a base front from the cathode. This process can significantly affect the soil zeta potential drop, as well as the solubility, ionic state and charge, and level of adsorption of the contaminant [28]. The variation of pH value of soil along the distance from anode to cathode is shown in Figure 4.

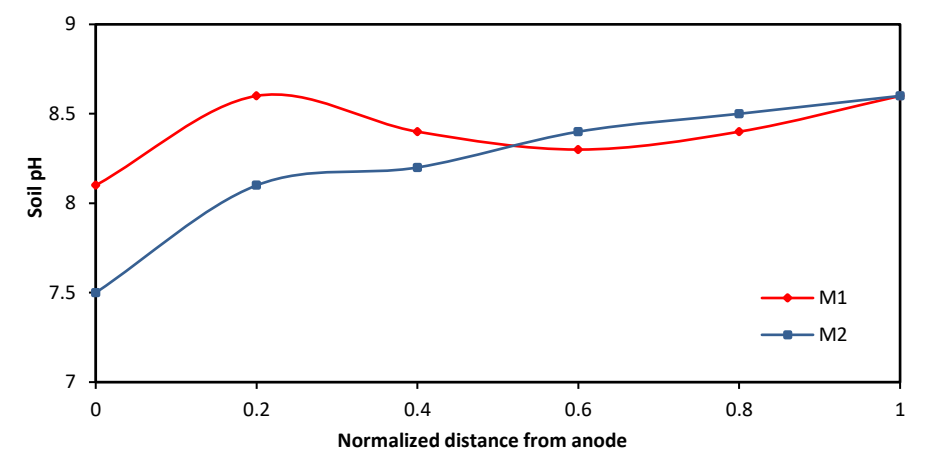


Figure 4. Profile of pH value of tested soil samples.

Electroosmosis flow (EOF)

Accumulative volumes of effluent from soil samples M1 and M2 are shown in Figure 5. According to the electroosmotic phenomenon, the water carries lead nitrate from anode to cathode compartment. The high concentration of lead nitrate may lead to the reverse flow from cathode to anode compartment. Also, the electroosmotic flow can be reversed, what occurs when the charge of soil surface is converted from negative to positive. The surface charge depends on pH and ionic strength and so, the high concentration of lead nitrate leads to increase of ionic strength that influenced the surface charge and zeta potential. Lowering the pH value of the soil causes alteration of the net surface charge of soil from negative to positive, what is due to the sorption of hydrogen ions on the surface of soil particles. In the soil with a positive surface charge, the direction of electroosmotic flow changed from the cathode to the anode, and so it is important to keep the negative charge of the soil surface to avoid the reversed EOF. Also, the pH value of the soil should

be maintained low enough to keep all contaminants in the dissolved phase [28,29]. The results of tests demonstrated that increase of the concentration of lead nitrate in the soil, increased the rate of EOF. This leads to increase of the ionic migration due to rise of the produced electrical current. Also, it is important to notice that EOF started 80 hours after the beginning of the experiment, what is due to low solubility of lead nitrate in water.

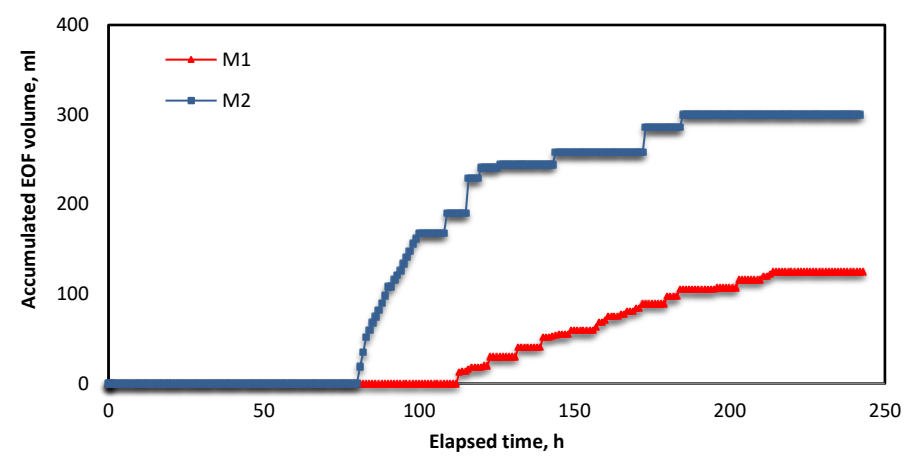


Figure 5. Accumulative volume of EOF in cathode compartment versus time

Removal efficiency

The residual concentrations of lead in the soil were measured using atomic absorption spectroscopy (AAS) device. The initial concentration of lead in the soil is calculated by Eq. (1):

$$c_{Pb} / \% = \frac{\text{atomic mass of lead} \times \text{used quantity}}{\text{atomic mass of lead nitrate}} 100$$
 (1)

The initial concentration of lead in the soil samples M1 and M2 were found equal to 4.17 and 12.512 g/kg, respectively. The removal efficiency is obtained by Eq. (2).

$$ER = \frac{c_i / c_f}{c_i} \tag{2}$$

In Eq. (2), ER is the the removal efficiency of lead from soil, while C_i and C_f are initial and final concentration of lead in the soil (g/kg). The removal efficiency of lead from soil samples M1 and M2 was determined as 12.4 and 21 %, respectively. Figure 6 shows the residual concentrations of lead in the soil after EK remediation.

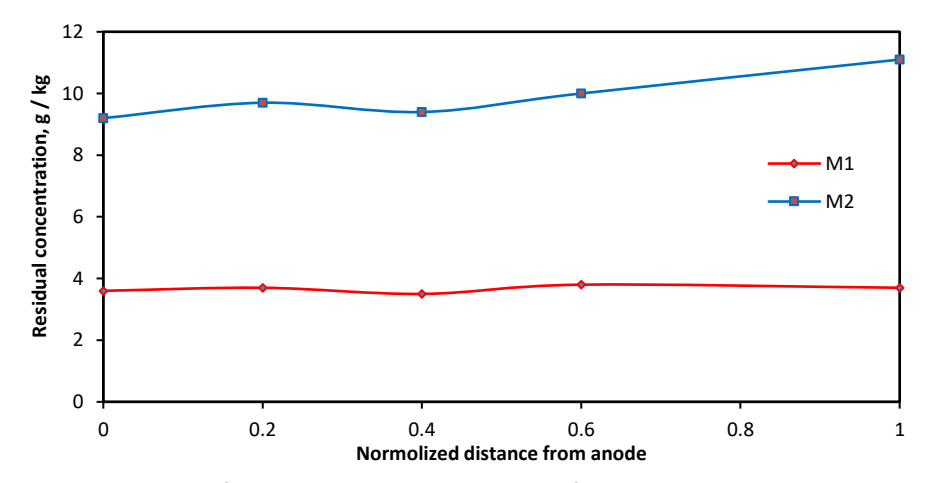


Figure 6. Variation of the residual concentration of lead in soil sample with distance

Conclusions

The lead nitrate as a soil contaminant has diverse impacts on the chemical and physical characteristics of tested soil samples. The impacts of contamination depend on the concentration and type of contaminant, as well as the type of soil, where geotechnical properties of soil are highly influenced with increasing the concentration of lead nitrate in the soil. From the results of this study, the following conclusions can be drawn out:

- 1) The electrokinetic method is very effective technique to remediate low permeability soils.
- 2) The pH value of soil increased in the soil specimen when moving towards the cathode compartment.
- 3) The volume of EOF increased with increasing the concentration of lead in the soil.
- 4) The removal efficiency of lead from soil samples M1 and M2 is 12.4 and 21 %, respectively. The low removal efficiency can be attributed to the high molar weight of lead nitrate which prevents moving and transportation of contaminant particles in the EK process. The extraction efficiency can be improved by increased the value of voltage gradient or by using another effective purging solution to remove lead from the contaminated soil.
- 5) Using of activated carbon is very effective to prevent reverse EOF. The ability of activated carbon to adsorb a contaminant increases with increased concentration of contaminant in the soil.
- 6) Using the mid compartment to enhance the EK technique is very useful in shortening the exiting path of contaminant particles from the soil sample.

For the concentration of lead in soil increased over 6.67 g/kg, the voltage gradient must be kept less than 1.3 V_{DC} / cm to avoid increasing temperature of EK cell what may cause a damage. Also, when the temperature exceeds 55 °C in the cathode compartment, production of gases is increased, what can be poisonous and have detrimental effects to the human health.

References

- [1] M. O. Karkush, A. T. Zaboon, H. M.Hussien, *Coupled Phenomena in Environmental Geotechnics, Taylor & Francis Group, London* (2013) 599-607.
- [2] M. K. Uddin, Chemical Engineering Journal 308 (2017) 438-462.
- [3] S. O. N. G. Yue, A. Benamar, S. Mezazigh, W. A. N. G. Huaqing, *Pedosphere* **280(1)** (2018) 35-43.
- [4] S. Chinthamreddy, Doctoral dissertation (1999).
- [5] K. R. Reddy, S. Chinthamreddy, *Journal of Geotechnical and Geoenvironmental Engineering* **129(3)** (2003) 263-277.
- [6] S. S. Kim, J. H. Kim, S. J. Han, Journal of Hazardous Materials 118(1-3) (2005) 121-131.
- [7] M. O.Karkush, T. A. Altaher, *Proceedings of the 19th International Conference on Soil Mechanics and Geotechnical Engineering*, Seoul (2017) 3139-3142.
- [8] M. A. Karim, Journal of Electrochemical Science and Engineering **4(4)** (2014) 297-313.
- [9] Z. Li, J.W. Yu, I. Neretnieks, *Journal of Hazardous Materials* **55(1-3)** (1997) 295-304.
- [10] P. E. Jensen, L. M. Ottosen, T. C. Harmon, Environmental Engineering Science 24(2) (2007) 234-244.
- [11] A. Shehzad, A. H. Khan, Z. Rehman, *International Journal of Advanced Structures and Geotechnical Engineering* **4** (2015) 138-147.
- [12] A. Chandrasekaran, R. Ravisankar, N. Harikrishnan, K. K. Satapathy, M. V. R. Prasad, K. V. Kanagasabapathy, *Spectrochimica Acta Part A: Molecular and Biomolecular Spectroscopy* **137** (2015) 589-600.
- [13] K. R. Reddy, M. R. Karri, Land Contamination & Reclamation 14(3) (2006) 685-698.
- [14] Annual Book of ASTM Standards, Soil and Rock. ASTM, Philadelphia, PA (2003).
- [15] R. F. Craig, Craig's soil mechanics. CRC Press (2004).
- [16] K. R. Reddy, C. Cameselle, Electrochemical remediation technologies for polluted soils, sediments and groundwater. John Wiley & Sons, 2009.

- [17] K. R. Reddy, Coupled Phenomena in Environmental Geotechnics, Taylor & Francis Group, London (2013) 131-147.
- [18] K. R. Reddy, K. Darko-Kagya, A. Z. Al-Hamdan, Water, Air, & Soil Pollution 221(1-4) (2011) 35-44.
- [19] C. Cameselle, K. R. Reddy, Electrochimica Acta 86 (2012) 10-22.
- [20] R. E. Saichek, K. R. Reddy, *Critical Reviews in Environmental Science and Technology* **35(2)** (2005) 115-192.
- [21] L. Rajić, B. Dalmacija, S. U. Perović, M. Bokorov, *International Journal of Electrochemical Science* **7** (2012) 58-67.
- [22] G. Dermont, M. Bergeron, G. Mercier, M. Richer-Laflèche, *Journal of Hazardous Materials* **152(1)** (2008) 1-31.
- [23] D. M. Zhou, C. F.Deng, L.Cang, Chemosphere **56(3)** (2004) 265-273.
- [24] J. S. Wong, R. E. Hicks, R. F. Probstein, Journal of Hazardous Materials 55(1-3) (1997) 61-79.
- [25] A. Giannis, E. Gidarakos, *Journal of Hazardous Materials* **123(1-3)** (2005) 165-175.
- [26] M. Saeedi, A. Jamshidi, N. Shariatmadri, A. Falamaki, *International Journal of Environmental Research* **3(4)** (2009) 629-636.
- [27] K. R. Reddy, R. E. Saichek, K. Maturi, P. Ala, *Indian Geotechnical Journal* **32(2)** (2002) 258-288.
- [28] J. Virkutyte, M. Sillanpää, P. Latostenmaa, Science of the Total Environment 289(1-3) (2002) 97-121.
- [29] D. H. Kim, B. G. Ryu, S. W. Park, C. I. Seo, K. Baek, *Journal of Hazardous Materials* **165(1-3)** (2009) 501-505.

©2019 by the authors; licensee IAPC, Zagreb, Croatia. This article is an open-access article distributed under the terms and conditions of the Creative Commons Attribution license (http://creativecommons.org/licenses/by/4.0/)